The Dissertation Committee for Liang Dong

certifies that this is the approved version of the following dissertation:

Adaptive Antenna Systems for Mobile Broadband Communications

Committee:

_____

Hao Ling, Supervisor

_____

Guanghan Xu, Supervisor

_____

Gustavo de Veciana

_____

Edward J. Powers

_____

Maruthi R. Akella

_____

Robert W. Heath

Adaptive Antenna Systems for Mobile Broadband Communications

by

Liang Dong, B.S., M.S.

Dissertation

Presented to the Faculty of the Graduate School of

The University of Texas at Austin

in Partial Fulfillment

of the Requirements

for the Degree of

Doctor of Philosophy

The University of Texas at Austin

August 2002

To Cliff and Delores, my American parents.

Acknowledgments

Many people have helped me in my Ph.D. research. The first two individuals who deserve special thanks are Professor Guanghan Xu and Professor Hao Ling, my dissertation advisors, for their guidance, support and encouragement throughout the course of my graduate research. I would like to express my deepest appreciation to Professor Xu, who, with great intelligence and incredible work ethic, provided me with both intellectual help for the theoretical aspects of my research and practical help for my applied work on the wideband smart antenna testbed. I am thankful to Professor Ling for broadening my knowledge in the research fields, and for his sharp scientific intuition, meticulous scholarship and warmheartedness, which have profoundly influenced me.

I would also like to thank my committee, Professor Gustavo de Veciana, Professor Edward J. Powers, Professor Maruthi R. Akella and Professor Robert W. Heath. Thanks to Professor de Veciana for encouraging me in rigorous analysis and thought, and sharing with me his expertise in communication networks. Thanks to Professor Powers, director of the Telecommunications and Signal Processing Research Center, for his suggestions, inspirations and the solid foundation of telecommunication knowledge that he has laid for me and many others. Thanks to Professor Akella for helping me take a quantum leap in the understanding of linear systems. Thanks to Professor Heath, director of the Wireless Systems Innovations Laboratory, for leading me into the exciting field of MIMO wireless, and for

his infectious research enthusiasm.

My association with Professors Xu and Ling's research groups has been an invaluable experience for me. I would like to thank my colleagues, past and present (in alphabetical order), Alberto Arredondo, Hosung Choo, Kapil Dandekar, Zhihui Deng, Lars Hansen, Shain-Shun Jeng, JoonHyuk Kang, Adnan Kavak, Sang-Youb Kim, Hang Li, Junfei Li, Garret Okamoto, Murat Torlak, Roberto Vargas, Weidong Yang, and Yaoqing Yang. I have very fond memories of our stimulating discussions at the group meetings, the days and nights working on experiments, the good humors and the precious friendships.

Finally, I would like to thank my parents for their love and support. I am indebted to Cliff and Delores Holubec, my "American parents": Their sacrificial love has made my graduate study at UT an extremely enjoyable journey.

LIANG DONG

The University of Texas at Austin

August 2002

Adaptive Antenna Systems for Mobile Broadband Communications

Publication No. _____

Liang Dong, Ph.D.

The University of Texas at Austin, 2002

Supervisors: Hao Ling and Guanghan Xu

Mobile broadband communication is experiencing rapid growth in technology, markets and range of services. This rapid growth has driven the recent surge of research and development activities for high-data-rate/high-mobility wireless systems, with improved network performance and enhanced economics. One technology thrust in wireless communications is the use of adaptive antennas at the transceivers, along with the associated advanced array signal processing, to improve cell coverage, link quality and system capacity.

This dissertation first provides a framework of adaptive antenna systems for wireless communications, and characterizes the multipath fading channels of mobile broadband systems. In particular, we consider antenna systems for the base station, as well as multiple-input multiple-output systems where antenna systems are utilized at both the base station and the mobile unit. It is proved that the channel fading can be modeled and predicted using linear models of low order. The correlation of fading at multiple antennas or over the wideband is exploited to perfect channel modeling and prediction.

Secondly, this dissertation develops the theory of adaptive antenna arrays with applications to mobile broadband systems. Through analysis of the propagation pattern and the channel structure, new techniques of uplink power control and downlink beamforming are derived to adapt to the rapid variation of the vector channel. The low variability of the channel subspace and the negligible distance between uplink and downlink channel subspaces are exploited to enhance the performance of adaptive transmission. Constraints are put on the model structure, which leads to a reduction of computational complexity of the channel estimation.

Finally, this dissertation describes the correlation of sub-channels embedded in the multiple-input multiple-output antenna systems, and discusses its effect on the channel capacity. Multiple antennas with dissimilar radiation patterns are employed to introduce decorrelation of the sub-channels, thus increasing channel capacity. Specifically, a prototype of compact antenna array at the mobile unit is proposed that exploits antenna pattern diversity.

In summary, this dissertation investigates the modeling and prediction of the time-varying multipath channels of antenna systems, while developing new techniques for mobile broadband communications that are based on the channel characterization. The general feasibility of the algorithms developed in this dissertation is demonstrated through a ray tracing simulator in various scattering environments.

Contents

List of Figures

xiv

Chapter 1

Introduction

1.1 Mobile Cellular Communications

The demand on information exchange has pushed the development of wireless communication systems at an unprecedented pace. As the wireless network matures and more users are added, a desire for high system capacity is inevitable. The radio spectrum for wireless communications is a limited resource, it will be stretched out to its limit to accommodate various current and emerging wireless services. To meet the capacity need of the explosive growth of wireless communications, new techniques are required to improve the quality and spectrum efficiency of communications over radio channels.

Cellular radio systems exploit the power falloff with distance of a transmitted signal to reuse a communication channel at spatially separated locations. The communication channel can be a frequency band, a time slot, or a unique code. The finite spectrum is made available throughout a geographical area by dividing the region into a number of smaller cells. In analog cellular systems, each cell uses a portion of the spectrum. Cells which are sufficiently far apart can reuse the same spectrum resources. A unique feature of code division multiple access (CDMA) sys-

1
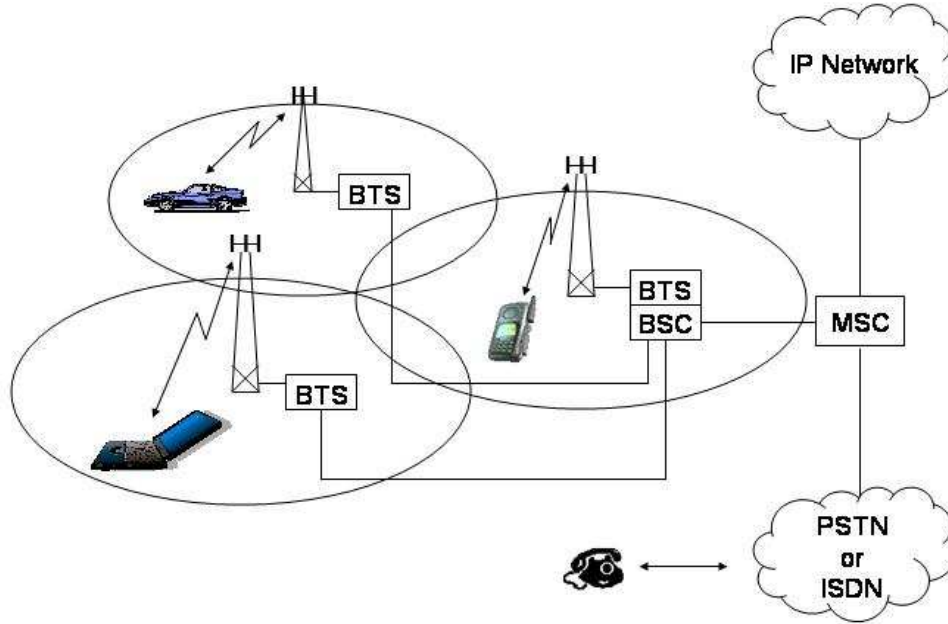
Figure 1.1: Architecture of a cellular network.

tems is that, the spectrum resources are reused from cell to cell. Each cell is served
by a base transceiver station (BTS), which is responsible for handling communica-
tions with mobile users within its respective cell. When a mobile user crosses the
boundary of two cells, its communication channel is handed off to the BTS in the
new cell. A group of BTSs are connected to a base station controller (BSC), which
may be integrated into a cell site. The BSC manages radio resources and network
functions between multiple BTSs. The BSC is connected to the mobile switching
center (MSC), which is responsible for all call handling as well as interfaces to other
switching elements. The MSC exchanges voice traffic with the public switching
telephone network (PSTN) or the integrated service digital network (ISDN), or ex-
changes data traffic with Internet-protocol networks. The top-level architecture of a

cellular network is illustrated in Figure 1.1. The physical limitations of the wireless channel present a fundamental challenge for reliable communications. The research conducted in this dissertation is focused on the wireless point-to-point link within a cell.

To utilize spectrum efficiently within a cell, two transmission techniques need to be investigated: one is the duplex scheme, which provides the two-way conversation between the base station and the mobile user, and the other is the multiple access scheme, which supports the concurrent conversations between the base station and multiple active users [1].

Most of the current mobile cellular systems employ channels that are separated in frequency for the uplink (mobile to base station) and the downlink (base station to mobile). This technique is called frequency division duplex (FDD). Other systems use the same frequency channels for both uplink and downlink, allowing the uplink and the downlink to use the frequency band during different time slots. This technique is called time division duplex (TDD). Recently, there is some development in using a set of smart codes, which have orthogonality among the codes for nonzero time shift, for simultaneous uplink and downlink in the same frequency band. This so called code division duplex (CDD) scheme can also effectively eliminate the interferences from adjacent cells [2]. Typically, the uplink and downlink channels are divided into different types of channels: the access channels (ACH) are used to set up calls and handle various control functions, and the traffic channels (TCH) are used to carry voice and data information.

When a base station communicates with multiple users, frequency division multiple access (FDMA) assigns different radio-frequency (RF) channels to individual mobile users. Each user is allocated a unique frequency band within the cell. Time division multiple access (TDMA) allows a number of users to access a single RF channel without interference by allocating unique time slots to each user. Each

mobile user occupies a set of cyclically repeating time slots. TDMA is a digital transmission technology because the system transmits data in a buffer-and-burst mode, therefore digital data and digital modulation must be used. Code division multiple access (CDMA) is a spread-spectrum technology that allows multiple users to use the same frequency band and to transmit simultaneously. CDMA codes every digital packet it sends with a unique key. A CDMA receiver responds only to the unique key and can pick out and demodulate the associated signal. CDMA's robust data performance leads the way to a plethora of enhanced services, with which the recent wireless industry has been established. Space division multiple access (SDMA), which exploits the use of an antenna array at the base station, controls the radiated energy for each user in space. SDMA serves different mobile users by forming antenna beams according to the physical location of the users. These different areas covered by the antenna beam may be served by the same frequencies (in TDMA or CDMA systems) or different frequencies (in FDMA systems).

1.2   3G Wireless Systems and Mobile Broadband Systems

While the step from the first to the second generation of wireless systems mainly brought the transition from analog to digital, the third generation (3G) systems are driven by the fast rise of the Internet and ever increasing need for high-speed data transmission capabilities while on the move. The requirement for high-speed data transmission, especially packet data transmission, brings a whole new set of challenges for 3G systems. With substantially enhanced capacity, quality, and data rates, 3G wireless technology provides customers with high-speed wireless access to the Internet and multimedia services, anytime and anywhere.

A whole family of standards are grouped together under the IMT-2000[1] label,

---

[1]IMT-2000 (International Mobile Telecommunications-2000) is the International Telecommuni-

such that mobile devices using different standards will be able to move seamlessly between all networks, thus providing global roaming. The 3G standard that has been agreed for Europe and Japan is known as Universal Mobile Telecommunications System (UMTS). UMTS is an upgrade from Global System for Mobile Communication (GSM) via General Packet Radio System (GPRS) or Enhanced Data Rates for GSM Evolution (EDGE). The terrestrial part of UMTS (i.e., non-satellite) is known as UMTS Terrestrial Radio Access (UTRA). The UTRA standard is a wideband CDMA (W-CDMA) technology that includes features that ensure easy integration with existing GSM technology. The FDD component of UTRA is based on the W-CDMA standard (a.k.a. UTRA FDD). It offers very high data rates up to 2 Mbps. The TDD component of UTRA is called TD-CDMA (or UTRA TDD). The main global competitor to UMTS is CDMA2000, the 3G standard developed in the United States by Qualcomm. CDMA2000 will deliver full IMT-2000 capabilities (data rates of up to 2 Mbps) in one-third as much spectrum as in W-CDMA. And CDMA2000 is backward compatible with the cdmaOne technology that has been already used by nearly 70 million subscribers. Other less-publicized standards include the TD-SCDMA, the Chinese national 3G standard. TD-SCDMA is a TDD standard similar to TD-CDMA, and it eliminates the uplink/downlink interference which affects other TDD methods by applying "terminal synchronization" techniques (the "S" in TD-SCDMA stands for "synchronization"). Because of this, TD-SCDMA allows full network coverage over macro-cells, micro-cells, and pico-cells. Hence, TD-SCDMA stands alongside W-CDMA and CDMA2000 as a fully-fledged 3G standard.

Wireless carriers provide the unique benefits of small device form, mobile access and location-based services that wired carriers can not offer. To remain competitive and to satisfy customer expectations, 3G operators must create a wireless network experience in a mobile environment that comes close to what subscribers

---

cation Union (ITU) globally coordinated definition of 3G covering key issues such as frequency spectrum use and technical standards.
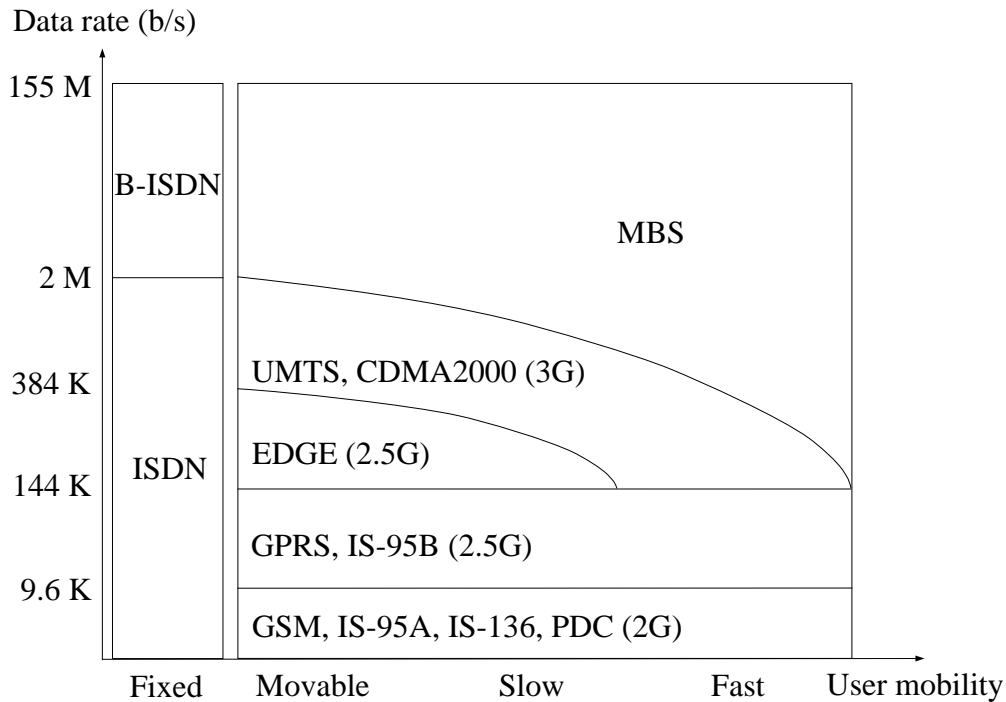
Figure 1.2: Service data rate versus user mobility of various systems.

currently receive over wired networks. Figure 1.2 compares the service data rate of the mobile systems of various standards to that of fixed Integrated Service Digital Network (ISDN) and Broadband-ISDN (B-ISDN). The figure indicates that 2 Mbps is achievable by very slow (movable) terminals of UMTS (or W-CDMA) and CDMA2000, whereas slow and fast mobile terminals can only access communications up to 384 and 144 Kbps, respectively. As for high-data-rate wireless access with a fast mobile, Mobile Broadband Systems (MBS) will play an important role in the wireless communications market in the near future [3]. In terms of terminal mobility and supported data rates, MBS operation begins where UMTS/CDMA2000 ends as shown in Figure 1.2. The achievable data rate of MBS is aimed at 155 Mbps as the upper bandwidth of B-ISDN, however, a decreasing shape (towards high mobility) is also likely to appear at the upper bound of the data rate.

6

This dissertation research has been prompted by the current thrust in wireless communications to look for new technologies to support the mobile broadband systems.

1.3 Antenna Systems for Broadband Wireless Access

Adaptive antenna systems (or smart antenna systems) offer a broad range of ways to improve the performance of wireless communications. The use of antenna arrays helps mitigate three major impairments caused by the wireless channel: fading, delay spread, and co-channel interference. An antenna array at the base station provides enhanced coverage through range extension, and it provides robustness to system perturbations and reduced sensitivity to non-ideal behavior. With antenna array, the base station can suppress the interference due to co-channel users (either from adjacent cell or same cell), and enhance the desired signal level by mitigating the impact of multipath or even exploiting the diversity inherent in multipath. Antenna array can be used to allow the mobile user and base station to operate at the same range as a conventional system, but at lower power. Antenna array can also be used to spatially separate signals, which is known as the *space division multiple access* (SDMA) technique. SDMA allows multiple users to operate in the same cell, on the same time/frequency slot provided. These two advantages of the adaptive antennas lead to improved system capacity. In this dissertation, if adaptive antennas are equipped at the base station but not at the user terminal, the wireless link is termed the *vector channel*; if adaptive antennas are equipped at both ends, the wireless link is termed the *matrix channel*.

The technologies of broadband wireless access must be able to cope with the hostile wireless environment, especially in the fast mobile scenarios. Antenna systems in the form of adaptive antenna array can provide an effective and promising solution while achieving reliable and robust high-mobility high-date-rate transmis-

sion [4]. The earliest form of antenna system for improving the performance of wireless communication systems is antenna diversity. It helps mitigate the effects of fading. Antenna diversity has been in commercial use at the base station of most wireless communications for many years. Over the last two decades, smart antenna systems, which attempt to actively mitigate co-channel interference, have also been developed [5]. The broadband channel and the fast Rayleigh fading experienced by the high-data-rate high-mobility wireless systems bring new challenges to the adaptive antenna systems. In this dissertation, we propose a series of new techniques of the adaptive antenna systems for the mobile broadband communications, which range from vector channel estimation/prediction to array processing, such as power control and beamforming.

Recently, there have been some important developments of the adaptive antenna systems, which include the idea of space-time receivers [6], space-time coding [7, 8, 9], and multiple-input multiple-output (MIMO) antenna systems [10, 11, 12]. MIMO antenna systems, which use multiple transmit and multiple receive antennas, are exploring the full potential of antenna systems for broadband wireless communications [13]. They can improve link reliability through diversity advantage and can increase potential data rate through multiplexing gain. MIMO systems for the mobile broadband communications is an ongoing topic of this dissertation research.

1.4 Dissertation Overview

In this introductory chapter, the recent development of mobile communication systems is presented. Mobile broadband systems, i.e. high-mobility wireless systems with performance comparable to the broadband wired networks, will be in huge market demand in the near future. Adaptive antenna system is one of the key technologies for increasing reliability and data rate of wireless communications. These

two facts have motivated this dissertation research.

Chapter 2 describes the wireless fading channel. It presents the radio propagation mechanism and introduces an uncorrelated scattering model. The frequency-selective fading of wideband signals is discussed. This chapter develops the wideband channel modeling, and proposes a prediction approach for the channel transfer function over the wideband.

Chapter 3 introduces the vector channel model of an antenna system. A dynamic uplink power control scheme is given to combat Rayleigh fading of the signals transmitted by a fast mobile. The power control relies on the channel prediction that exploits the fading correlation between the access channel and the traffic channel of an antenna system.

Chapter 4 proposes two novel downlink beamforming approaches for transmission over fast Rayleigh fading channels. The first approach is based on the prediction of the downlink channel, and the second one is based on the analysis of the uplink channel subspace.

Chapter 5 presents a blind estimation algorithm for the vector channels of wideband CDMA systems. The algorithm is computationally efficient because it takes into account the wideband channel constraints and reduces the number of unknown model parameters.

Although the main focus of this dissertation is on the wireless communications over vector channels, i.e. adaptive antenna array at one end of the communication link, MIMO systems (matrix channels) are also explored as the prolog of future research. Chapter 6 presents the ongoing research on the MIMO systems that exploit antenna pattern diversity. A ray-tracing simulator, FASANT, is used to study the channel capacity of MIMO systems, and its dependence on the characteristics of the scattering environment. Later, a prototype of MIMO handheld terminal is proposed, which has a compact antenna array that exploits antenna

pattern diversity.

Chapter 7 summarizes the dissertation and discusses future areas of research.

Several of the main ideas in this dissertation have been published or submitted for publication. The work on wideband channel prediction is published in [14]. The dynamic uplink power control based on channel prediction is published in [15]. The ideas of downlink beamforming for fast Rayleigh fading signals are presented in [16, 17]. The low-complexity channel estimation of wideband CDMA is published in [18]. The capacity study of MIMO systems that exploit antenna pattern diversity is presented in [19], and the design of compact antenna array at the handheld terminal is presented in [20].

Chapter 2

Modeling and Prediction of Mobile Radio Channels

2.1 Introduction

The mobile radio propagation environment places fundamental limitations on the performance of wireless communication systems. Signals arrive at a receiver via a scattering mechanism and the existence of multipath with different time delays, attenuations and phases give rise to a highly complex, time-varying, transmission channel. In order to mitigate the impairment caused by multipath propagation, it is essential to characterize the transmission channel. Under fast fading conditions, channel characteristics may change drastically over short period of time. Therefore, the dynamic behavior of the channel needs to be tracked for optimization of the adaptive functions of modems, such as automatic gain control (AGC), equalization, and timing recovery.

The radio channel in a wireless communication system is often characterized by multipath propagation. A fading signal results from interference between multipath components at the receiver. For transceivers moving at high speed, the channel

varies dramatically and undergoes deep fades within a typical time frame of several milliseconds. Future mobile systems will use higher carrier frequencies, with associated higher fading rates. Since the channel changes rapidly, usually the transceivers are not optimized for current channel conditions and thus fail to exploit the full potential of the wireless channels. To improve the system performance, adaptive transmission techniques are applied to combat the fast fading channel effect. To realize the potential of adaptive transmission methods, fading channel variations have to be reliably predicted at least several milliseconds ahead [21].

Recently, researchers have speculated that the fading process is in fact a deterministic sinusoidal process with time-varying parameters, and can be characterized using a discrete scatter propagation model [22]. Spectral estimation followed by linear prediction and interpolation is applied in [23] and [21] to predict the evolution of the channel. This algorithm characterizes the fading channel using an autoregressive (AR) model. Subspace-based methods are also used to predict the channel. A modified root-MUSIC algorithm is used in [24], and an ESPRIT algorithm is used in [25] to estimate the dominant sinusoids that make up the fading channel. Then these sinusoids are extrapolated to predict future channel samples. These algorithms predict the fading channels encountered in narrowband mobile communication systems. In [26], the statistical dependencies in sequences of wideband mobile radio channel data are measured, and a nonlinear model is used for the fading channel prediction.

In this chapter, we study the multipath fading effect of wireless channels, and later propose an ESPRIT-type [27] algorithm to predict the frequency-selective channel in wideband systems. The time-varying channel transfer function at different frequencies within the wideband are modeled and predicted jointly, assuming that the scatterers remain constant. Simulation results show that the joint-frequency prediction scheme has superior performance over conducting the channel prediction
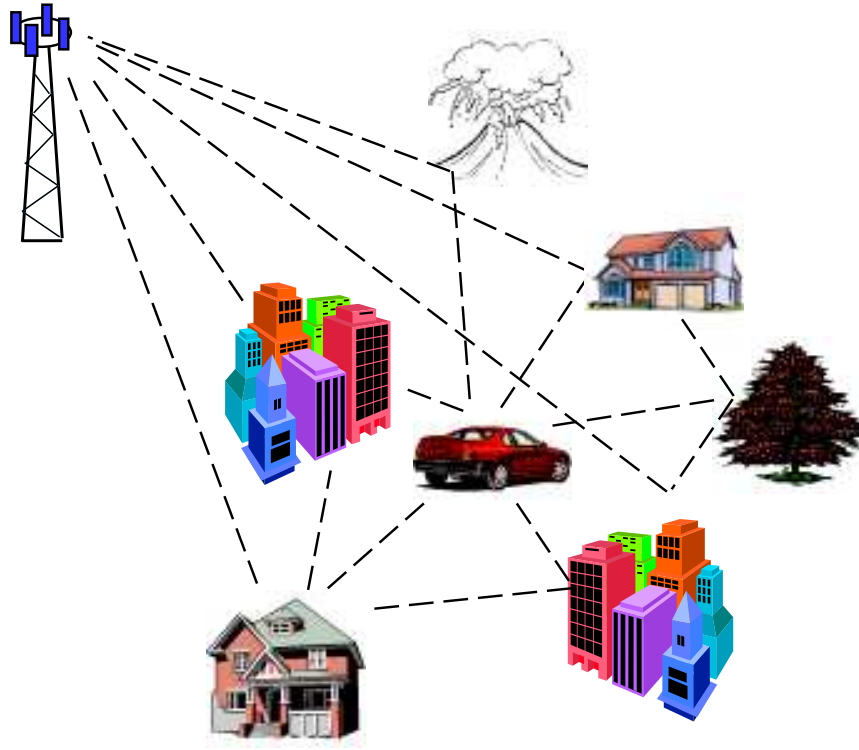
Figure 2.1: A typical mobile radio propagation environment.

on a single frequency.

2.2   Radio Propagation

Due to multipath propagation, the composite received signal is the sum of the signals arriving along different paths. As shown in Figure 2.1, except for the line-of-sight (LOS) path, all paths are going through at least one order of reflection or diffraction before arriving at the receiver. The average received signal power decreases as the distance from transmitter increases. In addition, phase alignment or cancellation of arriving paths results in considerable amplitude fluctuation of the composite received signal from one location to another. The time dispersion and random amplitude and

phase fluctuations in the received signal, a set of characteristics of channel effect, is termed *multipath fading*. The multipath channel impulse response is represented by

$$h(\tau;t) = \sum_{i=1}^{L} \beta_i(t)\delta(\tau - \tau_i(t)) \tag{2.1}$$

where L is the number of paths, β_i and τ_i represent the complex gain and the delay of the ith arriving path.

Delay Spread   The span of the time dispersion of arriving paths is referred to as *multipath delay spread* of the channel. Taken into account the signal intensity over the delay span, a good measure is the *root mean square (rms) delay spread*, given by

$$\tau_{rms} = \sqrt{\bar{\tau^2} - (\bar{\tau})^2} \tag{2.2}$$

where,

$$\bar{\tau^n} = \frac{\sum \tau_i^n |\beta_i|^2}{\sum |\beta_i|^2}, \quad n = 1, 2$$

The inverse of the rms delay spread is referred to as the *coherence bandwidth* of the channel. Wideband signal has high data rate in comparison to the coherence bandwidth.

Doppler Spread   With the relative motion of the transmitter and the receiver, or the change of the transmission media, e.g. movement of reflectors, the received signal experiences Doppler frequency shift. The spreading within the maximum frequency shift is referred to as the *Doppler spread*. Figure 2.2 shows the typical Doppler spectrum of the Clarke model [28]. For values of f close to $\pm f_m$ the height of the Doppler component rises to two high peaks at the edges of the spectrum. In the presence of a strong LOS component, the spectrum has an additional impulse representing the shift associated with the strong component. The mathematical definition of Doppler spectrum will be given in the next section.

14
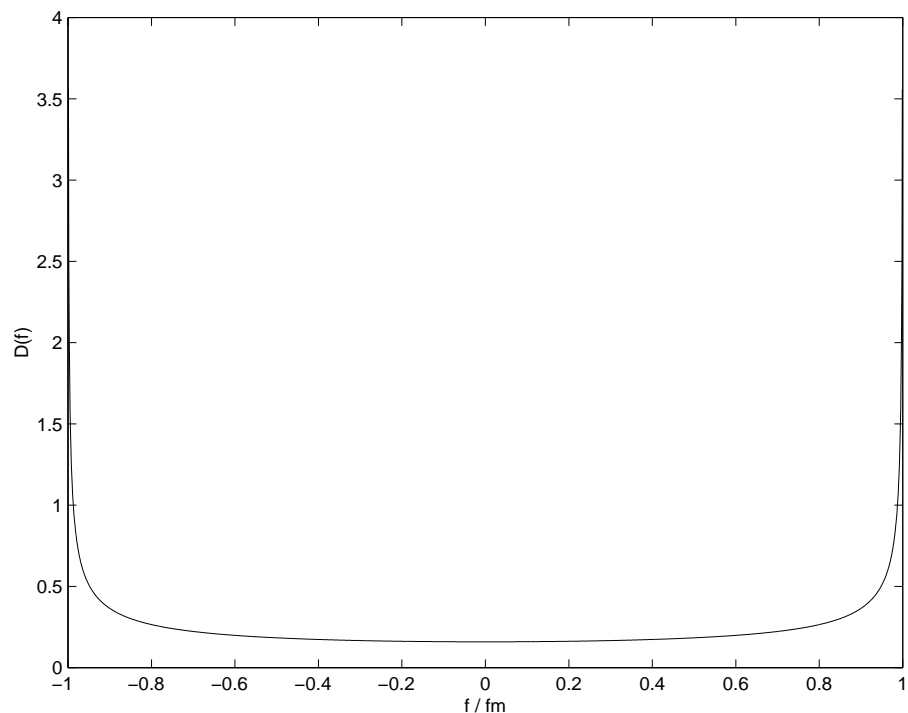
Figure 2.2: Doppler spectrum of mobile radio channel.

The adaptation time of algorithms used in the receiver must be faster than the Doppler spread of the channel in order to accurately track the fluctuations in the received signal. Ideally, a simulation should provide "snapshots" of the channel response, in either time or frequency domain, at a rate twice the maximum Doppler shift of the channel.

Received Signal Envelope   The received signal power is proportional to the distance between transmitter and receiver d, raised to a certain exponent which is referred to as the *distance-power gradient* α. Also, we expect different path losses in different directions due to the randomness of surrounding environment. This is usually referred to as *shadow fading* or *large-scale fading*. Results of measurements on indoor and urban radio channels show that a lognormal distribution best fits the

15
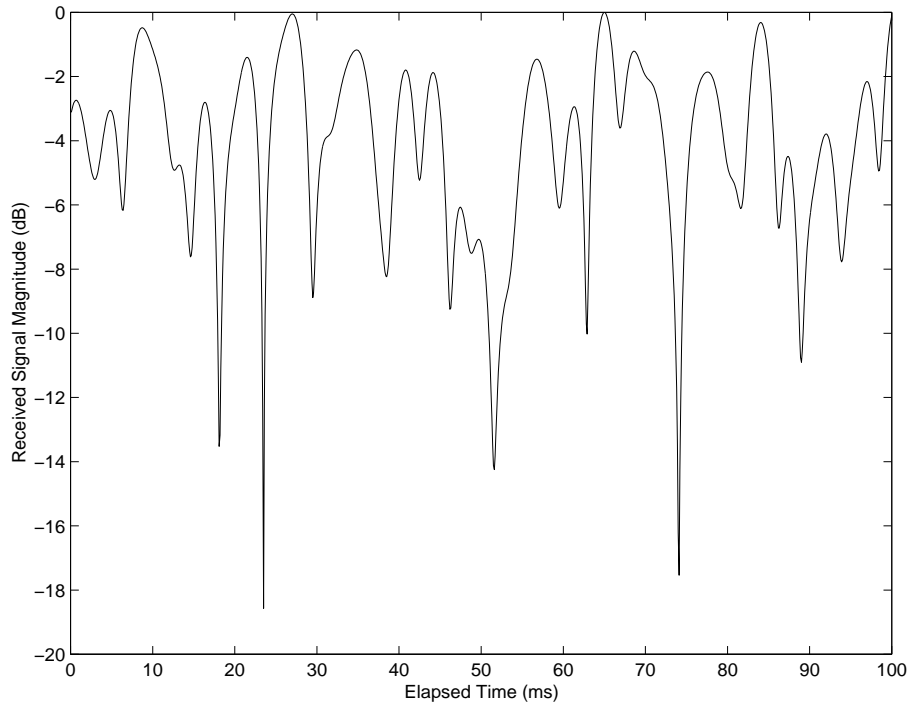
Figure 2.3: Magnitude of received signal: Carrier 2 GHz, Mobile speed 100 km/h.

large-scale variations of the signal amplitude. Therefore, the total path loss L_p in decibels is given by

$$L_p = L_0 + 10\alpha \log_{10} d + l \tag{2.3}$$

where, L_0 is defined as the path loss in decibels at an initial distance (e.g. 1 m), l is a lognormal-distributed random variable representing the shadow fading.

With multipath fading in areas with dimensions on the order of a wavelength of the carrier frequency, the statistical fluctuation of the amplitude of the received power is the superposition of fast local multipath fading over slow shadow fading. The slow shadow fading component causes changes in the mean value of the received power as the terminal moves from one area to another. The fast fading component changes rapidly as the transmitter or the receiver moves slightly or other objects are moved in the vicinity of the transmitter or the receiver. In this dissertation,

16

we focus on the problems caused by multipath fading, assuming the large-scale pass loss remains stationary.

Invoking the central limit theorem, the received signal amplitude experiencing multipath fading obeys a *Rayleigh* distribution in the absence of LOS (Figure 2.3). With the existence of LOS adding a nonzero mean, the received amplitude is assumed to be *Rician*. The same argument leads to the conclusion that the phase is uniformly distributed in the interval $[0, 2\pi)$.

2.3   The Uncorrelated Scattering Model

Bello [29] suggested the *wide-sense stationary uncorrelated scattering* (WSSUS) model, assuming that the signal variations on paths arriving at different delays are uncorrelated and the correlation properties of the channel are stationary. The autocorrelation of the observed impulse response at two different delays and two different times is given by

$$R_{hh}(\tau_1, \tau_2; t_1, t_2) = E\{h(\tau_1; t_1)h^*(\tau_2; t_2)\} = R_{hh}(\tau_1; \Delta t)\delta(\tau_1 - \tau_2) \qquad (2.4)$$

Given the assumption of uncorrelated scattering, the only nonzero value of the correlation is observed when the delays are the same; given stationary, the correlation values depend only on the time difference. For $\Delta t = 0$, this function is represented by $Q(\tau)$ and is referred to as the *delay power spectrum* of the channel:

$$Q(\tau) = R_{hh}(\tau; 0) \qquad (2.5)$$

Thus, the rms delay spread can be expressed as

$$\tau_{rms} = \sqrt{\frac{\int_{-\infty}^{\infty}(\tau - \bar{\tau})^2 R_{hh}(\tau)d\tau}{\int_{-\infty}^{\infty} R_{hh}(\tau)d\tau}} \qquad (2.6)$$

where

$$\bar{\tau} = \int_{-\infty}^{\infty} \tau R_{hh}(\tau)d\tau$$

If it is assumed that the channel does not change with time, the rms delay spread is the same as given by (2.2).

With wideband signaling, the frequency response over the signal band exhibits amplitude variations from one frequency to another. The multipath channel causes constructive interference and signal enhancement at certain frequencies but destructive interference and deep fades at other frequencies. This is referred to as *frequency selective multipath fading*. In order to characterize these variations statistically, the correlation in the frequency domain is exploited,

$$
\begin{aligned}
R_{Hh}(f_1, f_2; \Delta t) &= E\{H(f_1; t)H^*(f_2; t + \Delta t)\} \\
&= \int_{-\infty}^{\infty}\int_{-\infty}^{\infty} E\{h(\tau_1; t)h^*(\tau_2; t + \Delta t)\}e^{j2\pi(f_2\tau_2 - f_1\tau_1)}d\tau_1 d\tau_2 \\
&= \int_{-\infty}^{\infty} R_{hh}(\tau_1; \Delta t)e^{j2\pi\Delta f\tau_1}d\tau_1 \quad\quad (2.7)
\end{aligned}
$$

where $\Delta f = f_2 - f_1$. With WSSUS assumption, the channel response $h(\tau; t)$ is a wide sense stationary zero-mean Gaussian process in t. Therefore the frequency response $H(f; t)$, being obtained as a linear operation on $h(\tau; t)$, is also a wide sense stationary zero-mean Gaussian process in t. Hence,

$$
R_{Hh}(f_1, f_2; \Delta t) = R_{Hh}(\Delta f; \Delta t) \quad\quad (2.8)
$$

For a slowly time-varying channel,

$$
R_{Hh}(\Delta f; \Delta t) \simeq R_{Hh}(\Delta f; 0) \qu\quad (2.9)
$$

which is the Fourier transform of the delay power spectrum.

For general time-varying channel, the Fourier transform of R_{Hh} on the time variable yields

$$
R_{HH}(\Delta f; \lambda) = \int_{-\infty}^{\infty} R_{Hh}(\Delta f; \Delta t)e^{-j2\pi\lambda\Delta t}d(\Delta t) \qu\quad (2.10)
$$

for $\Delta f = 0$ if gives

$$
D(\lambda) = R_{HH}(0; \lambda) \qu\quad (2.11)
$$

18
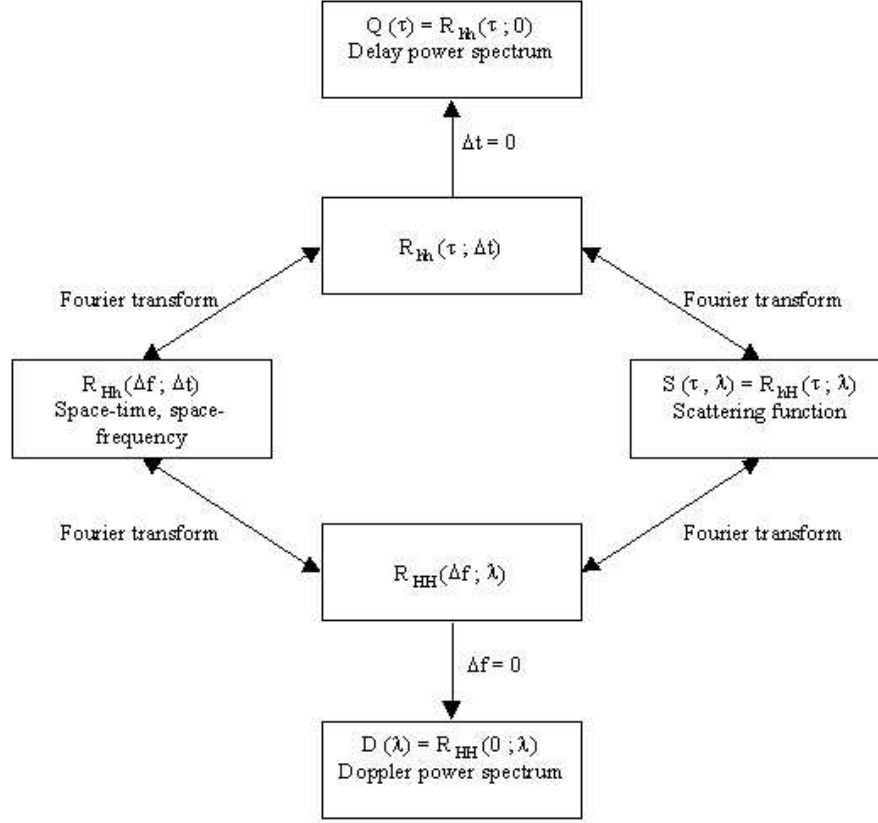
Figure 2.4: Correlation functions in WSSUS model.

the *Doppler power spectrum* of the channel, which represents the strength of the Doppler shift at different frequencies. The width of the Doppler power spectrum is referred to as the Doppler spread of the channel and provides a measure of the fading rate of the channel. The reciprocal of the Doppler spread is called the *coherence time* of the channel, which is a measure of the time interval over which a transmitted symbol will be relatively undisturbed by channel fluctuation.

The Fourier transform of $R_{hh}(\tau; \Delta t)$ over Δt is called the *scattering function*:

$$S(\tau, \lambda) = R_{hH}(\tau; \lambda) \tag{2.12}$$

which represents the rate of variations of the channel at different delays. In practice

it is usually assumed that the time and frequency components of the scattering function are independent. Therefore, scattering function can be decomposed into the delay and Doppler power spectra,

$$S(\tau, \lambda) = Q(\tau) \times D(\lambda) \tag{2.13}$$

Figure 2.4 summarizes the correlation functions of WSSUS model.

2.4 Wideband Signal and Frequency Selective Fading

As the signal bandwidth increases in the case of W-CDMA, i.e. the symbol duration gets shorter, the delay spread becomes relatively large such that it is comparable to the symbol duration:

$$\tau_i \sim T_s = \mathcal{B}^{-1} \tag{2.14}$$

As the multipath channel impulse response expressed in (2.1), with $\beta_i = \alpha_i e^{j\phi_i}$ for time-invariant channel, the channel transfer function is given by

$$H(f) = \sum_{i=1}^{L} \alpha_i \exp(j\phi_i - j2\pi f \tau_i) \tag{2.15}$$

For example, assuming there are 2 paths between the transmitter and the receiver and assuming that $\tau_1 = 0$, $\tau_2 = 0.1$, $\phi_1 = \phi_2 = 0$, $\alpha_1 = \alpha_2 = 1$ and $\mathcal{B} = 20$ Hz, the magnitude of the transfer function is showed in Figure 2.5. Clearly, in this wideband scenario with two equal strength paths, where $(\tau_2 = 0.1) \sim (T_s = 0.05)$, spectral components are distorted in the signal bandwidth.

2.5 Wideband Channel Modeling

The baseband equivalent channel between the base station (BS) and the mobile is modeled using the time-varying impulse response

$$h(\tau; t) = \sum_{k=1}^{L} \beta_k(t) \delta(\tau - \tau_k) \tag{2.16}$$
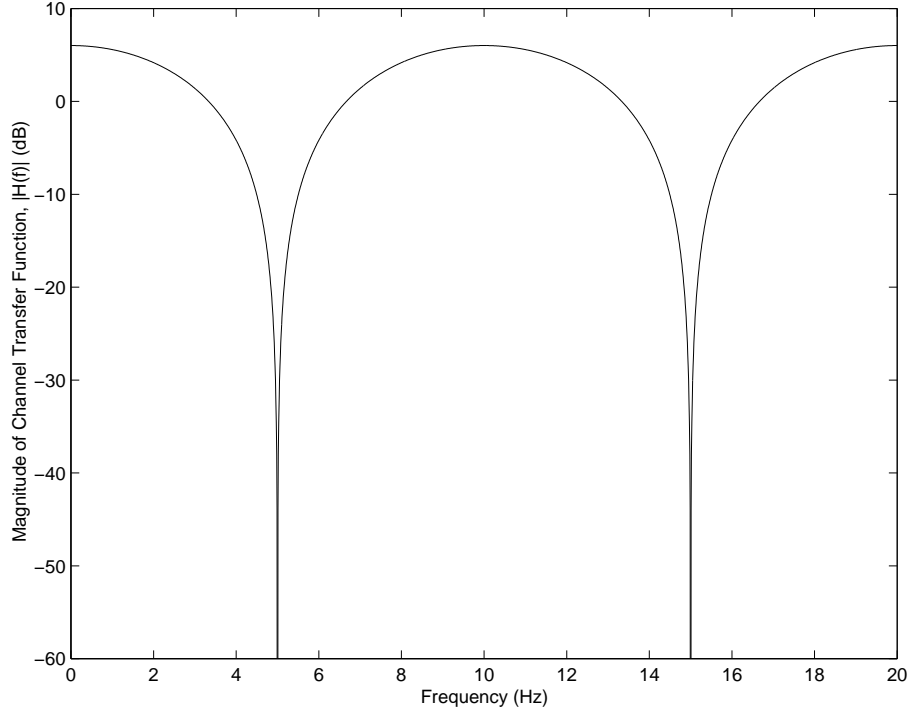
Figure 2.5: Magnitude of the channel transfer function: two equal strength paths.

where L is the total number of multipaths from discrete scatterers. The variable t indicates the time-varying property, and τ is the delay variable. β_k and τ_k are the complex amplitude and path delay of the kth multipath component, respectively.

Due to the motion of the mobile or the scatterers, the BS received signals experience Doppler frequency spread. The increased mobility results in fast fading in which the channel exhibits rapid temporal variations, such that the performance of the cellular radio system is substantially degraded. Fast-fading channels encountered in practice exhibit Doppler spreads on the order of 100-200 Hz. At higher and higher carrier frequencies of new generation wireless systems, the radio channel will vary dramatically within a typical data frame of several milliseconds. The complex amplitude $\beta_k(t)$ can be expressed as

$$\beta_k(t) = \alpha_k e^{j(2\pi f_k t + \phi_k)} \qquad (2.17)$$

21

where α_k, f_k, ϕ_k are the path loss, Doppler frequency shift and phase offset of the kth multipath component, respectively. The Doppler frequency is given by $f_k = f_c \frac{v}{c} \cos(\theta_k)$, where f_c is the carrier frequency, v is the speed of the mobile, c is the speed of light, and θ_k is the angle between the kth mobile incident ray and the mobile moving direction. The fading channel varies rapidly with increases in mobile speed. We assume a far-field condition, where the path loss and the phase offset remain constant during the short time of the channel analysis and prediction range. At carrier frequencies as high as several giga-hertz, typical motion of the mobile may be linearized over distances of several wavelengths.

For the frequency-selective fading channels in wideband systems, the knowledge of the channel transfer function over the entire frequency band is required. The channel transfer function which is the Fourier transform of the channel impulse response on the argument τ is

$$H(f;t) = \sum_{k=1}^{L} \beta_k(t) e^{-j2\pi f \tau_k} \tag{2.18}$$

In wideband channels, the difference between path delays $\{\tau_k\}$ can not be neglected. Therefore, a wideband channel undergoes frequency-selective multipath fading. The transfer function at one particular frequency f_m is given by

$$
\begin{aligned}
H(f_m;t) &= \sum_{k=1}^{L} \alpha_k e^{j(2\pi f_k t + \phi_k)} e^{-j2\pi f_m \tau_k} \\
&= \sum_{k=1}^{L} \alpha_k(f_m)\, e^{j2\pi f_k t} = \sum_{k=1}^{L} \alpha_{mk} z_k^t \tag{2.19}
\end{aligned}
$$

where $e^{-j2\pi f_m \tau_k}$ and ϕ_k are absorbed into the complex gain α_{mk}, and $z_k = e^{j2\pi f_k}$. $\{z_k^T, k = 1, \ldots, L\}$ are the so-called channel poles, where $1/T$ is the sampling rate. Although it requires a large L for $H(f_m;t)$ to experience Rayleigh fading, when deterministic Jakes model is used, the theoretical Doppler spectrum of the Rayleigh fading channel can be accurately approximated by a summation of a relatively small

22

number of dominant (in terms of energy) sinusoids [30]. The parameters α_{mk} and f_k of these significant multipath components are assumed constant in the model, and they are estimated in order to predict the composite fading channel in future time. The Doppler frequency shift f_k is independent of f_m. Therefore, the Rayleigh time-variations of the channel transfer function at different frequencies are highly correlated, as they have the same channel poles. This fact enables us to collect the channel samples at different frequencies and estimate the channel poles jointly.

2.6   Wideband Channel Prediction

The channel estimation/prediction problem is now reduced to a classical frequency estimation problem, with an unknown number of Doppler frequencies closely spaced around zero. Subspace-based methods are characterized by their ability to resolve closely spaced sinusoids on the basis of short sample sequences. In this paper, we consider an ESPRIT-type method to estimate the channel poles associated with D dominant sinusoids. When estimating channel parameters with the ESPRIT algorithm, the number of channel poles that can be resolved is limited by the number of channel samples in the analysis segment and the number of frequency points we choose from the entire wideband. However, near-optimum performance can be achieved if D is chosen large enough [25].

Estimation of Channel Poles   From (2.19), the discrete-time channel transfer function at frequency f_m can be expressed as

$$\mathbf{H}_m = \mathbf{Z}\,\alpha_m + \eta_m \tag{2.20}$$

23

where

$$\mathbf{H}_m = \begin{bmatrix} H(f_m;0) \\ H(f_m;T) \\ \vdots \\ H(f_m;(N-1)T) \end{bmatrix} \tag{2.21}$$

$$\mathbf{Z} = \begin{bmatrix} 1 & 1 & \cdots & 1 \\ z_1^T & z_2^T & \cdots & z_D^T \\ \vdots & \vdots & & \vdots \\ z_1^{(N-1)T} & z_2^{(N-1)T} & \cdots & z_D^{(N-1)T} \end{bmatrix} \tag{2.22}$$

$$\alpha_m = [\alpha_{m1} \; \alpha_{m2} \; \cdots \; \alpha_{mD}]' \tag{2.23}$$

η_m is the noise contribution, and superscript $'$ denotes the vector transpose operator. The observation interval is $[0,(N-1)T]$. Hereafter, we assume $T = 1$ in the analysis. Defining $\mathbf{Z}^{\downarrow}$ ($\mathbf{Z}^{\uparrow}$) as the matrix $\mathbf{Z}$ with the top (bottom) row deleted, we can write

$$\mathbf{Z}^{\uparrow}\Upsilon = \mathbf{Z}^{\downarrow} \tag{2.24}$$

where

$$\Upsilon = \mathrm{diag}\{z_1, z_2, \ldots, z_D\} \tag{2.25}$$

Collecting the channel transfer function samples in the observation interval at M frequency points within the wideband, we form the data matrix $\mathbf{H}$ as

$$\mathbf{H} = [\mathcal{H}_0 \; \mathcal{H}_1 \; \cdots \; \mathcal{H}_{M-1}] \tag{2.26}$$

$\mathcal{H}_m$ is an $L \times K$ Hankel matrix associated with the channel transfer function at frequency f_m

$$\mathcal{H}_m = \begin{bmatrix} H_m(0) & H_m(1) & \cdots & H_m(K-1) \\ H_m(1) & H_m(2) & \cdots & H_m(K) \\ \vdots & \vdots & & \vdots \\ H_m(L-1) & H_m(L) & \cdots & H_m(N-1) \end{bmatrix} \tag{2.27}$$

where $K + L = N + 1$. We need $L \geq KM$ to ensure that $\mathbf{H}$ is of full column rank. Thus, K is chosen as

$$K = \lfloor \frac{N+1}{M+1} \rfloor \tag{2.28}$$

A subspace decomposition can be performed on $\mathbf{H}$ by singular value decomposition (SVD) as

$$\mathbf{H} = [\mathbf{U}_s \ \mathbf{U}_n] \begin{bmatrix} \Sigma_s & \mathbf{0} \\ \mathbf{0} & \Sigma_n \end{bmatrix} \begin{bmatrix} \mathbf{V}_s^H \\ \mathbf{V}_n^H \end{bmatrix} \tag{2.29}$$

where $\mathbf{U}_s \in \mathcal{C}^{L \times D}, \Sigma_s \in \mathcal{R}^{D \times D}, \mathbf{V}_s \in \mathcal{C}^{KM \times D}$, and superscript H denotes Hermitian transpose operator. The orthonormal columns in $\mathbf{U}_s$ associated with the D largest eigenvalues corresponding to the dominant sinusoids span the D-dimensional signal subspace. Therefore, in the following expression

$$\mathbf{U}_s^{\uparrow} \Phi = \mathbf{U}_s^{\downarrow} \tag{2.30}$$

matrix Φ is similar to matrix Υ. So Φ and Υ have the same eigenvalues, which are the channel poles. The least squares estimate of Φ is given by

$$\hat{\Phi} = (\mathbf{U}_s^{\uparrow H} \mathbf{U}_s^{\uparrow})^{-1} \mathbf{U}_s^{\uparrow H} \mathbf{U}_s^{\downarrow} \tag{2.31}$$

The channel poles are projected onto the unit circle in accordance with the far-field channel model.

Estimation of Complex Path Gains   Based on the estimates of the channel poles $\{z_k\}$, the complex path gains α_m at each frequency can be determined by solving a set of linear equations as in (2.20). The least squares solution is given by

$$\hat{\alpha}_m = (\mathbf{Z}^H \mathbf{Z})^{-1} \mathbf{Z}^H \mathbf{H}_m \tag{2.32}$$

Channel Prediction   Once the channel poles and complex path gains are estimated, we can predict the channel transfer function $H(f_m; t)$ at future time from

25
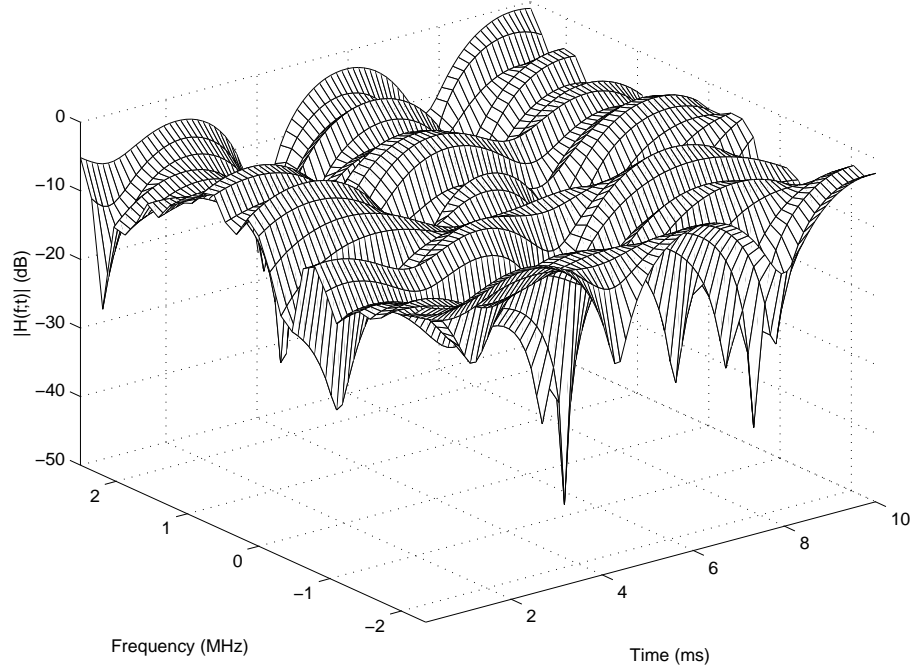
Figure 2.6: Channel transfer function.

(2.19) for $t = NT, (N + 1)T, \ldots$. The prediction error $e_m(k)$ $(k = N, N + 1, \ldots)$ is defined as the amplitude of the differences between predicted and actual channel samples

$$e_m(k) = |\hat{H}(f_m; kT) - H(f_m; kT)| \tag{2.33}$$

The performance of channel prediction is evaluated by the ratio of $e_m(k)$ to the root-mean-square (RMS) value of the envelope of the channel transfer function at frequency f_m. As a measure of prediction quality, we use the *prediction distance* defined in [22], for which the predicted and actual channels start to depart as this ratio becomes more than 20%. The prediction distance is converted to units of carrier wavelength λ in the simulation so that it is independent of the mobile speed.

26
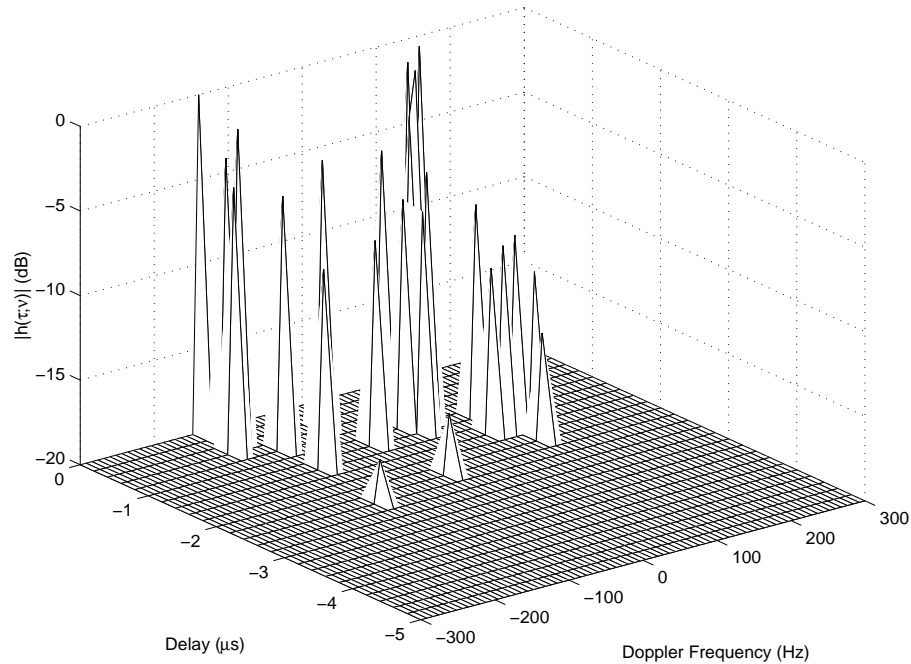
Figure 2.7: Channel impulse response.

2.7 Simulations

A wideband wireless system is simulated, in which the BS communicates with a mobile moving at a speed of 80 km/h. The carrier frequency is $f_c = 2$ GHz. Assume that the scatterers are uniformly distributed around the mobile. There are L significant multipath signals arriving at the BS, with the weakest having an amplitude no less than 20 dB lower than the amplitude of the most powerful one. The shortest multipath being as the reference, the propagation delay lengths and the phase offsets of the others are uniformly distributed on [0 m, 1000 m] and $[0, 2\pi)$, respectively.

Figure 2.7 illustrates the channel impulse response $h(\tau; \nu)$ in the domains of

27
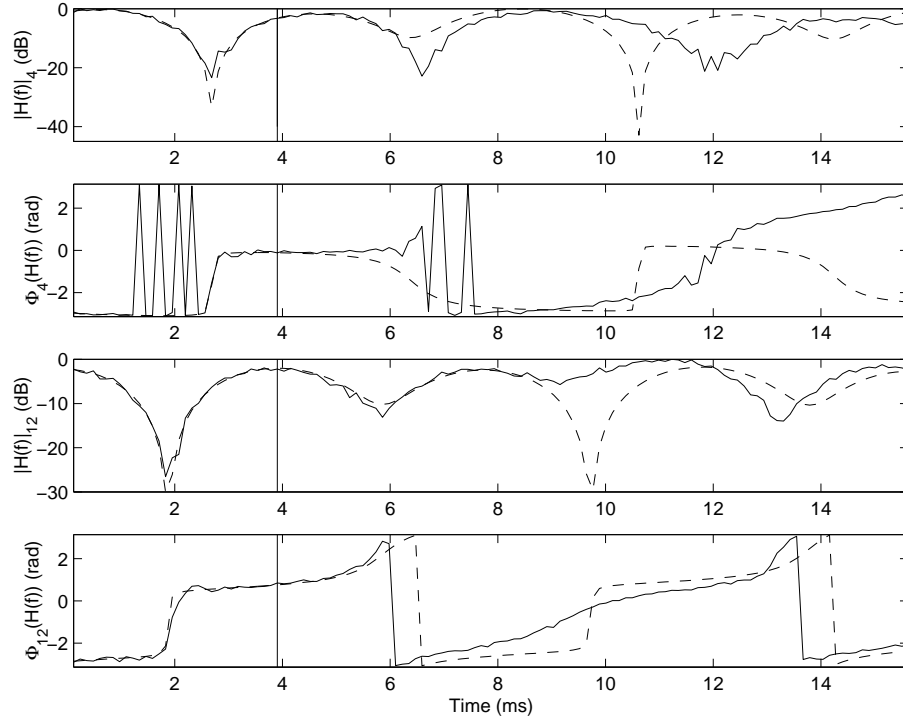
Figure 2.8: Channel prediction example. (— : actual channel, $\cdots$: predicted channel.)

delay and Doppler frequency as

$$h(\tau;\nu) = \sum_{k=1}^{L} \alpha_k \delta(\nu + f_k)\delta(\tau - \tau_k) \tag{2.34}$$

The figure shows $L = 25$ significant multipath components with no more than 20 dB variation. The maximum Doppler frequency shift is limited by the mobile speed. Performing the 2-dimensional FFT on $h(\tau;\nu)$ results in the time-varying channel transfer function $H(f;t)$. Figure 2.6 illustrates the baseband channel transfer function spanning a bandwidth of 5 MHz. The channel experiences fast fading and there are deep fades within a time frame of 10 ms.

The channel transfer function is sampled at $M = 32$ evenly spaced frequency points within the 5 MHz band. An example of channel prediction is demonstrated in

28
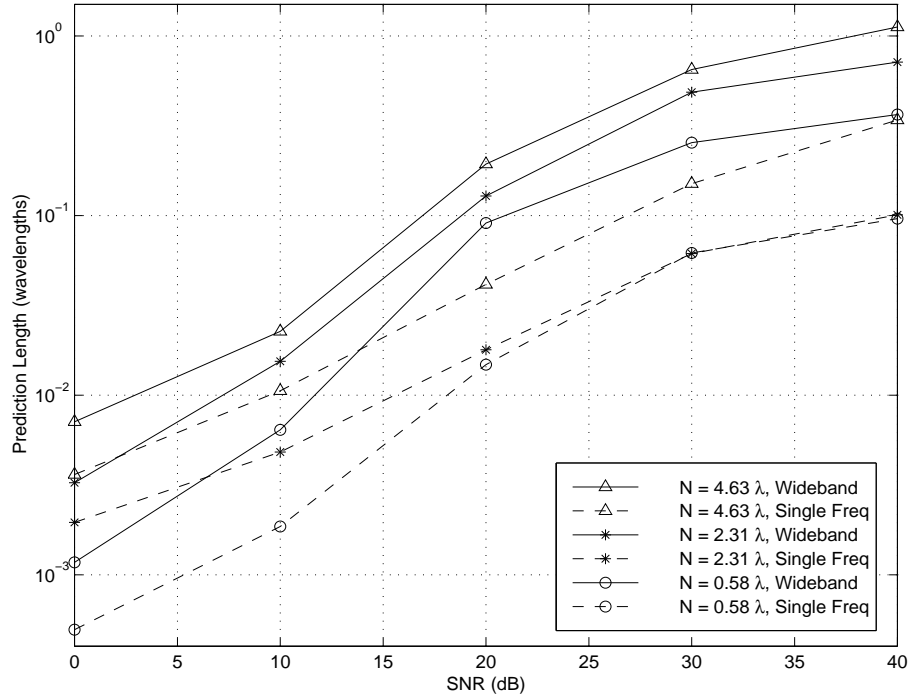
Figure 2.9: Channel prediction performance, $L = 10$.

Figure 2.8, which shows the amplitudes and phases of the channel transfer functions at the fourth and twelfth frequency points. The region to the left of the vertical line is the observation interval as the analysis segment, and the region to the right is the prediction segment. The observation interval is [0, 3.9 ms], which is $[0, 0.58\lambda]$ in wavelength units. At each frequency, 32 channel samples in the observation interval are used. Note that the sampling rate is higher than the Nyquist rate, which is twice the maximum Doppler frequency. It does not benefit by sampling the channel as densely as the data rate, because the channel variation is characterized by the Doppler frequencies. The Doppler frequencies $\{f_k\}$ are limited to a few hundred hertz, and T takes up only a few milliseconds, therefore the channel poles $\{z_k^T = e^{j2\pi f_k T}\}$ condense near 1 in the complex plan.

There are $L = 100$ significant multipath components with 20 dB variation
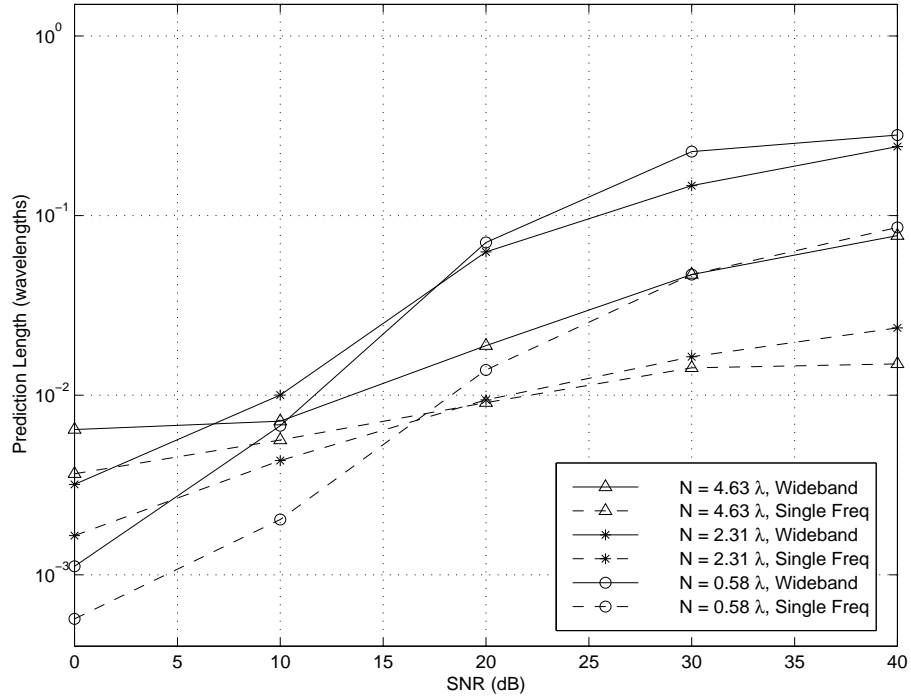
Figure 2.10: Channel prediction performance, $L = 100$.

range. The channel output SNR is fixed at 20 dB. We choose $D = 12$. Channel poles with amplitude larger than 1.1 or smaller than 0.9 are discarded, since they are usually not related to the Doppler frequencies of the channel. And the remaining poles are projected onto the unit circle.

Figure 2.9 and Figure 2.10 make the performance comparison between the joint-frequency channel prediction and the prediction conducted at each frequency individually, with the channel output SNR varying from 0 to 40 dB. The observation intervals are chosen as $[0, 0.58\lambda]$, $[0, 2.31\lambda]$ and $[0, 4.63\lambda]$, and a fixed number of 32 samples are taken from each interval. There are $L = 10$ significant multipath components simulated in Figure 2.9, and $L = 100$ in Figure 2.10. The number of Monte Carlo trials is 200. Because the joint-frequency wideband channel prediction uses more data in the observation interval to estimate the channel poles, it provides

better prediction performance.

2.8 Conclusions

Prediction of the frequency-selective fading channel in the wideband systems has been investigated in a fast fading environment. The simulations use a static model with far-field scatterers and constant mobile velocity. Applying the subspace method jointly at different frequencies within the wideband offers reliable prediction of the channel transfer function. The proposed prediction algorithm outperforms the channel prediction over a single frequency with an observation interval of the same length.

Chapter 3

Vector Channel Modeling and Dynamic Power Control

3.1 Introduction

In cellular wireless CDMA communication systems, mobile users adapt to time varying radio channels by regulating transmitted powers. The power control on the uplink attempts to adjust the transmitted power of each mobile such that the base station (BS) receives signals from each mobile with equal and constant nominal received power [31]. Optimal power control algorithms aim at minimizing the power transmitted by each mobile while maintaining required link quality.

The power control algorithms that have been developed to date assume slow fading radio channels. The channel characteristics vary slowly over several uplink and downlink frame periods. In TDD systems, the BS sends power control signals to an individual mobile according to the received signal power it measures from previous uplinks. However, when the mobile moves in the propagation environment, such that Doppler spread and multipath scattering cause rapid fluctuation in the received signal, the radio channel undergoes Rayleigh fading and varies drastically

within several frame periods [1]. This poses significant error in traditional power control, in which the mobile adjusts power based on the channel characteristics of the previous uplinks. Under fast fading, the control signaling from the BS is not suitable for the current uplink. Also, the constant transmitted power will not be able to cope with the deep fades within an uplink frame period.

When an antenna array is used at the BS, downlink beamforming technique exploits the spatial diversity of the mobiles to increase system capacity [32]. The BS assigns beamforming weights for the transmission to a particular user, and it combines with the vector channel to form the user-specified traffic channel (TCH).

In this chapter, we model the vector channels, and propose a new power control scheme, such that the mobile transmits at variable power levels based on the uplink traffic channel prediction. This control is open loop in the sense that the mobile user does not need BS signaling for power adjustment. Operating in TDD mode, the mobile extracts the most recent downlink channel from the received signal, and predicts the channel for uplink transmission. The AR model is employed for channel prediction. The mobile dynamically adjusts the transmitted power within an uplink frame according to the channel variation, such that the fast fading effect is compensated. Because imperfect beamforming gives rise to error of channel prediction, in this work, the uplink channel prediction relies on both the omni-directional access channel (ACH) and the user-specified traffic channel (TCH) to improve accuracy.

3.2   Propagation Environment and Vector Channel Model

A BS with an antenna array, serving multiple mobile users emitting narrowband signals is considered as in Figure 3.1. The multipaths which cause random phase change and angle spread at the receiver are a result of the following two mechanisms. First, the transmitted signals are scattered by objects local to the transmitter.
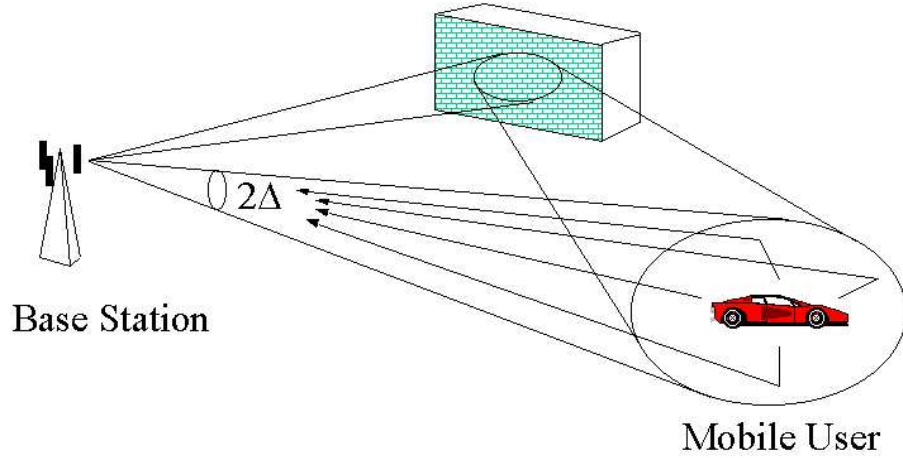
Figure 3.1: Multipaths caused by local and remote scatterers

Secondly, the scattering ray bundles are reflected or diffracted by objects remote to the transmitter. For local-scattering paths, it is reasonable to assume that the signal energy is dominant within a small spreading angle Δ with a uniform distribution. The reflection or diffraction by remote objects cause significant multipath delays and large angle spread.

Due to the motion of the mobile or the scatterers, the received signals at the BS experience Doppler spread. The increased mobility results in fast fading in which the channel exhibits rapid temporal variations, such that the performance of the cellular radio system is substantially degraded. Fast-fading channels encountered in practice exhibit Doppler spreads on the order of 100-200 Hz [33]. With carrier frequency 2 GHz and Doppler spread 100 Hz, the range of the channel envelope within 5 ms frame of uplink and downlink can be as large as 10 dB.

When an M-element antenna array is mounted on the BS, the channel between the BS and the mobile is modeled using the *Vector Channel Impulse Response* (VCIR). Without considering local scattering,

$$\mathbf{h}(t, \tau) = \sum_{i=0}^{L-1} \alpha_i(t, \tau) \mathbf{a}(\theta_i) \delta(t - \tau_i(\tau)) \tag{3.1}$$

where α_i, τ_i, $\mathbf{a}(\theta_i)$ are the complex amplitude, path delay and steering vector associated with DOA (θ_i) of the ith multipath component. There are a total of L multipath components. The complex amplitude can be expressed as

$$\alpha_i(t, \tau) = \rho_i(\tau)e^{j(2\pi f_i(\tau)t + \Psi_i(\tau))} \tag{3.2}$$

where ρ_i, f_i, and Ψ_i are the path gain, Doppler shift and phase offset. Assume that the parameters ρ_i, f_i, Ψ_i and τ_i remain constant during the short period of several TDD frames under consideration. Thus, the BS received baseband data vector from user j is given by

$$
\begin{aligned}
\mathbf{x}(t) &= \mathbf{h}(t, \tau) * u(t) + \mathbf{n}(t) \\
&= \sum_{i=0}^{L-1} \alpha_i(t)\mathbf{a}(\theta_i)u(t - \tau_i) + \mathbf{n}(t) \\
&= u(t - \tau_0)\mathbf{A}^{(j)}(t) + \mathbf{n}(t)
\end{aligned} \tag{3.3}
$$

where, $u(t)$ is the baseband transmitted signal which depends on the information-bearing symbol and the modulation waveform, $\mathbf{n}(t)$ is zero-mean, complex AWGN vector. The last step of (3.3) makes the narrowband channel assumption that $\tau_i \approx \tau_0$. $\mathbf{A}^{(j)}(t) = \sum_{i=0}^{L-1} \alpha_i(t)\mathbf{a}(\theta_i)$.

Consider locally scattered paths from one nominal DOA θ. The received data vector becomes [34]

$$
\begin{aligned}
\mathbf{x}(t) &= \sum_{k=0}^{N-1} \alpha_k(t)\mathbf{a}(\theta + \tilde{\theta}_k)u(t - \tau_k) + \mathbf{n}(t) \\
&= u(t - \tau_0)\mathbf{A}_i^{(j)}(t) + \mathbf{n}(t)
\end{aligned} \tag{3.4}
$$

where N is the total number of scattered paths within small angle spread Δ, and $\theta + \tilde{\theta}_k$ is the arrival angle of the kth scattered path. The delay spread of scattered paths are usually insignificant because of the small scattering radius. With $|\tilde{\theta}_k| \leq \Delta$,

a first-order Taylor series expansion yields

$$
\begin{aligned}
\mathbf{A}_i^{(j)} &= \sum_{k=0}^{N-1} \alpha_k \mathbf{a}(\theta + \tilde{\theta}_k) \\
&\cong \sum_{k=0}^{N-1} \alpha_k [\mathbf{a}(\theta) + \tilde{\theta}_k \mathbf{d}(\theta)] \\
&= (\sum_{k=0}^{N-1} \alpha_k) \mathbf{a}(\theta) + (\sum_{k=0}^{N-1} \alpha_k \tilde{\theta}_k) \mathbf{d}(\theta)
\end{aligned}
\tag{3.5}
$$

where, $\mathbf{d}(\theta) = \partial \mathbf{a}(\theta)/\partial \theta$ is the gradient.

Combining the effect of local scattering with that of large-angle reflection in (3.3) gives

$$
\begin{aligned}
\mathbf{x}(t) &= \sum_{i=0}^{L-1} [\gamma_i(t)\mathbf{a}(\theta_i) + \psi_i(t)\mathbf{d}(\theta_i)] \; u(t - \tau_i) + \mathbf{n}(t) \\
&= \mathbf{b}_j(t) \; u(t) + \mathbf{n}(t)
\end{aligned}
\tag{3.6}
$$

where

$$
\mathbf{b}_j(t) = \sum_{i=0}^{L-1} [\gamma_i(t)\mathbf{a}(\theta_i) + \psi_i(t)\mathbf{d}(\theta_i)]
$$

$$
\gamma_i(t) = \sum_{k=0}^{N_i-1} \alpha_{ik}(t), \quad \psi_i(t) = \sum_{k=0}^{N_i-1} \alpha_{ik}(t)\tilde{\theta}_{ik}
\tag{3.7}
$$

$\mathbf{b}_j(t)$, the composite multiplicative channel, is called the *spatial signature* of the narrowband channel for user j.

3.3 Mobile Received Signal

In TDD systems, radio channels for uplink and downlink are reciprocal. The signal transmitted by the BS antenna array can be described as

$$
\mathbf{u}(t) = \sum_{d=0}^{D} \mathbf{w}_d u_d(t)
\tag{3.8}
$$

where, $\mathbf{w}_d$'s are the beam-forming weight vectors. $\mathbf{w}_0 = \mathbf{1} \ (= ones(M, 1))$ is for the omni-directional access channel (ACH), whereas $\mathbf{w}_d$, $d \in \{1, \ldots, D\}$, is for the traffic channel (TCH) of each user. D is the number of mobile users. $u_0(t)$ is the common access signal, and $u_d(t)$ is the signal for user d. Therefore the signal received by user j is

$$x_j(t) = \mathbf{b}_j^T(t)\mathbf{u}(t) + n_j(t) \tag{3.9}$$

Suppose the signal-to-interference-and-noise-ratio (SINR) for user j is above the satisfactory threshold, then the received signal can be further expressed as

$$
\begin{aligned}
x_j(t) &= \mathbf{b}_j^T(t)\mathbf{w}_j u_j(t) + \mathbf{b}_j^T(t)\mathbf{w}_0 u_0(t) \\
&\quad + \sum_{d\neq 0, d\neq j} \mathbf{b}_j^T(t)\mathbf{w}_d u_d(t) + n_j(t) \\
&= \mathbf{b}_j^T(t)\mathbf{w}_j u_j(t) + \mathbf{b}_j^T(t)\,\mathbf{1}\,u_0(t) + \tilde{n}_j(t) \tag{3.10}
\end{aligned}
$$

Interference from signals for other users is absorbed into the noise component $\tilde{n}_j$. The two signal parts in (3.10) can be separated by CDMA orthogonal codes. Therefore, after detecting $u_j(t)$ and $u_0(t)$, the mobile user can extract the TCH as $\mathbf{b}_j^T(t)\mathbf{w}_j$ and the ACH as $\mathbf{b}_j^T(t)\mathbf{1}$. Now the task is to predict the TCH in the following uplink frame for the purpose of dynamic power control.

3.4 Access-Channel-Assisted Channel Prediction

The traffic channel $c(t)$ of user j is defined as

$$
\begin{aligned}
c(t) &= \mathbf{w}_j^T \mathbf{b}_j(t) \\
&= \mathbf{w}_j^T \sum_{i=0}^{L-1} [\gamma_i(t)\mathbf{a}(\theta_i) + \psi_i(t)\mathbf{d}(\theta_i)] \\
&= \mathbf{w}_j^T \sum_{i=0}^{L-1} \gamma_i(t) [\mathbf{a}(\theta_i) + \tilde{\mathbf{d}}_i] \\
&= \mathbf{w}_j^T [\mathbf{A} + \mathbf{D}] \, \mathbf{\Gamma} \tag{3.11}
\end{aligned}
$$

where,

$$\mathbf{A} = [\mathbf{a}(\theta_0), \ldots, \mathbf{a}(\theta_{L-1})], \quad \mathbf{D} = [\tilde{\mathbf{d}}_0, \ldots, \tilde{\mathbf{d}}_{L-1}],$$

$$\mathbf{\Gamma} = [\gamma_0(t), \ldots, \gamma_{L-1}(t)]^T$$

and

$$\tilde{\mathbf{d}}_i = \frac{\psi_i(t)}{\gamma_i(t)} \mathbf{d}(\theta_i)$$

Note that $\mathbf{w}_j$ and $\mathbf{A}$ are constant vector and matrix, $\|\mathbf{D}\|$ is of order $O(\Delta)$ and it is assumed that the derivatives exist and that they are bounded. From (3.2) and (3.7) we see that γ_i's are of harmonic forms that consist of a superposition of complex exponentials. As a result, sharp peaks are the predominant feature of the power spectrum of channel $c(t)$. Therefore, the *autoregressive* (AR) model is most appropriate for the channel [35]. The sharp peaks correspond to the poles near the unit circle. The AR model is closely tied to linear prediction, and the prediction coefficients $\mathbf{a}_p \overset{def}{=} [1, a_1, \ldots, a_p]^T$ satisfy the Yule-Walker equations

$$\hat{\mathbf{R}}_c \mathbf{a}_p = \epsilon_p \mathbf{u}_1 \tag{3.12}$$

where, $\hat{\mathbf{R}}_c$ is the (estimated) autocorrelation matrix of $c(t)$, ϵ_p is the modeling error, $\mathbf{u}_1 = [1, 0, \ldots, 0]^T$ is a unit vector of length $p+1$, and p is the model order. Thus, the prediction recursion is given by

$$\hat{c}(k) = -\sum_{l=1}^{p} a_l c(k-l) \tag{3.13}$$

In practice, forward and backward linear prediction is applied for stability [36].

Exploiting the BS antenna array, optimal beamforming weight vector $\mathbf{w}_j$ provides adequate signal quality for the desired mobile user while minimizing the interference from other user signals [37]. However, if the spatial signature $\mathbf{b}_j(t)$ changes rapidly, the downlink beamforming could actually result in received signal degradation. Consequently, the dedicated TCH for the mobile is sensitive to fast-fading, and it leads to large prediction error for uplink. The ACH, on the other hand,

38
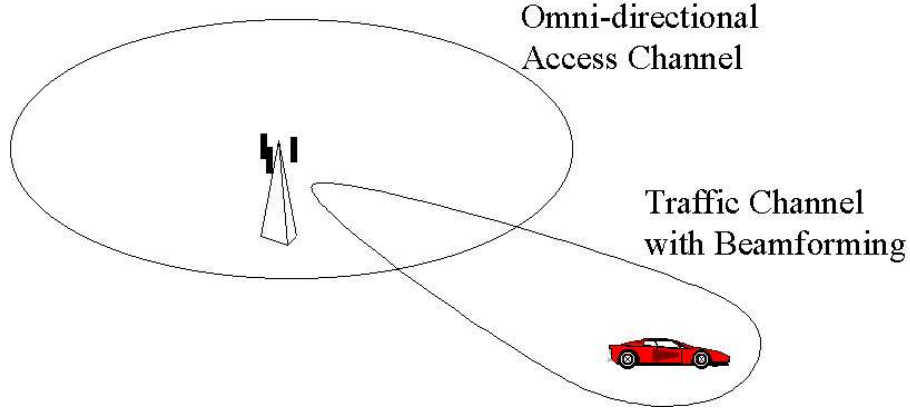
Figure 3.2: Access channel and traffic channel

is a broadcast channel, e.g. the universal sync channel, with $\mathbf{w}_0 = \mathbf{1}$. Therefore, the ACH provides relative robustness to channel perturbation and reduces sensitivity to fast-fading (Figure 3.2). From (3.11), the TCH and the ACH can be expressed as

$$c_T(t) = \mathbf{w}_j^T \left[\mathbf{A} + \mathbf{D} \right] \mathbf{\Gamma} \;, \qquad c_A(t) = \mathbf{w}_0^T \left[\mathbf{A} + \mathbf{D} \right] \mathbf{\Gamma} \tag{3.14}$$

As discussed before, sharp peaks are the predominant feature of the power spectrums of $c_T(t)$ and $c_A(t)$. The corresponding peaks in the TCH and the ACH spectrums have the same locations, since $\mathbf{w}$ is a constant complex vector. This yields the same corresponding poles in both AR models. As a result, (normalized) prediction coefficients of the TCH and the ACH using AR models of the same order are the same. Along with (3.12), stacking TCH and ACH samples provides an overdetermined linear equation

$$\left[\begin{array}{c} \tilde{\mathbf{R}}_T \\ \tilde{\mathbf{R}}_A \end{array} \right] \mathbf{a}_p = \mathbf{0} \tag{3.15}$$

where, $\tilde{\mathbf{R}}_T$ and $\tilde{\mathbf{R}}_A$ are $p \times (p+1)$ autocorrelation matrices of TCH and ACH

samples, respectively.

$$\tilde{\mathbf{R}} = \begin{bmatrix} r_c(1) & r_c(0) & r_c^*(1) & \cdots & r_c^*(p-1) \\ r_c(2) & r_c(1) & r_c(0) & \cdots & r_c^*(p-2) \\ \vdots & \vdots & \vdots & & \vdots \\ r_c(p) & r_c(p-1) & r_c(p-2) & \cdots & r_c(0) \end{bmatrix} \tag{3.16}$$

for both TCH and ACH.

Due to channel randomness, $\begin{bmatrix} \tilde{\mathbf{R}}_T \\ \tilde{\mathbf{R}}_A \end{bmatrix}$ usually has full column rank. There-
fore, (3.15) has a unique non-trivial least squares solution with $\mathbf{a}_p(1) = 1$.

3.5   Dynamic Uplink Power Control

Once the downlink symbols are detected, the mobile can extract its own TCH $c_T(t) = \mathbf{w}_j^T \mathbf{b}_j(t)$ and ACH $c_A(t) = \mathbf{w}_0^T \mathbf{b}_j(t)$ from the received signal. Channel samples are passed through a low-pass-filter (LPF) to suppress noisy variation, and are then used to predict the TCH of the next uplink frame. The mobile transmitted power is adjusted according to the predicted uplink channel by the "water-filling" scheme. The adjustment is dynamic in the sense that the transmitted power level changes as the channel changes during uplink. This can be expressed as

$$P_{TX}(t) = P_{BTh} + PL - F(t) \tag{3.17}$$

where, $P_{TX}(t)$ is the mobile transmitted power level in dB, P_{BTh} is the known BS received power threshold for this particular mobile user, PL is the large-scale path loss which does not change during the short period of time under consideration, $F(t)$ is the uplink traffic channel fading function. In the fast-fading environment, $F(t)$ changes rapidly proportional to the envelope of the predicted uplink TCH. The scale of $F(t)$ is chosen in such a way that the average transmitted power of an uplink frame is fixed.
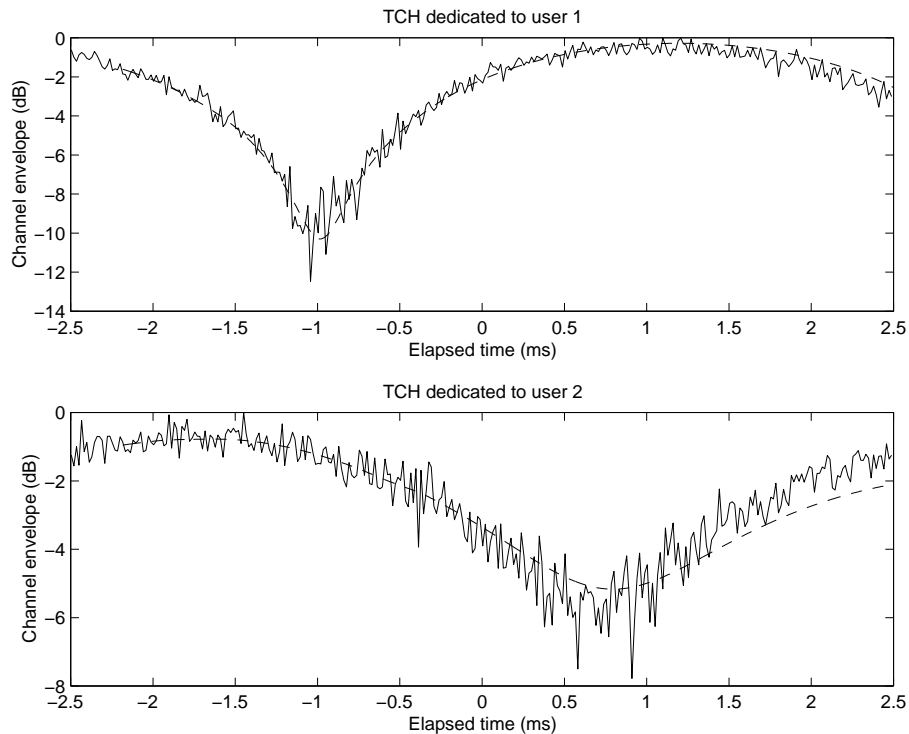
Figure 3.3: Downlink channel and (predicted) uplink channel.

Note that the channel sampling rate utilized for dynamic uplink power adjustment is much lower than the data symbol rate. Mobile user adjusts transmitted power a few times during uplink in an effort to combat deep fades within a frame.

3.6 Simulations

A wireless CDMA system of a base station communicating with two mobile users in the propagation environment as in Figure 3.1 is simulated. The BS has an 8-element uniform circular antenna array, which has half wavelength radius. We consider a typical vehicular scenario, in which the BS is located outdoors with a high antenna (thus no scatterers local to the BS), and the mobiles move at a speed of 80 km/h.

The received signals experience both local scattering and large-angle reflec-
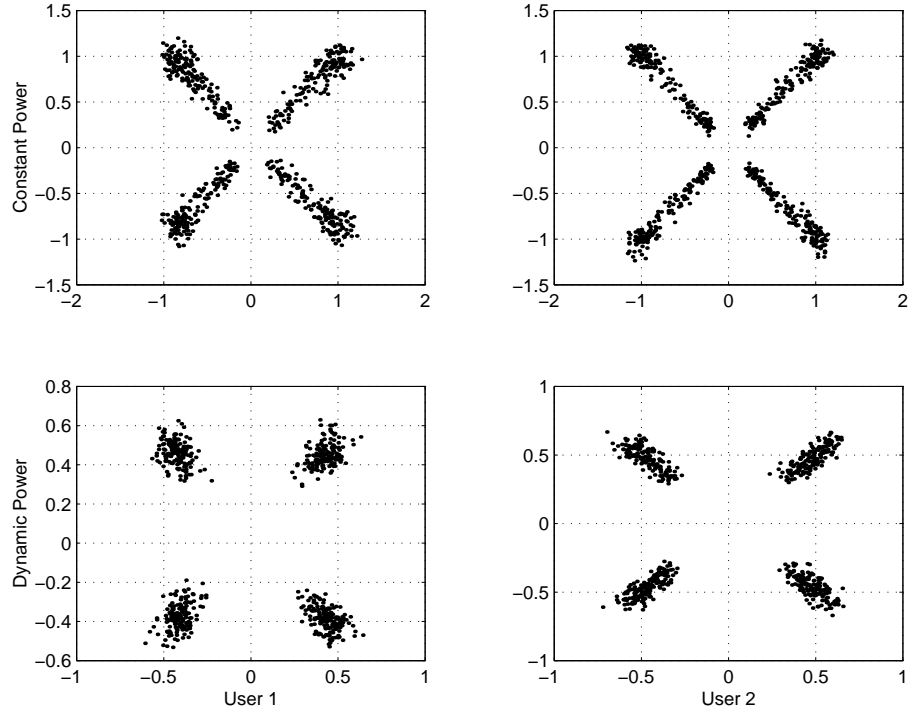
Figure 3.4: Base station received signal constellation.

tion. There are L dominant multipath bundles from each mobile arriving at the base station, with pass losses, delays and DOA's uniformly distributed on [0 dB, 20 dB], $[0, T]$ and $[0, 2\pi)$, respectively. T is the chip duration. The chip rate is 2.048 MHz. The integer L is uniformly distributed on $[1, 6]$. Each multipath bundle consists of $N = 100$ local scattering paths. There is 10 dB AWGN at the receiver. Communication is in TDD mode with 2.5 ms downlink and 2.5 ms uplink. Carrier frequency is 2 GHz. CDMA spreading factor is 8. The prediction order is $p = 12$. Assume perfect symbol detection at the BS.

Figure 3.3 illustrates the TCH of each mobile user during the time period of a consecutive downlink and uplink. The downlink TCH is passed through a LPF with cut-off frequency 200 Hz. The LPF output is represented by the dash line in the downlink. The dash line in the uplink period is the predicted TCH. Figure 3.4
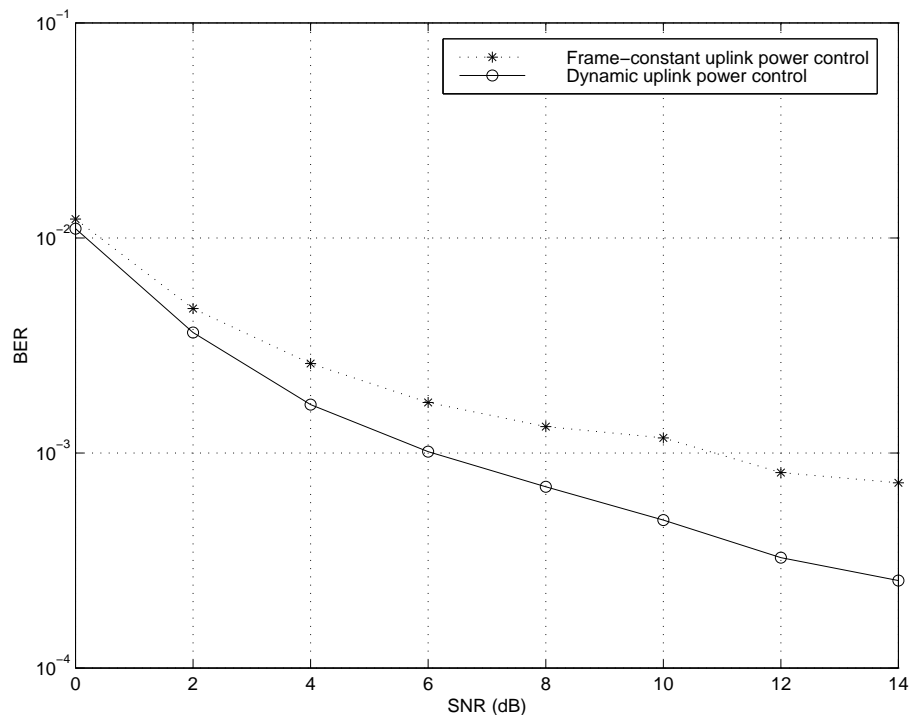
Figure 3.5: Performance of dynamic uplink power control.

shows the DQPSK constellations of BS received signals from each user, as the frame-constant uplink transmitted power compares with the dynamic uplink power. The performance comparison of the frame-constant uplink power control and dynamic uplink power control is made in Figure 3.5, in which it shows the average bit-error-rate (BER) of the received signals versus SNR at the BS. Figure 3.6 shows the average BER as the mobile moves at different speed. Here, SNR = 10 dB. The performance of power control based on ACH/TCH prediction is also compared with that of the prediction only with TCH samples. Clearly, the proposed method has the best performance over fast fading channels.
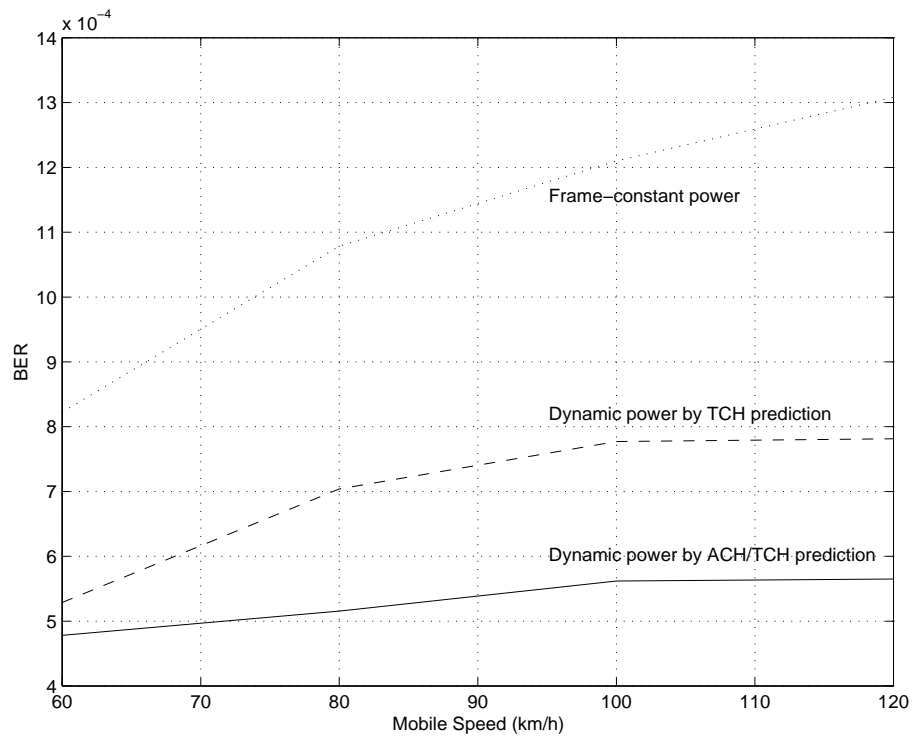
Figure 3.6: Performance of dynamic power control based on TCH or ACH/TCH prediction.

3.7 Conclusions

We have introduced an effective uplink power control scheme for wireless TDD systems under fast fading. The control intelligence is located at the mobile user end. The control is open-loop, as it is based on the prediction of the uplink channel. Prediction accuracy is improved by exploiting the antenna array technique. This mobile power control scheme aims at compensating channel fading fluctuation within a short period of time, usually several frame durations. It can also be combined with distributed iterative power control algorithms for optimal system performance.

Chapter 4

Downlink Beamforming for Fast Rayleigh Fading Signals

4.1 Introduction

Space diversity, obtained through antenna array processing, provides an attractive means to improve the performance of wireless communication systems [38, 39, 6]. When antenna array is equipped at the base station, the received signals in uplink (mobile to base station) are properly weighted and combined, and the transmitted signals in downlink (base station to mobile) are weighted on each array element before transmission, subject to a total radiated power constraint, to form beams toward the desired users. Both uplink combining and downlink beamforming endeavor to maximize the output signal-to-interference-plus-noise ratio (SINR) by using adaptive antenna array techniques, which combat the multipath fading of the desired signal [30] and the cochannel interference (CCI) [40, 32]. In code-division multiple access (CDMA) systems, the CCI is effectively reduced by the coding gain. Considering the signal after despreading as the signal of a single user case for the desired mobile, we herein focus our beamforming effort on combating the Rayleigh fading

experienced by each mobile caused by multipath propagation.

The increased mobility results in fast Rayleigh fading, in which the channel exhibits rapid temporal variations. The downlink beamforming algorithms that have been developed to date adapt only to slowly varying components in the channel and do not track fast Rayleigh fading which can vary significantly within a transmission data frame. This problem is mitigated by the adaptive downlink beamforming approach proposed in this chapter, in which the beamforming weights are adjusted multiple times within a transmission frame based on downlink channel prediction.

The linear predictability of mobile channel is reported in [23] and [21], in which the channel is modeled as a wide-sense stationary autoregressive (AR) process. Using the AR model, the vector channel modeling and prediction are introduced in [41], where an antenna array is implemented at the base station. The prediction of the vector channel benefits from the fact that the channel experienced by each array element can be modeled using the same AR model.

In this chapter, we exploit the prediction of vector channels for adaptive downlink beamforming to combat fast Rayleigh fading in the wireless link. The prediction order is estimated based on the information theoretic criteria for model order selection introduced by Akaike (AIC) [42] and by Schwartz and Rissanen (MDL) [43, 44]. When predicting the channel for the purpose of beamforming, we effectively decimate the observation interval of channel samples to improve the prediction performance. The beamforming rate, that is, the frequency of adjusting the antenna weights within a transmission frame, is closely related to the decimation in the channel prediction. The selection of the beamforming rate is discussed with its effect on the channel prediction performance, the receive bit error probability and the computational complexity of the algorithm.

Another issue that complicates downlink beamforming is the absence of accurate knowledge of the current downlink channels at the base station, especially in

frequency-division duplex (FDD) systems. In FDD systems, the instantaneous channels of uplink and downlink are uncorrelated when the channel coherence bandwidth is smaller than the carrier frequency separation [45]. Because of the uncorrelated fading in uplink and downlink, and the frequency dependency of array response, the direct use of the uplink weights for downlink beamforming is not sufficient. The existing approaches for FDD systems include the adaptive beamforming based on the mobile probing-feedback [46], and the adaptive beamforming based on the estimation of the direction of arrivals (DOA) [47]. However, the mobile feedback method requires additional bandwidth for control signaling, and introduces propagation delay, which can be intolerable under fast fading. And the DOA method can be impaired by the estimation resolution, which in many cases is limited by the dimension of the antenna array.

To circumvent this problem, in this chapter we propose another adaptive downlink beamforming approach that exploits the uplink channel subspace. It can realize transmit diversity gain without requiring knowledge of the current downlink channel. In [48, 49, 50, 51], the concept of channel subspace is applied to downlink beamforming to reduce the CCI, where the channel subspace is characterized by the channel covariance matrix. However, these algorithms are not able to cope with the fast Rayleigh fading of the desired signals. In our approach, the downlink beamforming weights are chosen according to the orthonormal basis of the uplink channel subspace. As the channel varies, the channel vector is confined to the channel subspace. In contrast to the time-varying channel vector, the channel subspace spanned by the array responses has a stable structure. Furthermore, the distance between the uplink channel subspace and the downlink channel subspace is negligible even with large uplink and downlink carrier separation. This makes the proposed beamforming technique applicable in a practical FDD system. The base station transmits the signal to a particular mobile through multiple code channels, each of the coded

signals being weighted by an orthonormal basis vector of the effective uplink channel subspace. The mobile combines the received signals of all the code channels, which results in the desired signal with its power preserved under fast fading. This is accomplished at the cost of the code-channel resource and by modifying the mobile receiving.

This chapter is organized as follows. In Section 4.2, we present the system model, together with the uplink space-time processing at the base station receiver. We propose the predictive downlink beamforming algorithm in Section 4.3, and discuss its implementation in time-division duplex (TDD) and frequency-division duplex (FDD) CDMA systems. In Section 4.4, the prediction order is estimated using information theoretic criteria for model order selection. In Section 4.5, we give the performance analysis of channel prediction for beamforming and system performance analysis. In Section 4.6, we propose the subspace-based downlink beamforming algorithm, and discuss its implementation in TDD and FDD systems. Section 4.7 gives the results of computer simulations, which are conducted through an electromagnetic ray tracer that uses an urban propagation model of downtown Austin, Texas. Finally, conclusions are drawn in Section 4.8.

4.2   System Model and Uplink Space-Time Processing

We consider a cell in which K mobile users, each with a single antenna element, communicate simultaneously with a base station with an M-element antenna array. The baseband signal received at the base station can be expressed in a vector form as

$$\mathbf{x}(t) = \sum_{k=1}^{K} \sum_{i=1}^{L_k} \mathbf{a}_{k,i}^{(u)}(t) \sqrt{p_k^{(u)}} s_k^{(u)}(t - \tau_{k,i}) + \mathbf{n}(t) \tag{4.1}$$

where superscript (u) denotes uplink, and

L_k total number of resolvable paths from mobile k;

$\mathbf{a}_{k,i}(t)$ time-varying channel vector of the ith path from mobile k;

$\tau_{k,i}$ path delay of the ith path from mobile k;

p_k transmit power of mobile k;

$s_k(t)$ transmitted signal of mobile k;

$\mathbf{n}(t)$ receiver background noise vector, each element of which is independent additive white Gaussian noise (AWGN) with one-sided spectrum density N_0.

A path can be resolved by a RAKE receiver, if its temporal separation to other paths is larger than the chip duration T_c. Each of the resolvable paths is itself a cluster of temporally unresolvable multipath components, which may arrive at the receiver from different directions. Suppose there are L_s unresolvable subpaths which contribute significantly to the ith path from mobile k, the channel vector $\mathbf{a}_{k,i}(t)$ can be written as

$$\mathbf{a}(t) = \sum_{j=1}^{L_s} \alpha_j(t)\mathbf{v}(\theta_j) \tag{4.2}$$

Here we omit the subscripts k and i. For an M-element circular array with radius R, the array response $\mathbf{v}(\theta_j)$ associated with the direction of arrival (DOA) θ_j is given by

$$\mathbf{v}(\theta_j) = [e^{j2\pi Rf_c \cos(\theta_j)/C}, e^{j2\pi Rf_c \cos(\theta_j+2\pi/M)/C}, \cdots, e^{j2\pi Rf_c \cos(\theta_j+2\pi(M-1)/M)/C}]^T \tag{4.3}$$

where f_c is the carrier frequency. $\alpha_j(t)$ is the complex amplitude of the jth subpath, which can be expressed as

$$\alpha_j(t) = \rho_j e^{j2\pi(f_j t-(f_c+f_j)\tau_j)} \tag{4.4}$$

where ρ_j and f_j are the complex path loss and the Doppler frequency shift of the jth subpath, respectively. The Doppler frequency is given by $f_j = f_c \frac{v}{c}\cos(\psi_j)$, where v

49

is the relative speed of the mobile, c is the speed of light, and ψ_j is the angle between the incident wave of the jth subpath at the mobile and the mobile moving direction. The received signals experience Doppler frequency spread due to the motion of the mobile or the scatterers. We consider only Rayleigh fading but no path loss or shadowing, that is to assume the DOA θ_j, the path loss ρ_j, the path delay τ_j and the Doppler frequency f_j remain constant over a period of several data frames.

The transmitted signal $s_k(t)$ depends on the information-bearing bit stream $\{b_k(n)\}$ and the modulation waveform $g_k(t)$ as

$$s_k(t) = \sum_n b_k(n)g_k(t - nT_s) \tag{4.5}$$

where T_s is the symbol duration. For CDMA systems, the modulation waveform is of the form

$$g_k(t) = \sum_{n=0}^{N-1} c_k(n)p(t - nT_c) \tag{4.6}$$

where $\{c_k(0), c_k(1), \ldots, c_k(N-1)\}$ is the binary (± 1) spreading code, $p(t)$ is the chip pulse-shaping function. T_c is the chip duration, N is the code length, and we have $T_s = NT_c$. Suppose the RAKE receiver has a finger aligned with each resolvable path, and a matched filter, which is given by $g_k^*(-t)$, is present at each finger. With the assumption of white Gaussian noise, the output of a matched filter is a sufficient statistic for the estimation of the transmitted signal [45]. The output of the matched filter for the ith path from mobile k sampled at the symbol rate is

$$
\begin{aligned}
\mathbf{y}_{k,i}(n) &= \int_{(n-1)T_s+\tau_{k,i}}^{nT_s+\tau_{k,i}} g_k(t - nT_s - \tau_{k,i})\mathbf{x}(t)dt \\
&= \sqrt{Gp_k}\mathbf{a}_{k,i}(n)b_k(n) + \mathbf{i}(n) + \tilde{\mathbf{n}}(n)
\end{aligned}
\tag{4.7}
$$

where G is the processing gain. $\mathbf{i}(n)$ is the undesired component due to multiple access interference (MAI) and self interference, and $\tilde{\mathbf{n}}(n)$ is the noise component:

$$
\begin{aligned}
\mathbf{i}(n) &= \sum_{k \neq l \text{ or } i \neq j} \sqrt{p_l}\mathbf{a}_{l,j}(n) \sum_m b_l(m) \int g_k(t - nT_s - \tau_{k,i})g_l(t - mT_s - \tau_{l,j})dt \\
\tilde{\mathbf{n}}(n) &= \int g_k(t - nT_s - \tau_{k,i})\mathbf{n}(t)dt
\end{aligned}
$$

50

We assume that the modulation waveforms of the interfering users or with different delays appear as mutually uncorrelated noise. Therefore, the desired signal is stronger than each of the interferers at the output of the matched filter. Receivers employing antenna arrays adjust their beam patterns by assigning a weight vector $\mathbf{w}_k$, such that the array output is weighted and added to maximize the signal-to-interference-and-noise-ratio (SINR). Due to the fast time-varying property of the channel vector $\mathbf{a}(n)$, the weight vector needs to be adjusted several times during an uplink frame to compensate fading. We assume the channel is piecewise stationary, that is, the channel vector is constant during each beamforming group, which is defined as a time span of tens to hundreds of symbols to calculate each weight. The average output power of the symbols of the lth beamforming group is

$$
\begin{aligned}
\mathcal{P}_l &= E\{\mathbf{w}_{k,i}^H \mathbf{y}_{k,i}(n)\mathbf{y}_{k,i}^H(n)\mathbf{w}_{k,i}\} \\
&= \mathbf{w}_{k,i}^H E\{\mathbf{y}_{k,i}(n)\mathbf{y}_{k,i}^H(n)\}\mathbf{w}_{k,i} \\
&= \mathbf{w}_{k,i}^H \mathbf{R}_{yy}(l)\mathbf{w}_{k,i}
\end{aligned}
\tag{4.8}
$$

where $\mathbf{R}_{yy}(l)$ is the spatial covariance matrix of the matched filter output, which can be written as

$$
\mathbf{R}_{yy}(l) = Gp_k\mathbf{a}_{k,i}(l)\mathbf{a}_{k,i}^H(l) + \mathbf{R}_{in}(l)
\tag{4.9}
$$

with $\mathbf{R}_{in}(l)$ being the spatial covariance matrix of total interference plus noise. The weight vector which maximizes the SINR

$$
\Gamma_l = \frac{Gp_k\mathbf{w}_{k,i}^H\mathbf{a}_{k,i}(l)\mathbf{a}_{k,i}^H(l)\mathbf{w}_{k,i}}{\mathbf{w}_{k,i}^H\mathbf{R}_{in}(l)\mathbf{w}_{k,i}}
\tag{4.10}
$$

is given by the optimum Wiener solution as [52]

$$
\mathbf{w}_{k,i} = \zeta\mathbf{R}_{in}^{-1}(l)\mathbf{a}_{k,i}(l)
\tag{4.11}
$$

where ζ is an arbitrary constant that does not change the value of the SINR obtained after combining. Assuming that the interference is spatially white, we can show that

$\mathbf{R}_{in}$ is proportional to an identity matrix, therefore a suboptimal solution for the weight vector is

$$\mathbf{w}_{k,i} = \zeta \mathbf{a}_{k,i}(l) \tag{4.12}$$

The optimum combining and suboptimum combining have similar performance as shown in [53]. In order to compensate fading, we maintain constant received signal strength by forming the suboptimal weight vector as

$$\mathbf{w}_{k,i} = \xi \beta_{k,i}^{-1}(l) \tilde{\mathbf{a}}_{k,i}(l) \tag{4.13}$$

where $\tilde{\mathbf{a}}_{k,i}(l)$ is the normalized channel vector, and $\beta_{k,i}(l) = ||\mathbf{a}_{k,i}(l)||$. ξ is a constant that takes into account the total power constraint. The average signal power of the lth beamforming group becomes independent of l as

$$\mathcal{P}_{s,l} = G p_k \mathbf{w}_{k,i}^H \mathbf{a}_{k,i}(l) \mathbf{a}_{k,i}^H(l) \mathbf{w}_{k,i} = G p_k \xi^2 \tag{4.14}$$

Given that the desired signal is sufficiently stronger than interference and noise after matched filtering, $\tilde{\mathbf{a}}_{k,i}(l)$ and $\beta_{k,i}(l)$ are obtained as the principal unit norm eigenvector and its corresponding eigenvalue of $\mathbf{R}_{yy}(l)$.

Applying spatial diversity combining and RAKE reception is indeed a space-time filtering process. We adopt the scheme of performing beamforming before RAKE combining on the received data for better performance [54]. However in doing so, a weight vector needs to be assigned for each resolvable path, compared to only one weight vector for all paths from a particular mobile when beamforming is performed after RAKE combining.

4.3   Predictive Downlink Beamforming

In uplink, both the beamformer and the RAKE receiver are implemented in the base station. In downlink, the beamformer and the RAKE receiver are implemented in the base station and the mobile, respectively. The delay spread does not change

from uplink to downlink. However, the vector channel representing each resolvable path varies drastically over a *duplex time* under fast Rayleigh fading. A duplex time is the time gap between two consecutive transmission frames in the TDD systems. In the FDD systems, the feedback of the downlink channel state information has a time delay for the current base station transmission, which is also refer to as the duplex time in this context. Furthermore, the vector channel exhibits deep fades during each transmission. Therefore, the prediction of future downlink and the fine adjustment of beamforming weights within a transmission frame are crucial to guarantee receive performance.

Downlink Beamforming for TDD   In TDD systems with the same carrier frequency, radio channels for uplink and downlink are reciprocal. The uplink channel vector $\mathbf{a}_{k,i}$ for the ith path from mobile k is extracted from the received data at the base station and can be used to predict the future downlink. Similar to (4.13), the downlink beamforming weights are formed according to the predicted downlink channel, which varies during the transmission frame, but is assumed piecewise stationary for each beamforming group. Hereafter we omit the subscripts k and i with the understanding that we are dealing with the ith path of mobile k.

Recall that the output of the matched filter at the base station can be expressed as in (4.7). Suppose perfect detection of the symbol bit $b(n)$. The base station can extract the uplink channel vector samples from $\mathbf{y}(n)$ as

$$
\begin{aligned}
\mathbf{c}(n) &= b^*(n)\mathbf{y}(n) \\
&= \sqrt{Gp_k}\mathbf{a}(n) + \eta(n) \\
&= \sqrt{Gp_k}\sum_j \alpha_j(n)\mathbf{v}(\theta_j) + \eta(n)
\end{aligned}
\tag{4.15}
$$

where $\eta(n) = b^*(n)(\mathbf{i}(n) + \tilde{\mathbf{n}}(n))$ is the interference plus noise component. Assume that the mobile transmit power is fixed over a few duplex time intervals. Note that

$\mathbf{v}(\theta_j)$ is a constant vector, and the Rayleigh fading effect is due to the variation of each complex amplitude $\alpha_j(n)$ caused by Doppler frequency shifts. As $\alpha_j(n)$ can be expressed as in (4.4), it is clear that $\mathbf{c}(n)$ is of harmonic form that consists of a superposition of complex exponentials in noise. As a result, sharp peaks are the predominant feature of the power spectrum of the channel samples at each array element. This justifies an all-pole model for the channel. The channel vector is modeled as a pth order Gaussian *autoregressive* (AR(p)) process

$$\mathbf{c}(n) = -\sum_{l=1}^{p} q_l \mathbf{c}(n-l) + \mathbf{e}(n) \tag{4.16}$$

where $\{\mathbf{e}(n)\}$ is a white Gaussian sequence. The locations of the sharp peaks correspond to the poles near the unit circle as $z_j = e^{j2\pi f_j T_s}$, which are determined by the Doppler frequency shifts of the p dominant subpaths. The AR coefficients are the same for channel samples of all array elements, because the arriving signals, though combined with different phases at different array elements, experience the same Doppler frequency shifts, which yield the same poles in the AR models.

As shown in (4.13), the suboptimal weight vectors are derived from the channel vectors of the desired mobile. Therefore, the prediction coefficients can be applied directly onto the uplink weights to generate a series of downlink beamforming weights, with a simple modification on the scale of the norms. Accordingly, the uplink channel samples forming the observation interval for prediction are decimated to the beamforming rate. The decimator consists of a downsampler preceded by a low-pass filter (LPF), which functions as an anti-aliasing filter [36]. We bandlimit the channel samples to a frequency band which includes the expected Doppler frequency shifts and then downsample the resulting data to the beamforming rate. The beamforming rate is usually higher than twice the maximum Doppler frequency. The downsampled version of the Gaussian AR(p) process can be written as

$$\mathbf{c}(n) = -\sum_{l=1}^{p} q_l \mathbf{c}(n-lL_b) + \mathbf{e}(n) \tag{4.17}$$

where L_b is the length of a beamforming group. A simpler linear structure is a tapped-delay-line configuration, which makes one-step prediction via an FIR filter as

$$\hat{\mathbf{c}}(n) = -\sum_{l=1}^{p} q_l \mathbf{c}(n - lL_b) \tag{4.18}$$

The coefficients $\mathbf{q}_p = [1, q_1, \ldots, q_p]^T$ are determined as the least square solution to the linear equations

$$\mathbf{C}\mathbf{q}_p = 0 \tag{4.19}$$

where $\mathbf{C}$ is a matrix of channel samples after decimation, assuming that $\{\mathbf{c}(0), \mathbf{c}(1), \ldots, \mathbf{c}(N-1)\}$ is observed

$$\mathbf{C} = \begin{bmatrix} \mathbf{c}(N-1) & \mathbf{c}(N-1-L_b) & \cdots & \mathbf{c}(N-1-pL_b) \\ \mathbf{c}(N-2) & \mathbf{c}(N-2-L_b) & \cdots & \mathbf{c}(N-2-pL_b) \\ \vdots & \vdots & & \vdots \\ \mathbf{c}(pL_b) & \mathbf{c}((p-1)L_b) & \cdots & \mathbf{c}(0) \\ \mathbf{c}^*(0) & \mathbf{c}^*(L_b) & \cdots & \mathbf{c}^*(pL_b) \\ \vdots & \vdots & & \vdots \\ \mathbf{c}^*(N-1-pL_b) & \mathbf{c}^*(N-1-(p-1)L_b) & \cdots & \mathbf{c}^*(N-1) \end{bmatrix} \tag{4.20}$$

The forward and backward linear prediction is applied to ensure the Toeplitz structure of the normal equations along with the guaranteed stability of the AR model.

The AR coefficients $\mathbf{q}_p$ varies slowly and can be easily adapted using, for example, the least-mean squares (LMS) algorithm [35]

$$\mathbf{q}_p(n) = \mathbf{q}_p(n - L_b) + \mu \mathcal{C}^H(n)(\mathbf{c}(n) - \hat{\mathbf{c}}(n)) \tag{4.21}$$

where $\mathbf{q}_p(n)$ denotes the prediction coefficients to be applied at time n, μ is a tuning constant, and $\mathcal{C}(n) = [\mathbf{c}(n - L_b), \ldots, \mathbf{c}(n - pL_b)]^T$.

Downlink Beamforming for FDD   In FDD systems, radio channels for uplink

and downlink have independent fading. The instantaneous channels of uplink and downlink are uncorrelated when the channel coherence bandwidth is smaller than the carrier frequency separation [45]. When mobile probing-feedback is applied in FDD systems [46], we modify the AR coefficients obtained from the uplink channel samples, and apply them to the feedbacks of previous downlink for prediction. The downlink beamforming weights can therefore be found, provided the probing rate is higher than or equal to the beamforming rate. The prediction coefficients can be obtained from the channel poles by Newton's relations as

$$q_l = (-1)^l \sum_{}^{l} \underbrace{z_i z_j \cdots z_k}_{l} \qquad l = 1, \ldots, p \qquad (4.22)$$

where $z_i, z_j, \ldots, z_k$ are distinct poles with $z_i = e^{j2\pi f_i T_b}$. f_i is the Doppler frequency, $1/T_b$ is the downlink channel probing rate. Assuming the probing rate is equal to the beamforming rate, we have $T_b = T_s L_b$. Fast fading channels encountered in practice exhibit Doppler spreads on the order of $100 - 200$ hertz [33]. With $T_b \sim 1 \times 10^{-3}$ second, the poles $\{z_i\}$ have no 2π-phase ambiguity on the complex plan. Therefore the uplink channel poles can be transformed to downlink channel poles by modifying the phase components as

$$\Phi(z_i^{(d)}) = \frac{f_c^{(d)}}{f_c^{(u)}} \Phi(z_i^{(u)}) \qquad (4.23)$$

In most FDD implementations, $\frac{f_c^{(d)}}{f_c^{(u)}} \approx 1$. As we will see in the simulations, it is credible to apply the prediction coefficients of uplink directly to the downlink without any modification.

4.4 Model Order Selection

We rewrite the Gaussian AR(p) process in a downsampled version as follows, assuming that $\{\mathbf{c}(0), \mathbf{c}(1), \ldots, \mathbf{c}(N-1)\}$ is observed,

$$\mathbf{c}(n) + \sum_{l=1}^{p} q_l \mathbf{c}(n - lL_b) = \mathbf{e}(n), \quad n = pL_b, \ldots, N-1. \tag{4.24}$$

where the model order p satisfies $p \leq (N-1)/L_b$. $\mathbf{e}(n)$ is drawn i.i.d. by the complex multivariate Gaussian distribution of zero mean and covariance matrix $\mathbf{C}_e = \sigma_\varepsilon^2 \mathbf{I}$. Suppose that the observed channel vectors are of one uplink frame, which is evenly divided into g beamforming groups as $N = gL_b$. The model order p is selected, therefore in the range $0 < p \leq g-1$, to minimize the total squared prediction error as

$$\hat{p} = \arg \min_{0 < p \leq (g-1), q_1, \ldots, q_p} \sum_{n=pL_b}^{N-1} ||\mathbf{e}(n)||^2 \tag{4.25}$$

Let $q_1, \ldots, q_p, \sigma_\varepsilon^2$ comprise the AR(p) parameter vector $\Theta^{(p)}$. Regarding the prediction errors as spatially white, independent vectors with zero mean, the joint probability density is given by

$$f(\mathbf{e}(pL_b), \ldots, \mathbf{e}(N-1); \Theta^{(p)}) = \prod_{i=pL_b}^{N-1} \frac{1}{(\pi \sigma_\varepsilon^2)^M} e^{-\frac{1}{\sigma_\varepsilon^2} \mathbf{e}^H(i) \mathbf{e}(i)} \tag{4.26}$$

where M, the dimension of the vector, is the number of antenna elements at the base station. The optimum model order $\hat{p}$ is found by selecting the model which minimize the Akaike information criterion (AIC) [42]

$$\text{AIC}(p) = -2 \ln f(\mathbf{e}(pL_b), \ldots, \mathbf{e}(N-1); \hat{\Theta}^{(p)}) + 2k \tag{4.27}$$

or the minimum description length criterion (MDL) [44, 55]

$$\text{MDL}(p) = -\ln f(\mathbf{e}(pL_b), \ldots, \mathbf{e}(N-1); \hat{\Theta}^{(p)}) + \frac{1}{2} k \ln(N - pL_b) \tag{4.28}$$

where $\hat{\Theta}^{(p)}$ is the maximum likelihood (ML) estimate of the parameter vector $\Theta^{(p)}$, and k is the degree of freedom in $\Theta^{(p)}$. When $\mathbf{e}(n)$ is considered Gaussian, the ML

estimates are exactly the MMSE estimates given by the Yule-Walker equations

$$
\begin{aligned}
\hat{\mathbf{q}} &= -\mathbf{R}^{-1}\mathbf{r}_0 \\
\hat{\sigma}_\varepsilon^2 &= r_{00} - \mathbf{r}_0^H \mathbf{R}^{-1}\mathbf{r}_0
\end{aligned}
\tag{4.29}
$$

where

$$
\hat{\mathbf{q}} = [\hat{q}_1, \ldots, \hat{q}_p]^T, \quad \mathbf{r}_0 = [r_{10}, \ldots, r_{p0}]^T, \quad \mathbf{R} = \begin{bmatrix} r_{11} & r_{12} & \cdots & r_{1p} \\ r_{21} & r_{22} & \cdots & r_{2p} \\ \vdots & \vdots & & \vdots \\ r_{p1} & r_{p2} & \cdots & r_{pp} \end{bmatrix}
$$

and

$$
r_{kl} = \frac{1}{M(N - pL_b)} \sum_{i=pL_b}^{N-1} \mathbf{c}^H(i - kL_b)\mathbf{c}(i - lL_b)
$$

Substituting the ML estimates in the log-likelihood function, and recalling that the prediction coefficients are complex and the prediction error variance is real, which follows that $\Theta^{(p)}$ has $2p + 1$ degrees of freedom, we obtain $(0 < p \leq g - 1)$

$$
\begin{aligned}
\mathrm{AIC}(p) &= 2M(N - pL_b)(\ln(\pi(r_{00} - \mathbf{r}_0^H\mathbf{R}^{-1}\mathbf{r}_0)) + 1) + 2(2p + 1) \tag{4.30} \\
\mathrm{MDL}(p) &= M(N - pL_b)(\ln(\pi(r_{00} - \mathbf{r}_0^H\mathbf{R}^{-1}\mathbf{r}_0)) + 1) + \frac{2p + 1}{2}\ln(N - pL_b)
\end{aligned}
$$
$$\tag{4.31}$$

For another approach of model order selection, recall that the channel vectors can be expressed as

$$
\mathbf{c}(n) = \sqrt{Gp_k} \sum_{i=1}^{p} \mathbf{v}(\theta_i)\beta_i e^{j2\pi f_i nT_s} + \eta(n)
\tag{4.32}
$$

where the model order p is interpreted as the number of dominant multipaths with Doppler frequencies $f_1, f_2, \ldots, f_p$. We write the channel sample matrix of the jth

antenna as

$$
\mathbf{C}_j = \begin{bmatrix} c_j(0) & c_j(K) & \cdots & c_j(\lfloor \frac{L_b-1}{K} \rfloor K) \\ c_j(L_b) & c_j(L_b+K) & \cdots & c_j(L_b+\lfloor \frac{L_b-1}{K} \rfloor K) \\ \vdots & \vdots & & \vdots \\ c_j((g-1)L_b) & c_j((g-1)L_b+K) & \cdots & c_j((g-1)L_b+\lfloor \frac{L_b-1}{K} \rfloor K) \end{bmatrix}
$$
(4.33)

where the downsampling factor L_b makes the channel poles $\{e^{j2\pi f_i L_b T_s}\}$ distinguishable on the complex plan, and the leaping factor K is chosen large enough such that the columns of $\mathbf{C}_j$ can be regarded as statistically independent complex Gaussian random vectors. The channel sample covariance matrix is defined by

$$
\hat{\mathbf{R}}_c = \frac{1}{MN'} \sum_{j=1}^{M} \mathbf{C}_j \mathbf{C}_j^H
$$
(4.34)

where $N' = \lfloor \frac{L_b-1}{K} \rfloor + 1$. Based on the eigenvalues of the channel sample covariance matrix, the model order can be estimated as similar to [56, 57].

4.5 Performance Analysis

Prediction Performance The relative amplitude change and the relative angle change of the channel vector $\mathbf{c}(n)$ at time n referring to $\mathbf{c}(n_0)$ at time n_0 are defined as [41]

$$
\mathcal{A}(\mathbf{c}(n), \mathbf{c}(n_0)) = 20 \log_{10} \frac{||\mathbf{c}(n)||}{||\mathbf{c}(n_0)||}
$$
(4.35)

$$
\cos(\widehat{\mathbf{c}(n), \mathbf{c}(n_0)}) = \frac{\mathbf{c}^H(n_0)\mathbf{c}(n)}{||\mathbf{c}(n_0)|| \cdot ||\mathbf{c}(n)||}
$$
(4.36)

We measure the time-variation of the vector channel as the amplitude change and the angle change of the current channel vector from the one at the beginning of the transmission frame. The relative amplitude change is usually small, because it is quite unlikely that all vector components vanish simultaneously. However,

59

the relative angle change of channel vectors can be drastic within a transmission frame. With a range of $[0, 1]$, the absolute value of the relative angle approaches 0 quickly in fast Rayleigh fading, which means then the channel vector becomes almost orthogonal to the one at the beginning of the frame.

Let $\mathbf{c}(n)$ and $\hat{\mathbf{c}}(n)$ denote the exact and the predicted channel vectors at downlink time n, respectively, we define the normalized root mean square error (RMSE) of the prediction of the channel as

$$\text{RMSE}(n) = \frac{\sqrt{E\{||\hat{\mathbf{c}}(n) - \mathbf{c}(n)||^2\}}}{\sqrt{E\{||\mathbf{c}(n)||^2\}}} \tag{4.37}$$

When the application of vector channel prediction is in beamforming to combat fast Rayleigh fading, both the relative amplitude and the relative angle between the exact and the predicted channel vectors should be incorporated in the evaluation of the prediction quality. We define the ratio $\gamma(n)$ as

$$\gamma(n) = \frac{||P_{\hat{\mathbf{c}}(n)}\mathbf{c}(n)||}{||\hat{\mathbf{c}}(n)||} \tag{4.38}$$

where $P_{\hat{\mathbf{c}}(n)}$ denotes the projection onto the subspace spanned by $\hat{\mathbf{c}}(n)$. From (4.13), (4.14) and (4.15), we know that the received signal power is proportional to $\gamma^2(n)$ as

$$\mathcal{P}_{s,l} \propto \gamma^2(l) = \left| \frac{\hat{\mathbf{c}}^H(l)\mathbf{c}(l)}{||\hat{\mathbf{c}}(l)||^2} \right|^2 \tag{4.39}$$

where l is the index of the beamforming group. We define the mean fluctuation of the received signal power in decibel as

$$\kappa_l = E\{|20\log_{10}\gamma(l)|\} \tag{4.40}$$

Suppose one sets the tolerance level of the received signal power fluctuation to κ dB. Then it is valid to indicate the prediction length, which is defined as the distance in wavelength from the last observed channel vector when $\gamma(n)$ starts to exceed the range $[10^{-\kappa/20}, 10^{\kappa/20}]$.

In the predictive downlink beamforming scheme, the N-symbol downlink frame is segmented evenly into g consecutive beamforming groups, each with L_b symbols. The prediction sampling rate is equal to the beamforming rate, which is determined by the speed of the mobile, that is, how rapidly the vector channel varies. In practice, the beamforming rate is much higher than twice the maximum Doppler frequency. For a fixed model order, increasing the beamforming rate will generally shorten the prediction length at low SNR . Besides the prediction length, there are other performance issues related to the beamforming rate, such as receive bit error probability and computational complexity of the algorithm.

Bit Error Probability on a Rayleigh Fading Channel with AWGN Suppose differential QPSK modulation is implemented in the system. For fading channels, the carrier phase changes rapidly when the channel exhibits a deep fade. This leads to an error floor that increases with the Doppler frequency. The bit error probability for DQPSK with Gray coding can be expressed as [45]

$$P_b(\gamma_b) = Q(a, b) - \frac{1}{2} e^{-\frac{1}{2}(a^2 + b^2)} I_0(ab) \tag{4.41}$$

where $Q(a, b)$ is the Marcum Q function, $I_0(x)$ is the modified Bessel function of order zero, and

$$a = \sqrt{2\gamma_b \left(1 - \frac{1}{\sqrt{2}}\right)} \tag{4.42}$$

$$b = \sqrt{2\gamma_b \left(1 + \frac{1}{\sqrt{2}}\right)} \tag{4.43}$$

γ_b is the received bit-energy-to-noise ratio

$$\gamma_b = \frac{|\alpha|^2 E_b}{N_0} = \frac{E_b}{N_0} \mathbf{w}^H \mathbf{a} \mathbf{a}^H \mathbf{w} \tag{4.44}$$

where E_b is the bit energy, N_0 is the variance of the Gaussian noise along the symbol vector, and $\alpha = \mathbf{w}^H \mathbf{a}$ is defined as the traffic channel of the particular mobile. The

code-processing gain is not included in the derivation. If the communication is over a Rayleigh fading channel without beamforming, $|\alpha|$ is a Rayleigh random variable, and the probability density function (PDF) of γ_b is

$$p_{\gamma_b} = \frac{1}{\bar{\gamma}_b} e^{-\frac{x}{\bar{\gamma}_b}} \tag{4.45}$$

where $\bar{\gamma}_b$ is the average received bit-energy-to-noise ratio. Assuming that the g predicted weight vectors perfectly compensate the channel fading at the middle of each beamforming group, i.e.

$$\mathbf{w}^H(l)\mathbf{a}(lL_b - \frac{L_b}{2}) = 1, \qquad l = 1, \ldots, g. \tag{4.46}$$

we have

$$\gamma_b(\tau)|_{\mathbf{a}(n_0)} = \frac{E_b}{N_0} \cdot \frac{\mathbf{a}^H(n_0)\mathbf{a}(n_0 + \tau)\mathbf{a}^H(n_0 + \tau)\mathbf{a}(n_0)}{||\mathbf{a}(n_0)||^4} \tag{4.47}$$

where n_0 indicates the middle point of a beamforming group. If the channel is Rayleigh faded, the elements of $|\mathbf{a}(n_0)|$ are independent Rayleigh random variables of the same mean. Suppose the PDF of $\gamma_b(\tau)$ for a fixed τ is $p_{\gamma_b(\tau)}$. Since τ can be chosen from $[-\frac{L_b}{2}, \frac{L_b}{2} - 1]$ with equal probability, γ_b has the PDF as

$$p_{\gamma_b} = \frac{1}{L_b} \sum_{\tau=-\frac{L_b}{2}}^{\frac{L_b}{2}-1} p_{\gamma_b(\tau)} \tag{4.48}$$

Finally, the average probability of bit error is given by

$$P_b = \int_0^\infty P_b(x) p_{\gamma_b}(x) dx \tag{4.49}$$

Without the piecewise stationary assumption for the channel, increasing the beamforming rate will likely reduce the bit-error-rate (BER) given perfect channel prediction. However at low SNR, this reduction of BER is shadowed by the degradation of prediction performance at high beamforming rate, especially for FDD systems without modification of the prediction coefficients as we will see in the simulations.

Algorithm Complexity   When calculating the prediction coefficients of the complex AR(p) model, the increase of the computational complexity from an implementation using g_1 beamforming groups to another using g_2 beamforming groups is

$$\Delta(g_1, g_2) = 8MN(2p^3 + p^2)\left(\frac{1}{g_1} - \frac{1}{g_2}\right). \tag{4.50}$$

where M is the channel vector dimension, and N is the length of the observation interval. The two implementations have the same estimated model order p satisfying $p+1 \leq g_1 < g_2$. On top of the low-complexity property of the AR model, this shows that, for relatively large number of beamforming groups in a frame, the increase in segmentations causes modest increase in the computational complexity of the prediction algorithm. However, frequent adjustment of the beamforming weights adds burden to the system hardware.

4.6   Subspace-Based Downlink Beamforming

Recall that there are two problems in the aforementioned conventional beamforming approach for signals over fast Rayleigh fading channels. First, the fast variation of the channel vector $\mathbf{a}(n)$ causes deep fades within an uplink frame or a downlink frame, which can not be compensated by a combining weight fixed over the frame. Secondly, the beamforming weights obtained during uplink may not function for downlink transmission, because the channel vector $\mathbf{a}(n)$ changes over duplex time. These problems have been successfully solved by the predictive downlink beamforming algorithm. However, radio channels for FDD uplink and downlink have independent fading. The beamforming weights obtained using received data through uplink can not be applied directly to downlink in FDD systems.

In order to combat fast Rayleigh fading, we construct the downlink beamforming weights using the uplink data, and transmit the weighted signal through
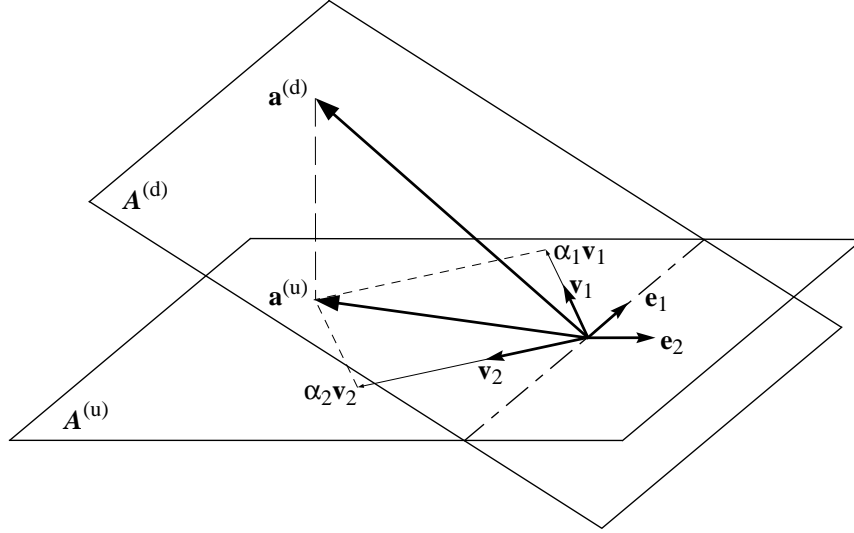
Figure 4.1: Uplink and downlink channel subspaces.

separable communication pipes. The combined signal power at the mobile is preserved despite the channel fades within the downlink frame. This beamforming approach is directly applicable in both TDD and FDD systems.

Downlink Beamforming for TDD   The uplink channel vector and the downlink channel vector, as expressed in (4.2), are the linear combinations of the array responses $\{\mathbf{v}^{(u)}(\theta_i)\}$ and $\{\mathbf{v}^{(d)}(\theta_i)\}$, respectively. Therefore,

$$
\begin{aligned}
\mathbf{a}^{(u)}(t) &\in \mathcal{A}^{(u)} = \operatorname{span}\{\mathbf{v}^{(u)}(\theta_1), \mathbf{v}^{(u)}(\theta_2), \ldots, \mathbf{v}^{(u)}(\theta_{L_s})\} \\
\mathbf{a}^{(d)}(t) &\in \mathcal{A}^{(d)} = \operatorname{span}\{\mathbf{v}^{(d)}(\theta_1), \mathbf{v}^{(d)}(\theta_2), \ldots, \mathbf{v}^{(d)}(\theta_{L_s})\}
\end{aligned}
\tag{4.51}
$$

where L_s is the total number of unresolvable multipaths in the link. $\mathcal{A}^{(u)}$ and $\mathcal{A}^{(d)}$ are defined as the uplink channel subspace and the downlink channel subspace, respectively. Assuming $L(< L_s)$ multipaths have prominent amplitudes, and the array responses $\{\mathbf{v}(\theta_i)\}$ of these dominant multipaths are independent, we define L as the effective rank of $\mathcal{A}^{(u)}$ and $\mathcal{A}^{(d)}$. Because the DOAs are large-scale parameters

64

of the time-varying channel, the array responses $\{\mathbf{v}(\theta_i)\}$, which are a basis of the channel subspace, change slowly compared to the channel fading rate. Therefore it is credible to assume that the channel subspaces are fixed over the time period of consideration. As the channel vector $\mathbf{a}(t)$ changes due to the variation of the complex amplitudes $\{\alpha_i(t)\}$, it is confined in the channel subspace as shown in Figure 4.1. In TDD systems with the same carrier frequency for both uplink and downlink, the array responses in both links are the same, and the uplink and downlink channel subspaces are identical. In Figure 4.1, the uplink channel subspace $\mathcal{A}^{(u)}$ and the downlink channel subspace $\mathcal{A}^{(d)}$ should coincide for TDD systems.

As in (4.7), the uplink signal as the output of the matched filter at the base station can be expressed as

$$\mathbf{y}(n) = \sqrt{Gp_k}\mathbf{a}(n)b(n) + \eta(n) = \sqrt{Gp_k}b(n)\sum_i \alpha_i(n)\mathbf{v}(\theta_i) + \eta(n) \qquad (4.52)$$

where $\eta(n)$ is the interference plus noise component. $\mathbf{v}(\theta_j)$ is assumed constant following previous discussion, and the mobile transmitting power p_k is assumed fixed over an uplink frame. The channel Rayleigh fading is caused by the Doppler effect of each complex amplitude $\alpha_i(n)$. Suppose the amplitudes of the path losses $\{|\rho_i|\}$ do not change over several frame periods, the spatial sample-covariance matrix of the uplink signal can be obtained by

$$\mathbf{R}_{yy} = \frac{1}{N}\sum_{n=1}^{N}\mathbf{y}(n)\mathbf{y}^H(n) = Gp_k\mathbf{V}\mathbf{P}\mathbf{V}^H + \mathbf{R}_{in} \qquad (4.53)$$

where

$$\mathbf{V} = [\mathbf{v}(\theta_1) \ \cdots \ \mathbf{v}(\theta_L)], \quad \mathbf{P} = \mathrm{diag}\{|\rho_1|^2, \ldots, |\rho_L|^2\}$$

and $\mathbf{R}_{in}$ includes the noise component and small cross-correlation between multipaths. The L principle eigenvectors of $\mathbf{R}_{yy}$, corresponding to the L largest eigenvalues, form an orthonormal basis $\{\mathbf{e}_i, i = 1, \ldots, L\}$ of the *effective channel subspace*. The effective rank L can be determined subjectively as the number of dominant

eigenvalues of $\mathbf{R}_{yy}$, provided that $L < M$. Or, it can be determined based on the application of the information theoretic criteria for model selection such as the one introduced in [56]. In TDD systems, the basis $\{\mathbf{e}_i\}$ obtained from uplink signal is an orthonormal basis of the effective downlink subspace, so the downlink channel vector $\mathbf{a}^{(d)}(t)$ approximates a linear combination as

$$\mathbf{a}^{(d)}(t) \approx \sum_{i=1}^{L} \mathbf{e}_i^H \mathbf{a}^{(d)}(t)\mathbf{e}_i = \sum_{i=1}^{L} \beta_i(t)\mathbf{e}_i \qquad (4.54)$$

with

$$||\mathbf{a}^{(d)}(t)||^2 = \sum_{i=1}^{L} |\beta_i(t)|^2. \qquad (4.55)$$

The base station uses L code channels to transmit the downlink signal to mobile k, and assigns the orthonormal basis vector as the antenna weight for each copy of the signal. The total transmitted signal can be written as

$$\mathbf{s}(t) = \sum_{i=1}^{L} \mathbf{e}_i^H s_i(t) \qquad (4.56)$$

where

$$s_i(t) = \sum_n b_k(n)g_i(t - nT_s)$$

Therefore, the signal received by the mobile is

$$x(t) = \mathbf{s}(t)\mathbf{a}^{(d)}(t) + n(t) = \sum_{i=1}^{L} \mathbf{e}_i^H \mathbf{a}^{(d)}(t)s_i(t) + n(t) \qquad (4.57)$$

By CDMA despreading, the mobile can divide the received signal into L copies which are transmitted using L code channels as

$$x_i(n) = \mathbf{e}_i^H \mathbf{a}^{(d)}(n)b_k(n) + \eta(n) = \beta_i(n)b_k(n) + \eta(n), \quad i = 1, \ldots, L \qquad (4.58)$$

The received power of each signal copy fluctuates within a downlink frame due to fast Rayleigh fading, whereas, the total signal power in the channel subspace remains

almost constant. One can combine separated signal copies after phase compensation, for example, using the differential phase shift keying (DPSK) modulation scheme as

$$
\begin{aligned}
\hat{x}(n) &= \sum_{i=1}^{L} x_i^*(n-1)x_i(n) = \sum_{i=1}^{L} |\beta_i(n)|^2 b_k^*(n-1)b_k(n) + w(n) \\
&= \sum_{i=1}^{L} |\beta_i(n)|^2 d_k(n) + w(n) = ||\mathbf{a}^{(d)}(n)||^2 d_k(n) + w(n) \quad (4.59)
\end{aligned}
$$

where $\{d_k(n)\}$ are the original bits, $\{b_k(n)\}$ are the differentially encoded bits. The downlink channel vector is assumed to be fixed over a symbol period, such that $\beta_i(n) = \beta_i(n-1)$. $w(n)$ is the interference plus noise component. The original symbol bit $d_k(n)$ is detected from $\hat{x}(n)$. Notice that

$$
\begin{aligned}
||\mathbf{a}^{(d)}(n)||^2 &= \mathbf{a}^{(d)H}(n)\mathbf{a}^{(d)}(n) \\
&= \sum_p \sum_q \alpha_p^*(n)\alpha_q(n)\mathbf{v}^H(\theta_p)\mathbf{v}(\theta_q) \\
&= \sum_{p,q} \beta_{p,q} e^{j2\pi(f_q - f_p)nT_s} \\
&= M \sum_{p=1}^{L} |\rho_p|^2 + 2\Re e\{\sum_{p<q} \beta_{p,q} e^{j2\pi(f_q - f_p)nT_s}\} \quad (4.60)
\end{aligned}
$$

where $\beta_{p,q} = \rho_p^*\rho_q \mathbf{v}_p^H \mathbf{v}_q e^{j2\pi(f_p\tau_p - f_q\tau_q + f_c(\tau_p - \tau_q))}$. $|\mathbf{v}_p^H \mathbf{v}_q| < ||\mathbf{v}_p||^2 = M$ when $p \neq q$. $||\mathbf{a}^{(d)}(n)||^2$ has a large positive term as in (4.60), and the fading is greatly ameliorated because it is quite unlikely that all vector components will vanish simultaneously. One observation is that when the number of dominant multipaths L is 1 or 2, there is no fading in $||\mathbf{a}^{(d)}(n)||^2$.

For a spatially white channel, $||\mathbf{a}^{(d)}(n)||^2$ has a χ_M^2 distribution. The channel amplitude $||\mathbf{a}^{(d)}(n)||$ varies slowly compared to the angle of the channel vector. The relative angle of two channel vectors at symbol time m and n is defined as

$$
\cos(\widehat{\mathbf{a}(m), \mathbf{a}(n)}) = \frac{\mathbf{a}^H(n)\mathbf{a}(m)}{||\mathbf{a}(n)|| \cdot ||\mathbf{a}(m)||} \quad (4.61)
$$

For fast Rayleigh fading channels, the relative angle changes rapidly when $|m - n|$ increases from 0 to the number of symbols of a data frame. With a range of $[0, 1]$,

the absolute value of the relative angle has a high probability to approach 0, which means then the two channel vectors are almost orthogonal to each other. The deep fades within a data frame attribute to the rapid change in the channel vector angle, and can not be compensated by the conventional beamforming. The proposed beamforming algorithm effectively eliminates the factor of angle change in the fading of the vector channel, and the combined signal is scaled by the more tractable amplitude of the vector channel.

Downlink Beamforming for FDD   In FDD systems, the base station assigns the L orthonormal basis vectors of the effective uplink channel subspace as the downlink beamforming weights. Therefore, $\beta_i(n) = \mathbf{e}_i^H \mathbf{a}^{(d)}(n)$ is the projection of the downlink channel vector onto the basis vector $\mathbf{e}_i$ of the effective uplink channel subspace. Similar to (4.59), the combined signal at the mobile reception is

$$\hat{x}(n) = \sum_{i=1}^{L} |\beta_i(n)|^2 d_k(n) + w(n) = ||P^{(u)} \mathbf{a}^{(d)}(n)||^2 d_k(n) + w(n) \qquad (4.62)$$

where $P^{(u)} \in \mathbb{C}^{M \times M}$ is the orthogonal projection onto the effective uplink subspace $\mathcal{A}^{(u)}$.

Although the instantaneous channels of uplink and downlink are uncorrelated when the channel coherence bandwidth is smaller than the carrier frequency separation [45], the DOAs are the same in uplink and downlink, and the distance between the uplink channel subspace and downlink channel subspace is negligible in a practical FDD system. As shown in Figure 4.1, the downlink channel vector $\mathbf{a}^{(d)}(n)$ almost lies in the uplink channel subspace $\mathcal{A}^{(u)}$, with $||P^{(u)} \mathbf{a}^{(d)}(n)|| \approx ||\mathbf{a}^{(d)}(n)||$. (See Appendix A).
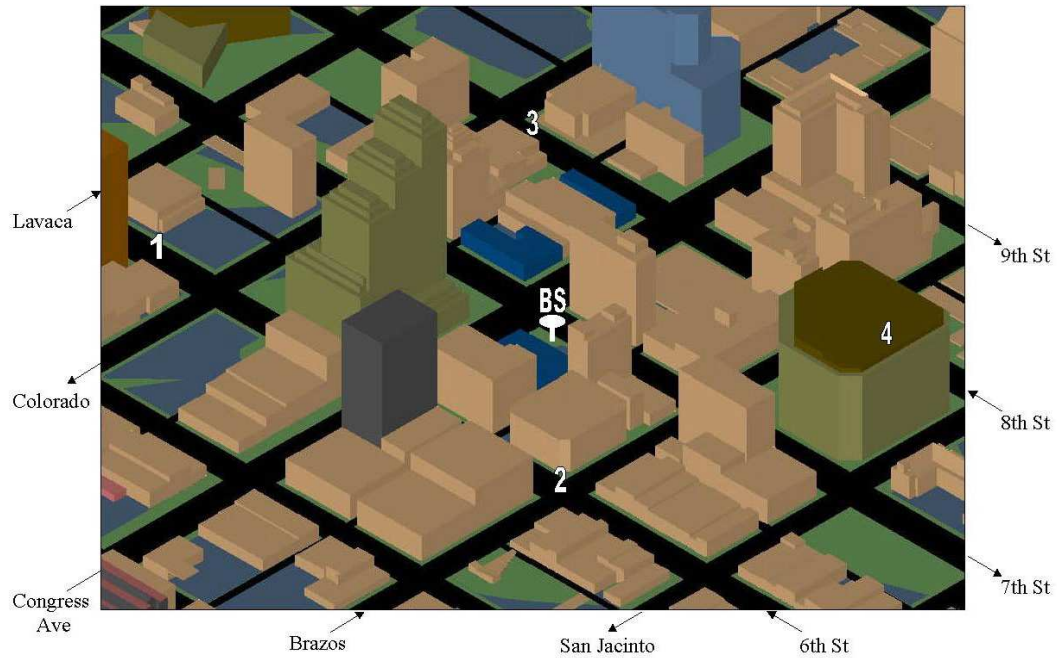
Figure 4.2: A wireless CDMA system which consists of a base station and four mobiles in the urban environment (CAD model) of downtown Austin, Texas. (Mobile 4 shown here is behind the building on 8th Street.)

4.7 Simulations

Simulations were conducted through an electromagnetic ray tracer FASANT [58, 59]. It was a deterministic ray tracing technique based on the geometric optics and the uniform theory of diffraction. (See Appendix B). We used the computer-aided design (CAD) model of downtown Austin, Texas (Figure 4.2) as the geometry input for the simulator. The material properties of the CAD model were: relative permittivity $\epsilon = 9.0$, relative permeability $\mu = 1.0$, conductivity $\sigma = 0.1$ for the building walls, and $\epsilon = 2.0$, $\mu = 1.0$, $\sigma = 0.001$ for the ground. Figure 4.2 shows a wireless CDMA system in the vehicular scenario, in which a base station communicates with four mobile users. The base station is located near the corner of 7th Street and Congress Avenue. Mobiles 1 and 2 move along 6th Street, and mobiles 3 and 4 move along

69
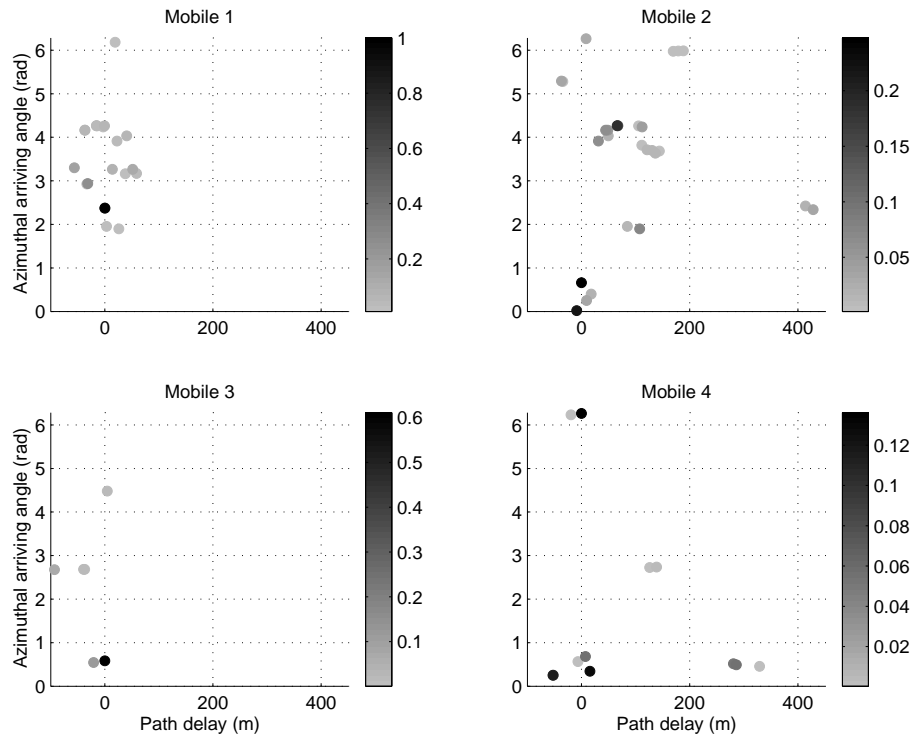
Figure 4.3: Azimuthal arriving angles versus path delays of multipaths viewed at the base station. The gray bar indicates the relative signal strength of each multipath.

8th Street, all at the city speed limit of 30 mph east to west. The base station has an 8-element uniform circular antenna array at a height of 20 m, with a radius of 0.085 m about half the carrier wavelength. The rooftop heights in this area range from approximately 8 m to 100 m. Each mobile has a single antenna, 1.5 m off the ground. The average direct distance from the mobiles to the base station is 250 m. All the mobiles experience non-line-of-sight (NLOS) propagation channels.

The ray tracing output of the dominant (in terms of received power) paths is shown in Figure 4.3 and Figure 4.4. The figures indicate the DOA, path delay and field strength of each multipath viewed at the base station and at each mobile, respectively. The receiving frame and the transmitting frame have equal length of 320 symbols over a time period of 5 ms. With a CDMA spreading gain of 8, the chip
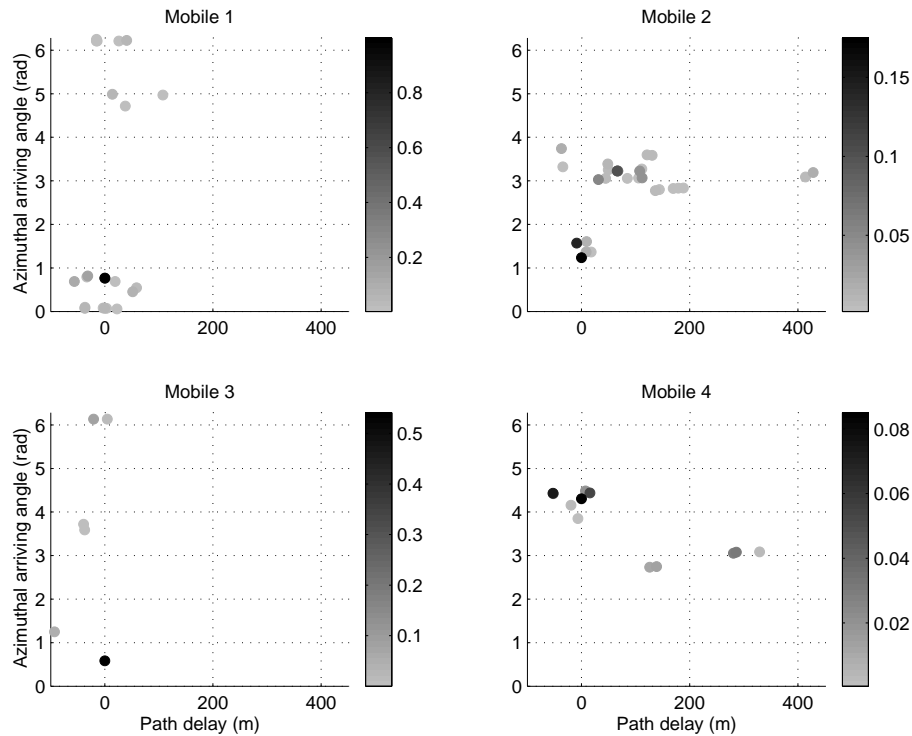
Figure 4.4: Azimuthal arriving angles versus path delays of multipaths viewed at each mobile. The gray bar indicates the relative signal strength of each multipath.

rate is 512 KHz, and the propagation length of one chip period is approximately 586 meters. The maximum delay spread of all the mobiles as shown in Figure 4.3 and Figure 4.4 is less than a chip period. Therefore we use one RAKE finger for base station reception, assuming that the finger is aligned to the arrival of the strongest multipath from each mobile. The signals are modulated by the differential quadrature phase shift keying (DQPSK). The pulse-shaping filter is a raised cosine function with rolloff factor 0.5.

For the predictive beamforming, the system is operated in FDD mode with uplink carrier of 1.8 GHz and downlink carrier of 2.0 GHz. Although the frequency spacing is as large as 10% of the carrier, we apply the prediction coefficients derived from the uplink channel directly to downlink channel feedbacks to simplify
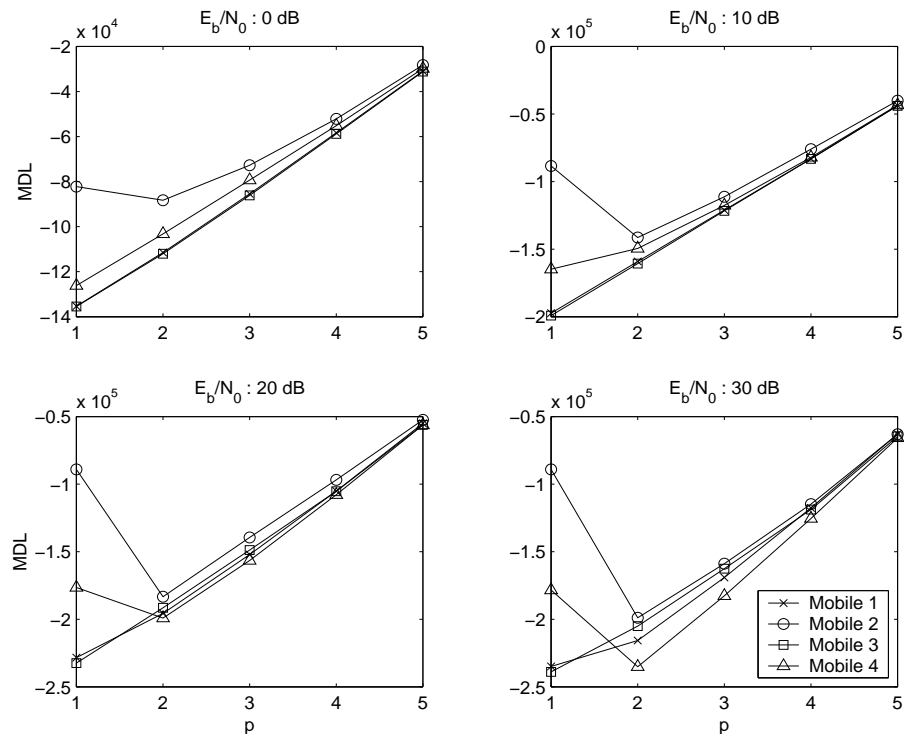
Figure 4.5: Model order selection by minimum description length criterion (MDL).

the implementation. Using the MDL criterion for the AR model order selection, Figure 4.5 shows, at high receive SNR, the estimated model orders are 1 for mobiles 1 and 3, and 2 for mobiles 2 and 4. This is in agreement with the multipath distribution exhibited in Figure 4.4, as the model order can be interpreted as the number of dominant multipaths with large angle difference from each other when arriving at the mobile. This difference in arriving angles at the mobile results in different Doppler components. In the prediction of downlink vector channels, we use the highest model order $p = 2$ for all 4 mobiles.

The channel prediction performance is demonstrated in Figure 4.6 and Figure 4.7. Figure 4.6 shows the normalized RMSE of the predicted downlink vector channels averaged over four mobiles. The RMSE of the predicted downlink channel is compared with that when the last channel feedback is assumed for current down-
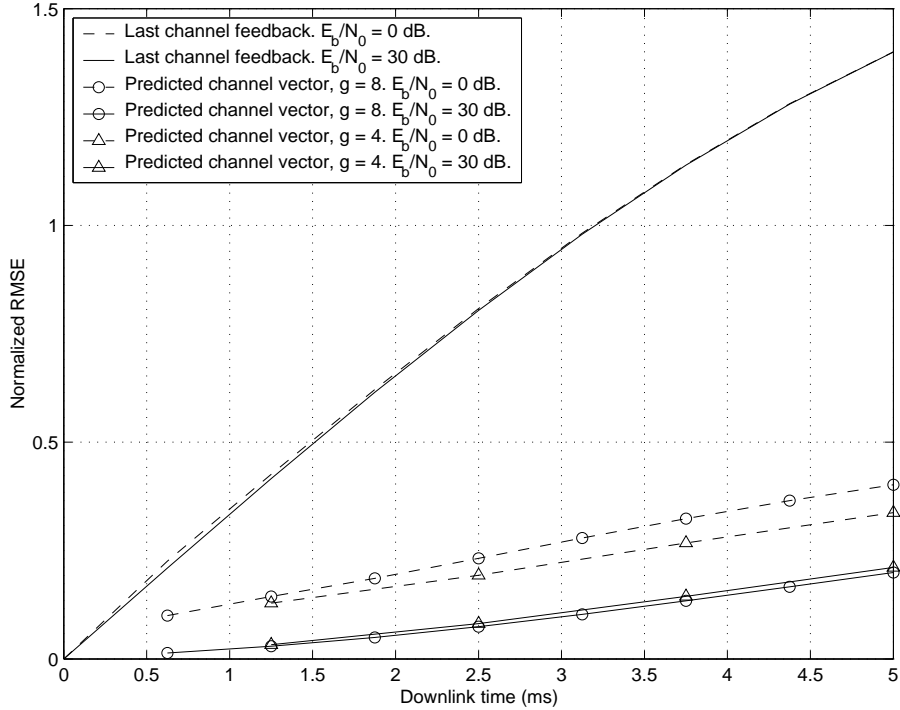
Figure 4.6: Normalized RMSE of vector channels averaged over four mobiles.

link. Although the prediction is performed in a FDD system without coefficient modification, the reduction in RMSE shows that the prediction provides sufficient knowledge of future channel variation, especially at high SNR when the prediction is more accurate. Two beamforming rates are chosen for comparison, with $g = 4$ and $g = 8$ accordingly. Comparing the predicted channel samples at corresponding downlink time, we see that at low SNR, the RMSE of low beamforming rate (low sampling rate), is smaller than that of high beamforming rate. Figure 4.7 compares the mean received signal power fluctuation κ of the predicted downlink with the mean power fluctuation when the last channel feedback is used to obtain the beamforming weights. κ is a measure of more importance to evaluate the performance of the prediction for beamforming. The downlink beamforming based on the channel prediction lowers the signal power fluctuation at the mobile receiving under fast

73
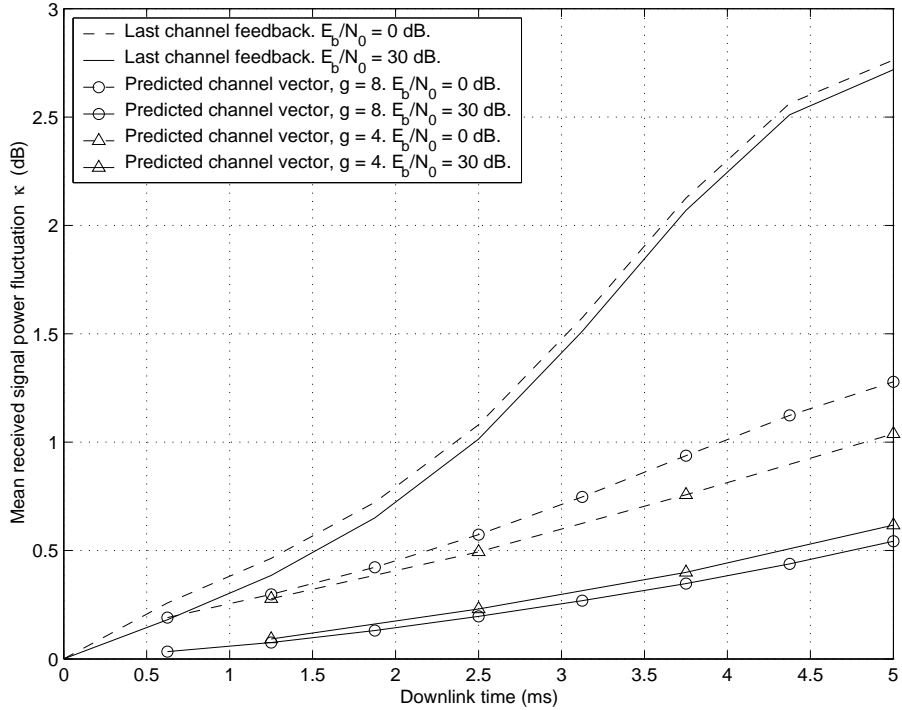
Figure 4.7: Mean fluctuation of the received signal power averaged over four mobiles.

Rayleigh fading as shown in Figure 4.7. At low SNR, the appropriate reduction in the beamforming rate provides better prediction performance as we compare $g = 4$ with $g = 8$.

Figure 4.8 gives the system performance in the average BER of the four mobiles on Rayleigh fading channels with AWGN. The BER of the link applying predictive beamforming is compared with that with no Rayleigh fading, and with that applying conventional beamforming, where the downlink weights are set according to the last channel feedback. The predictive downlink beamforming offers significant performance improvement. And not surprisingly, at low SNR, the predictive downlink beamforming using $g = 4$ outperforms the one using $g = 8$ due to its better channel prediction performance.

For subspace-based beamforming, the system is operated either in TDD mode
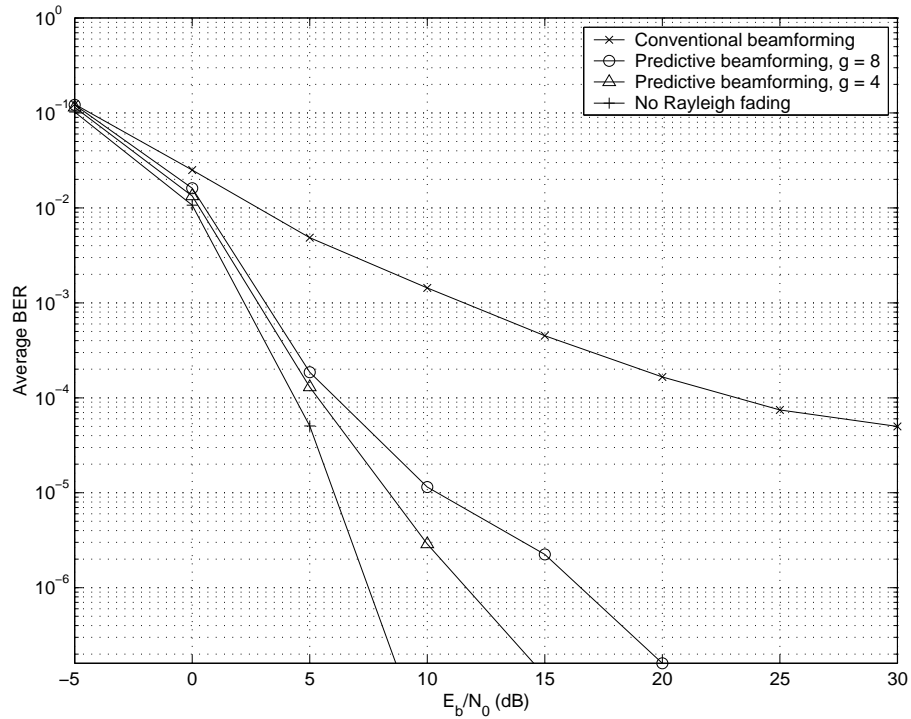
Figure 4.8: Average bit error rate for DQPSK on a Rayleigh fading channel with AWGN.

with uplink and downlink carriers of 1.8 GHz, or in FDD mode with an uplink carrier of 1.8 GHz and a downlink carrier of 2.0 GHz. Since the multipaths of mobile 2 have the largest angle spread (weighted by the field strength) at the base station as shown in Figure 4.3, and the largest angle spread at the mobile site as shown in Figure 4.4, the signal received by mobile 2 has the most severe Rayleigh fading. Therefore, we elaborate on mobile 2 to demonstrate the performance of the proposed downlink beamforming in the single user case. Figure 4.9 compares the 8 eigenvalues of the normalized spatial covariance matrix of the despreaded uplink signal of mobile 2, with interference from other mobile uplinks, and AWGN of 0, 10, 20 and 30 dB averaged over the receive antennas. At low and high SNR, all the plots show two dominant eigenvalues, with the rest more than 20 dB down. Therefore, the effective
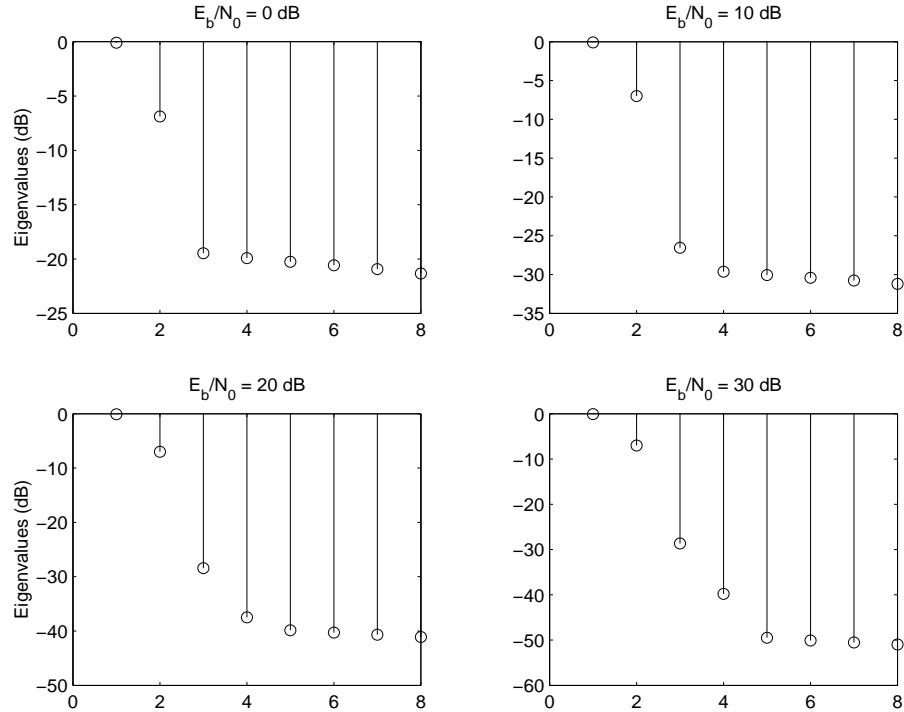
Figure 4.9: Eigenvalues of the normalized spatial covariance matrix of the de-spreaded uplink signal of mobile 2.

rank of the uplink channel subspace is $L = 2$.

Figure 4.10 shows the receiving bit error rate (BER) of mobile 2 in the single user case, in which the received signal has no multiple access interference but self interference. The AWGN at the mobile receiver ranges from -5 dB to 30 dB. As a comparison, we choose $L = 1, 2, 3$ to generate the beamforming weights from the uplink channel subspace, and use 1 code channel, 2 code channels and 3 code channels accordingly to transmit the downlink signal to mobile 2 in both TDD and FDD modes. The BER curves are lower-bounded by the BER with no Rayleigh fading. The proposed downlink algorithm using 1 code channel is merely the conventional beamforming, where the weight is constructed as the principle eigenvector of the spatial covariance matrix. The receiving performance is essentially
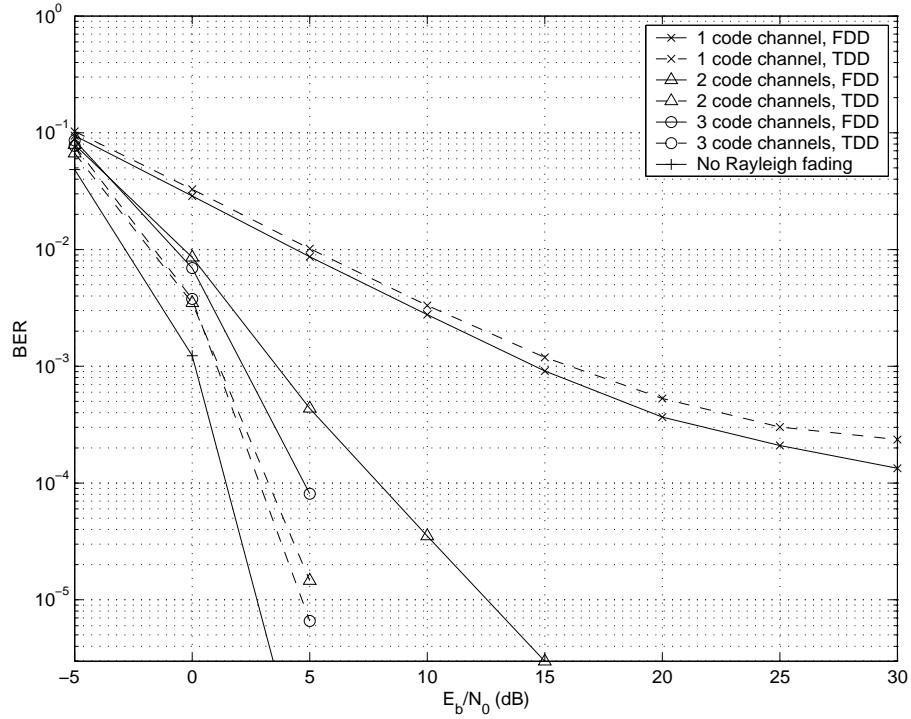
Figure 4.10: Bit error rate for DQPSK on a Rayleigh fading channel with AWGN. Single user case: mobile 2.

the same for TDD and FDD as indicated by the BER curves in the figure. When 2 sets of weights are used for downlink transmission through 2 code channels, the receiving BER reduces more than 10 dB in both TDD and FDD modes, especially at high SNR. And the merit of the algorithm in TDD is distinguished from that in FDD due to the estimation accuracy of the effective channel subspace in TDD systems. When 3 sets of weights are used for downlink transmission through 3 code channels, the receiving BER reduces even more. We observe that the beamforming advantage of using 3 sets of weights over using 2 sets of weights is not as big as that of 2 over 1. This is not unexpected since the effective rank of the channel subspaces is 2.

For the multiple user case, Figure 4.11 shows the eigenvalues of the normal-
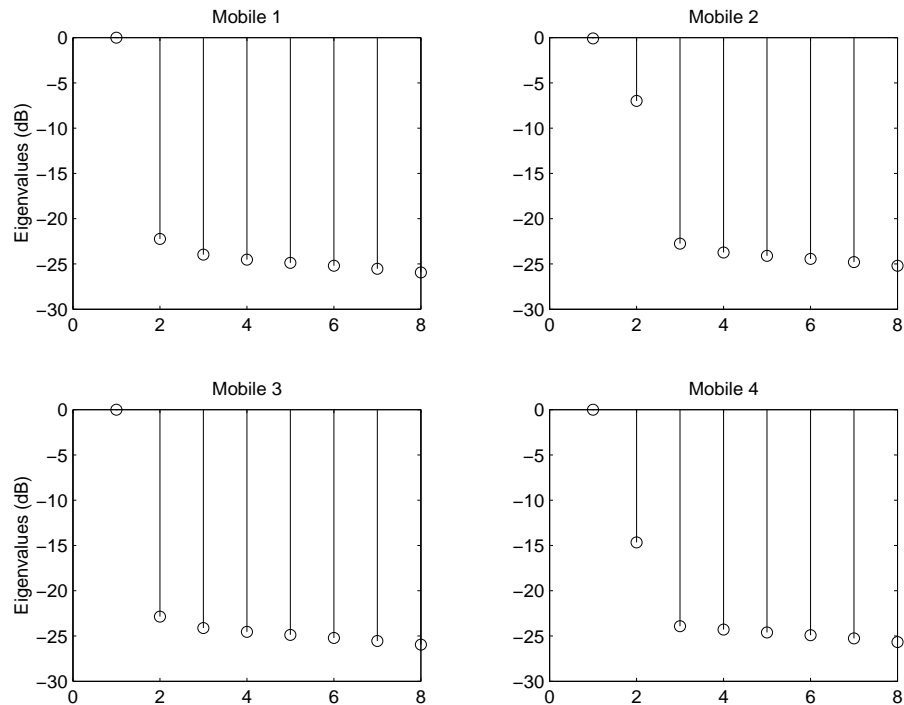
Figure 4.11: Eigenvalues of the normalized spatial covariance matrices of the despreaded uplink signals of the 4 mobiles. $E_b/N_0 = 10$ dB.

ized spatial covariance matrices of the despreaded uplink signals of the 4 mobiles. At a receiving SNR of 10 dB, there is one dominant eigenvalue of each of the spatial covariance matrices of mobiles 1 and 3, and two dominant eigenvalues of each of those of mobiles 2 and 4. The rest of the eigenvalues are all 20 dB down the largest ones. This is in agreement with the multipath angle distribution exhibited in Figure 4.3. Therefore, we infer that the effective rank of the uplink channel is 1 for mobiles 1 and 3, and 2 for mobiles 2 and 4.

We apply three schemes as a comparison to construct beamforming weights and to allocate the code channels accordingly for downlink transmission to all mobiles . In Scheme 1, one beamforming weight vector is used and 1 code channel is allocated for the transmitted signal to each mobile. In Scheme 2, 1 set of weight
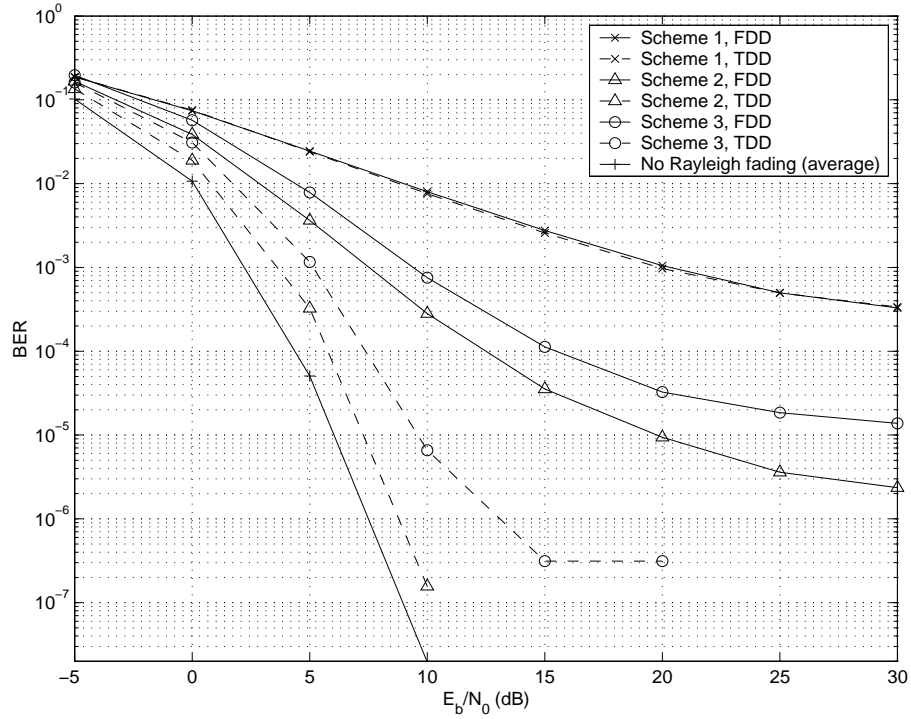
Figure 4.12: Bit error rate for DQPSK on a Rayleigh fading channel with AWGN. Mobile 2 in multiple user case.

is used and 1 code channel is allocated for the transmission to mobiles 1 and 3, and 2 sets of weights and 2 code channels for the transmission to mobiles 2 and 4. In Scheme 3, 2 sets of weights are used and 2 code channels are allocated for each mobile.

Figure 4.12 and Figure 4.13 illustrate the performance of the downlink reception of mobiles 2 and 4 in the multiple user case, respectively. Each BER is bounded by the BER with no Rayleigh fading averaged over 4 mobiles. As for mobiles 1 and 3, the channel has hardly any Rayleigh fading because there is only one dominant multipath in the link. The BERs of different beamforming schemes are almost the same and are close to the BER with no Rayleigh fading. For mobile 2, there are 2 dominant multipaths with nearly equal strength. The proposed
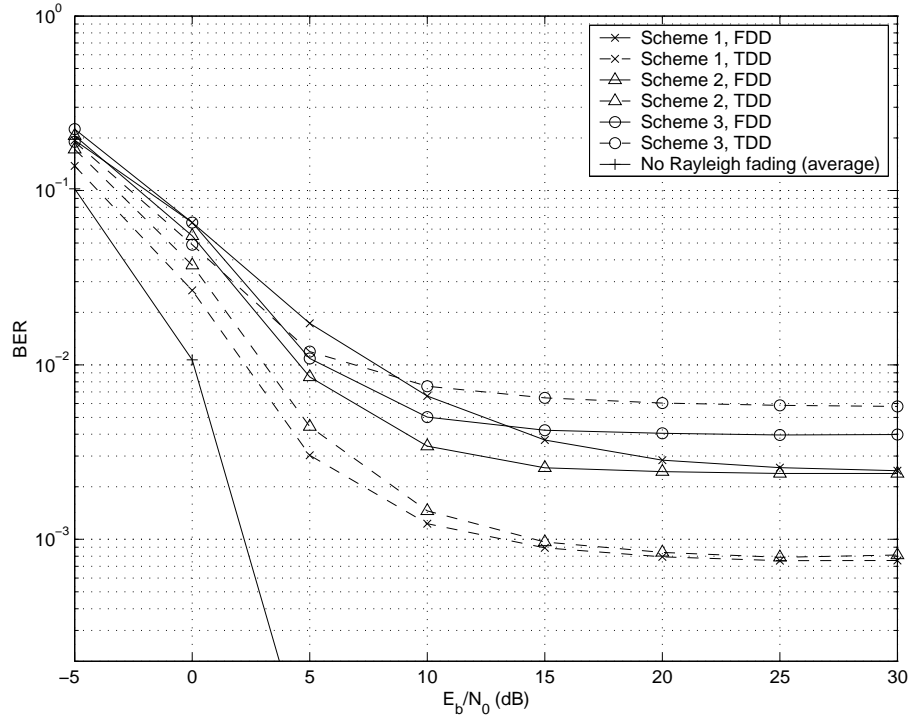
Figure 4.13: Bit error rate for DQPSK on a Rayleigh fading channel with AWGN. Mobile 4 in multiple user case.

beamforming algorithm which exploits the effective channel subspace (as in Scheme 2 and 3) outperforms the conventional beamforming (as in Scheme 1). However, the performance of Scheme 3 degrades compared to that of Scheme 2, even though additional resources of code channels are consumed. This is because it does not help combating the channel fading by using additional beamforming weights for over-estimated rank of the effective channel subspace, however, more code channels introduce more interference due to imperfect code orthogonality. For mobile 4, there are 2 dominant multipaths in the link, however, one is 15 dB weaker than the other as shown in Figure 4.11. Therefore, the advantage of exploiting 2-dimensional channel subspace for downlink transmission is limited, and it is overwhelmed by the extra interference as more code channels are used in the system.

80
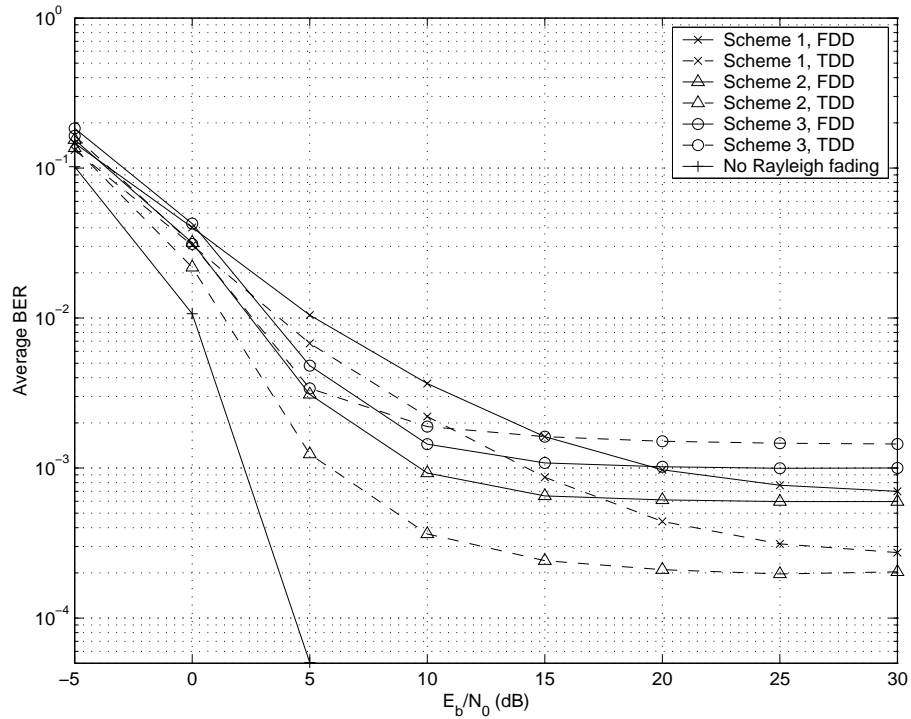
Figure 4.14: Average bit error rate for DQPSK on a Rayleigh fading channel with AWGN.

Figure 4.14 compares the average receiving BER of the 4 mobiles of different beamforming schemes. Despite the extra interference of using additional code channels, Scheme 2 gives the optimum overall performance, since its beamforming weight construction and code channel allocation fit well with the effective ranks of the channel subspaces. When we use more code channels than the effective ranks, the system performance degradation is mainly attributed to the situation of mobile 4.

4.8   Conclusions

The predictive downlink beamforming and the subspace-based downlink beamforming were proposed to combat the fast Rayleigh fading in the wireless channel. The

predictive beamforming enhances the system performance significantly even when implemented in FDD base stations without modification of the channel prediction coefficients, while maintaining the simplicity of mobile receiving. The algorithm has moderate complexity because it is based on the low-complexity channel prediction using the AR model.

The subspace-based beamforming outperforms the conventional one, provided that the effective rank of the channel subspace is well estimated. It can be implemented in TDD systems where the uplink and downlink channels are reciprocal, and in practical FDD systems with moderate performance degradation, thanks to the negligible distance between the uplink and downlink channel subspaces. The beamforming approach is not restricted to CDMA systems for which we exploited the code channels. In fact, using multiple CDMA code channels is just a means for the mobile to separate the signal copies weighted by the orthonormal basis vectors of the uplink channel subspace. There may be other methods for the effective separation, for instance, using the subcarriers of the orthogonal frequency division multiplexing (OFDM) systems.

Physical layer simulations have shown reduction in the receiving BER for both beamforming algorithms, compared to the systems using conventional downlink beamforming. The two proposed downlink beamforming approaches are bandwidth-efficient due to their open-loop nature, and each of them can be combined with iterative beamforming schemes for optimal system performance.

Chapter 5

Subspace-Based Estimation for Wideband CDMA Channels

5.1 Introduction

In this chapter, we consider the estimation of multiuser vector channels for wideband CDMA systems. In wideband CDMA (W-CDMA) systems, the intersymbol interference (ISI) introduced by multipath propagation can be significant due to the large multipath delay spread. ISI, together with the user asynchronism in the reverse link, distorts the code orthogonality. Therefore, explicit knowledge of all user channels is needed for equalization and multiuser detection. One of the key features of W-CDMA systems is the pilot-assisted channel estimation, in which a large portion of the bandwidth is reserved for the training sequence overhead. If the pilots are inserted sparsely in the transmitted data stream, the performance of channel estimation is limited in a fast-fading environment.

Alternatively, blind channel estimation offers better spectrum efficiency, and has received increasing attention [60, 61, 62, 63, 64]. Subspace-based channel estimation for CDMA systems exploits the eigenstructure of the received data matrix,

allowing reconstruction of signature waveforms without the knowledge of input signals. By assuming knowledge of the user codes but no training sequences, these subspace-based blind techniques model each of the user channels as an FIR filter and identify it by exploiting the second-order statistics of the channel output. In W-CDMA, the order of an FIR filter identifying the entire user channel can be quite large.

Improved performance in statistical estimation can be expected if one can put enough constraints on the model structure. Modifications have been made in [65] to reduce the number of unknown parameters, where the knowledge of the structure of the propagation channel is incorporated in the subspace methods. However, an extensive multidimensional optimization search is required in this parametric subspace approach.

In this chapter, we propose a deterministic approach to estimate the user channels in W-CDMA systems. Taking into account the *a priori* information of the structure of the propagation channel, we describe the channel by a reduced number of model parameters, i.e. two separable sets of spatial and temporal parameters. Our approach is computationally more efficient than the traditional subspace method on the unstructured channel. The nominal path arrival angles and delays, which describe the general propagation structure, vary slowly compared to the multipath fading rate. They can be estimated and tracked using a small number of pilot symbols over a long period of time. In the following sections, the reverse link (uplink) of the W-CDMA communication systems is considered.

5.2 An Overview of Wideband CDMA Systems

CDMA systems do not have the same hard channel limits as other systems (such as a fixed number of time slots, RF carriers); capacity is usually determined not by the number of channel processing element available, but by the total available transmit

RF bandwidth (MHz)	Downlink rates (Kb/s)	Uplink rates (Kb/s)
1.25	$1.2 - 307.2$	$1.2 - 307.2$
3.75	$1.2 - 1036.8$	$1.2 - 1036.8$
7.5	$1.2 - 2073.6$	$1.2 - 2073.6$
11.25	$1.2 - 2457.6$	$1.2 - 2073.6$
15	$1.2 - 2457.6$	$1.2 - 2073.6$

Table 5.1: Channel bandwidths and data rates supported by cdma2000

power or total interference. Therefore, CDMA radio technology is considered a better choice to satisfy the requirements of 3G wireless systems. Furthermore, services that offer multimedia and high data rates demand a wider bandwidth spectrum for CDMA. W-CDMA radio transmission technologies provide a true multimedia system that offers improved capacity for both voice and data applications and accessibility to Internet applications at high data rate. The goal is to support at least 384 Kb/s with wide area coverage and up to 2 Mb/s with local area coverage.

The cdma2000 radio transmission technology (RTT) proposed by North America meets the IMT-2000 requirement and also retains backward compatibility with existing cdmaOne networks without any compromise in system performance or capabilities [66]. Table 5.1 shows the RF bandwidths and data rates supported by the cdma2000 radio interface. Two spreading options, namely multi-carrier (MC) and direct-spread (DS), are identified in the W-CDMA RTT.

1. MC-CDMA allows operator to cascade many 1.25-MHz bandwidth carriers to form a wideband system. The modulation symbols after coding and interleaving are demultiplexed onto N carriers of 1.25 MHz each ($N = 3, 6, 9, 12$), where each carrier has a chip rate of 1.2288 Mc/s.

2. DS-CDMA has a single wideband carrier. The modulation symbols are direct sequence spread using a chip rate of $N \times 1.2288$ Mc/s ($N = 1, 3, 6, 9, 12$) and
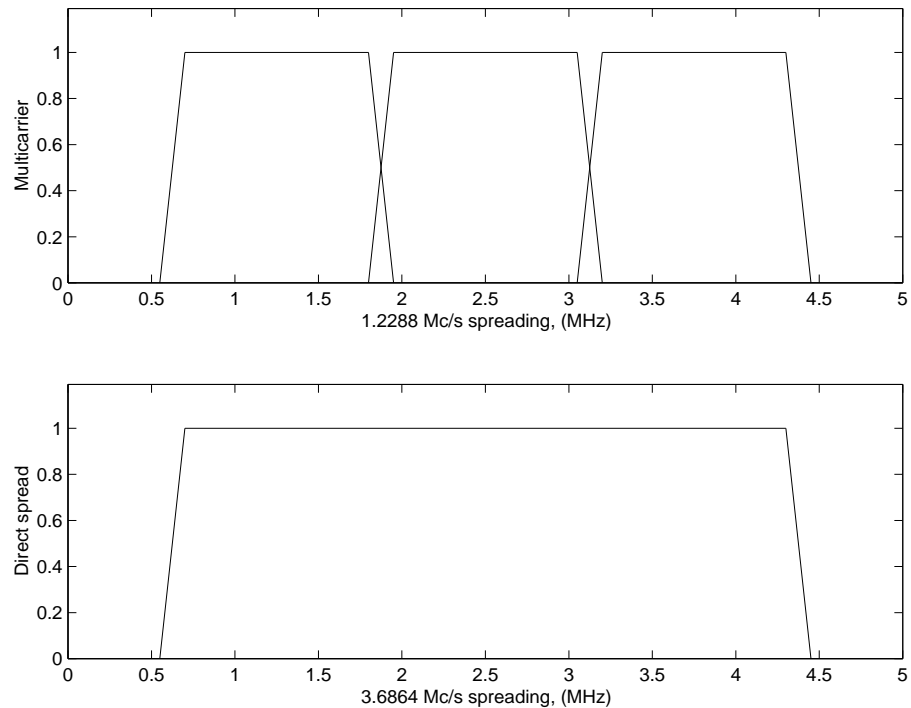
Figure 5.1: W-CDMA spreading options for an N = 3 system.

the spread signal is modulated onto a single carrier.

Figure 5.1 illustrates the two options for an $N = 3$ system.

IMT-2000 has targeted PCS systems at bands around 2 GHz. In addition, IEEE 802.11-based WLANs operate in the 2.4-GHz ISM band. The frequencies in this region have several attractive features, such as wide coverage and less requirement for antenna size and separation.

5.3 Analytical Model of W-CDMA Systems

Structured Channel Model   Consider the case of a mobile user communicating with a base station (BS) with an array of M antenna elements. The baseband

multipath fading vector channel response can be described as [45]

$$\mathbf{h}(t) = \sum_{i=1}^{P} \mathbf{a}(\theta_i)\beta_i p(t - \tau_i) \tag{5.1}$$

where P is the total number of paths. $p(t)$ is the chip pulse shaping filter. $\mathbf{a}(\theta_i)$, β_i and τ_i are the array response, the complex amplitude and the delay associated with the ith path, respectively. In W-CDMA systems, the multipath delay spread may span several symbol periods.

In the reverse link, the signals transmitted by the mobile users are first scattered by objects local to the mobile, and then the scattering ray bundles are reflected or diffracted by objects remote to the mobile. Within each bundle of rays from a remote reflector, the scattering rays come with arrival angles close to the nominal direction-of-arrival (DOA) and arrive at the BS with a small delay spread. The delay difference between ray bundles are relatively large. Assume that the nominal delays of ray bundles are separable by the W-CDMA receiver. This propagation structure causes BS path arrivals to cluster in a 2-D direction-of-arrival (DOA) vs. time-of-arrival (TOA) plot.

Suppose there are Q DOA-TOA clusters viewed by the BS. The channel response corresponding to the qth cluster can be described as

$$\mathbf{h}_q(t) = \sum_{k=1}^{P_q} \mathbf{a}(\theta_q + \tilde{\theta}_{qk})\beta_{qk} p(t - \tau_{qk}) \tag{5.2}$$

where P_q is the number of scattering paths within. $\theta_q + \tilde{\theta}_{qk}$ is the arrival angel with nominal DOA θ_q. With $|\tilde{\theta}_{qk}|$ being small, a first-order Taylor series expansion of (5.2) yields (we drop the subscript q on the right side)

$$
\begin{aligned}
\mathbf{h}_q(t) &\simeq \sum_k (\mathbf{a}(\theta) + \tilde{\theta}_k \mathbf{d}(\theta))\beta_k p(t - \tau_k) \\
&= \mathbf{a}(\theta) \sum_k \beta_k p(t - \tau_k) + \mathbf{d}(\theta) \sum_k \tilde{\theta}_k \beta_k p(t - \tau_k) \\
&= \mathbf{a}(\theta) g_1(t - \tau) + \mathbf{d}(\theta) g_2(t - \tau) \tag{5.3}
\end{aligned}
$$

where $\mathbf{d}(\theta) = \partial \mathbf{a}(\theta)/\partial \theta$ is the gradient. Therefore the entire vector channel response follows as

$$\mathbf{h}(t) = \sum_{q=1}^{2Q} \mathbf{a}_q \ g_q(t - \tau_q) \tag{5.4}$$

where, each path cluster as a dispersive channel is modeled as two FIR filters $g_{2i-1}(t)$ and $g_{2i}(t)$ $(i = 1, \ldots, Q)$, with short supports compared to the symbol period. $\{\tau_q\}$ are the nominal delays and are assumed to be pre-estimated by the BS. Note that because $\{g_q(t)\}$ are somewhat arbitrary, the nominal delays do not need to be estimated precisely, and they can be easily tracked when channel varies. We process $\{\mathbf{a}_q\}$ as arbitrary vectors.

Data Model   In CDMA systems, the transmitted symbols are spread to chip-rate data by the user-specified spreading code of length L_c. The signal received at BS antenna array is $\mathbf{x}(t) = \mathbf{w}(t) * s(t)$, where $s(t)$ is the transmitted signal. Vector $\mathbf{w}(t)$ is the user signature waveform, which is the convolution of the spreading code and the channel response $\mathbf{w}(t) = c(t) * \mathbf{h}(t)$. We introduce the notation for the discrete-time data sampled at the chip rate

$$\bar{\mathbf{x}}(k) \;=\; [\mathbf{x}^T(kL_c - L_c + 1) \;\cdots\; \mathbf{x}^T(kL_c)]^T \tag{5.5}$$

$$\bar{\mathbf{h}} \;=\; [\mathbf{h}_1^T \ \mathbf{h}_2^T \;\cdots\; \mathbf{h}_{L_h}^T]^T \tag{5.6}$$

$$\bar{\mathbf{w}} \;=\; [\mathbf{w}_1^T \ \mathbf{w}_2^T \;\cdots\; \mathbf{w}_{L_c+L_h-1}^T]^T \tag{5.7}$$

where L_h is the channel length of $\mathbf{h}(t)$. The signature waveform $\bar{\mathbf{w}}$ can be expressed

as

$$
\bar{\mathbf{w}} = \underbrace{\left[\begin{array}{cccc} c_1 & & & \\ \vdots & \ddots & & \\ c_{L_c} & & c_1 & \\ & \ddots & & \vdots \\ & & & c_{L_c} \end{array}\right]}_{\mathbf{C}} \otimes \mathbf{I}_M \ \bar{\mathbf{h}} \tag{5.8}
$$

where $\{c_k, \ k = 1, 2, \ldots, L_c\}$ is the spreading code, and $\otimes$ denotes the Kronecker product. From (5.4), the discrete vector channel can be expressed as

$$
\bar{\mathbf{h}} = \mathbf{G} \ \bar{\mathbf{a}} \tag{5.9}
$$

where $\bar{\mathbf{a}} = [\mathbf{a}_1^T \cdots \mathbf{a}_{2Q}^T]^T$ and $\mathbf{G} = \mathcal{G} \otimes \mathbf{I}_M$. $\mathcal{G}$ is a $L_h \times 2Q$ matrix whose columns are defined as

$$
\mathrm{Col}^{(q)}\{\mathcal{G}\} = \underbrace{\left[\begin{array}{c} \mathbf{0}_{\mathrm{I}} \\ --- \\ \mathbf{I}_{L_g} \\ --- \\ \mathbf{0}_{\mathrm{II}} \end{array}\right]}_{\mathcal{F}_q} \underbrace{\left[\begin{array}{c} g_q(1) \\ g_q(2) \\ \vdots \\ g_q(L_g) \end{array}\right]}_{\mathbf{g}_q} \tag{5.10}
$$

where $\mathbf{0}_{\mathrm{I}}$ and $\mathbf{0}_{\mathrm{II}}$ are zero matrices with dimensions $l_q \times L_g$ and $(L_h - L_g - l_q) \times L_g$, respectively. l_q is the known nominal delay index. L_g is the maximum order of FIR filters $\{\mathbf{g}_d, \ d = 1, \ldots, 2Q\}$.

The vector channel from (5.4) can also be expressed as

$$
\bar{\mathbf{h}} = \mathbf{A} \ \bar{\mathbf{g}} \tag{5.11}
$$

where $\bar{\mathbf{g}} = [\mathbf{g}_1^T \cdots \mathbf{g}_{2Q}^T]^T$ and $\mathbf{A}$ is a $ML_h \times 2QL_g$ matrix defined as

$$
\mathbf{A} = [\mathcal{F}_1 \otimes \mathbf{a}_1, \ \mathcal{F}_2 \otimes \mathbf{a}_2, \cdots, \mathcal{F}_{2Q} \otimes \mathbf{a}_{2Q}] \tag{5.12}
$$

Suppose signature waveform $\bar{\mathbf{w}}$ spans L symbols, i.e. $L = \lceil \frac{L_h - 1}{L_c} \rceil + 1$, we partition vector $\bar{\mathbf{w}}$ into L parts, each having length ML_c. If the last one does not have sufficient elements, it is padded with zeros. Each part is denoted as

$$\bar{\mathbf{w}}_k = [\mathbf{w}_{kL_c - Lc + 1}^T \quad \mathbf{w}_{kL_c - Lc + 2}^T \quad \cdots \quad \mathbf{w}_{kL_c}^T]^T \tag{5.13}$$

Therefore the noiseless baseband signal received by the BS over a symbol period sampled at the chip rate is

$$\bar{\mathbf{x}}(k) = [\bar{\mathbf{w}}_L \; \bar{\mathbf{w}}_{L-1} \cdots \bar{\mathbf{w}}_1] \begin{bmatrix} s(k-L+1) \\ s(k-L+2) \\ \vdots \\ s(k) \end{bmatrix} \tag{5.14}$$

where $\{s(k)\}$ are the information bearing symbols, which belong to a finite alphabet. Collecting data $\bar{\mathbf{x}}(k)$ from N consecutive symbol periods, we form a Hankel matrix as

$$\mathbf{X} = \begin{bmatrix} \bar{\mathbf{x}}(1) & \bar{\mathbf{x}}(2) & \cdots & \bar{\mathbf{x}}(N-K+1) \\ \bar{\mathbf{x}}(2) & \cdots & \cdots & \bar{\mathbf{x}}(N-K+2) \\ \vdots & & & \vdots \\ \bar{\mathbf{x}}(K) & \cdots & \cdots & \bar{\mathbf{x}}(N) \end{bmatrix} = \mathbf{WS} \tag{5.15}$$

where $K (< N)$ is defined as the *smoothing factor*, and

$$\mathbf{W} = \begin{bmatrix} \bar{\mathbf{w}}_L & \cdots & \bar{\mathbf{w}}_1 & & \\ & \bar{\mathbf{w}}_L & \cdots & \bar{\mathbf{w}}_1 & \\ & & \ddots & & \ddots \\ & & & \bar{\mathbf{w}}_L & \cdots & \bar{\mathbf{w}}_1 \end{bmatrix}_{ML_cK \times (K+L-1)} \tag{5.16}$$

$$\mathbf{S} = \begin{bmatrix} s(-L+2) & \cdots & s(N-K-L+2) \\ s(-L+3) & \cdots & s(N-K-L+3) \\ \vdots & & \vdots \\ s(K) & \cdots & s(N) \end{bmatrix} \tag{5.17}$$

90

5.4 Subspace-Based Channel Estimation

In the presence of additive white noise, the data matrix in (5.15) becomes

$$\mathbf{X} = \mathbf{W}\mathbf{S} + \mathbf{N} \qquad (5.18)$$

We construct the data matrix by choosing K as $\frac{L-1}{ML_c-1} < K < \frac{N-L}{2} + 1$, such that $\mathbf{W}$ is a tall matrix and $\mathbf{S}$ is a wide matrix. Due to channel independence and the randomness of symbol sequences, it is safe to assume that $\mathbf{W}$ is of full column rank and $\mathbf{S}$ is of full row rank. Perform singular value decomposition (SVD) on $\mathbf{X}$ as

$$\mathbf{X} = [\mathbf{U}_s\ \mathbf{U}_n] \begin{bmatrix} \boldsymbol{\Sigma}_s & \mathbf{0} \\ \mathbf{0} & \boldsymbol{\Sigma}_n \end{bmatrix} \begin{bmatrix} \mathbf{V}_s^H \\ \mathbf{V}_n^H \end{bmatrix} \qquad (5.19)$$

where $\mathbf{U}_s$ is a $ML_cK \times (K+L-1)$ matrix, and $\mathbf{U}_n$ is a $ML_cK \times (ML_cK-K-L+1)$ matrix. The orthonormal vectors in $\mathbf{U}_s$ associated with the signal eigenvalues span the *signal subspace*, which is also the column space of $\mathbf{W}$, whereas the orthonormal vectors in $\mathbf{U}_n$ associated with the noise eigenvalues span the *noise subspace*. Due to the orthogonality between the signal subspace and the noise subspace, the columns of $\mathbf{W}$ are orthogonal to any vector in the noise subspace. Since the matrix $\mathbf{W}$ depends linearly on $\bar{\mathbf{w}}$, we have

$$\mathbf{U}_n \perp \mathbf{W} \Rightarrow\ \mathcal{U}_n^H \bar{\mathbf{w}} = \mathbf{0} \qquad (5.20)$$

where $\mathcal{U}_n = [\mathcal{T}(\mathbf{u}_1)\ \cdots\ \mathcal{T}(\mathbf{u}_r)]$ with $r = ML_cK - K - L + 1$. $\mathcal{T}(\mathbf{u}_i)$ is a $ML_cL \times (K+L-1)$ block-Hankel matrix. $\mathbf{u}_i$ is the ith column of $\mathbf{U}_n$ and is partitioned into K blocks with each being a vector of length ML_c. Following (5.8), (5.9) and (5.11), the linear equation (5.20) can be written as

$$\mathcal{U}_n^H \mathbf{C}\mathbf{A}\bar{\mathbf{g}} = \mathbf{0} \qquad (5.21)$$

$$\text{or} \qquad \mathcal{U}_n^H \mathbf{C}\mathbf{G}\bar{\mathbf{a}} = \mathbf{0} \qquad (5.22)$$

We choose the array response $\mathbf{a}(\theta_i)$ and its gradient $\mathbf{d}(\theta_i)$ from a point source for the nominal DOA θ_i as the initial values for $\mathbf{a}_{2i-1}$ and $\mathbf{a}_{2i}$ $(i = 1, \ldots, Q)$. Under the

non-triviality constraint $||\bar{\mathbf{g}}|| = 1$, (5.21) can be solved for fixed $\{\mathbf{a}_q\}$ in the least-square sense, i.e. $\hat{\bar{\mathbf{g}}}$ is the normalized eigenvector corresponding to the minimum eigenvalue of the matrix $\mathbf{A}^H \mathbf{C}^H \mathcal{U}_n \mathcal{U}_n^H \mathbf{C} \mathbf{A}$. Substituting $\hat{\bar{\mathbf{g}}}$ into matrix $\mathbf{G}$, we can obtain $\{\mathbf{a}_i\}$ as the least-square solution of (5.22), under the constraint $||\bar{\mathbf{a}}|| = 1$. Thus we have identified $\bar{\mathbf{a}}$ and $\bar{\mathbf{g}}$, and can construct the signature waveform matrix $\mathbf{W}$ up to a phase ambiguity.

In the algorithm development, we assumed that L_g, the maximum order of FIR filters $\{g_q(t)\}$, and the channel length L_h are known *a priori*. In practice, one may select the maximum local scattering channel spread value for L_g in a particular application [45], and overestimate the channel order as $\hat{L}_h$. Therefore, the subspace spanned by $\hat{\mathbf{U}}_n$ is included in the (true) noise subspace, and the linear equation (5.20) is still established.

The extension of the algorithm to multi-user systems is straight forward. Suppose there are R active mobile users in the BS cell, we can rewrite (5.18) as

$$\mathbf{X} = \mathbf{W}\mathbf{\Gamma}\mathbf{S} + \mathbf{N} \tag{5.23}$$

where,

$$\mathbf{W} = [\mathbf{W}_1 \ \mathbf{W}_2 \ \cdots \ \mathbf{W}_R] \tag{5.24}$$

$$\mathbf{\Gamma} = \mathrm{diag}(\underbrace{\gamma_1, \ldots, \gamma_1}_{K+L-1}, \ldots, \underbrace{\gamma_R, \ldots, \gamma_R}_{K+L-1}) \tag{5.25}$$

$$\mathbf{S} = [\mathbf{S}_1^T \ \mathbf{S}_2^T \ \cdots \ \mathbf{S}_R^T]^T \tag{5.26}$$

γ_i $(i = 1, \ldots, R)$ is the channel gain of the ith user. Assume that both symbol and noise are zero-mean i.i.d. random variables with variance σ_s^2 and σ_n^2, respectively. And assume σ_s^2 is known to be 1. The data covariance matrix is therefore

$$\mathbf{R}_x = \frac{1}{N - K + 1} \mathrm{E}\{\mathbf{X}\mathbf{X}^H\} = \mathbf{W}\mathbf{\Gamma}\mathbf{\Gamma}^H \mathbf{W}^H + \sigma_n^2 \mathbf{I} \tag{5.27}$$

Hence, a good estimate of the user channel gain is given by

$$\hat{\mathbf{\Gamma}}\hat{\mathbf{\Gamma}}^H = \mathrm{diag}\{\hat{\mathbf{W}}^\dagger (\hat{\mathbf{R}}_x - \hat{\sigma}_n^2 \mathbf{I})(\hat{\mathbf{W}}^\dagger)^H\} \tag{5.28}$$
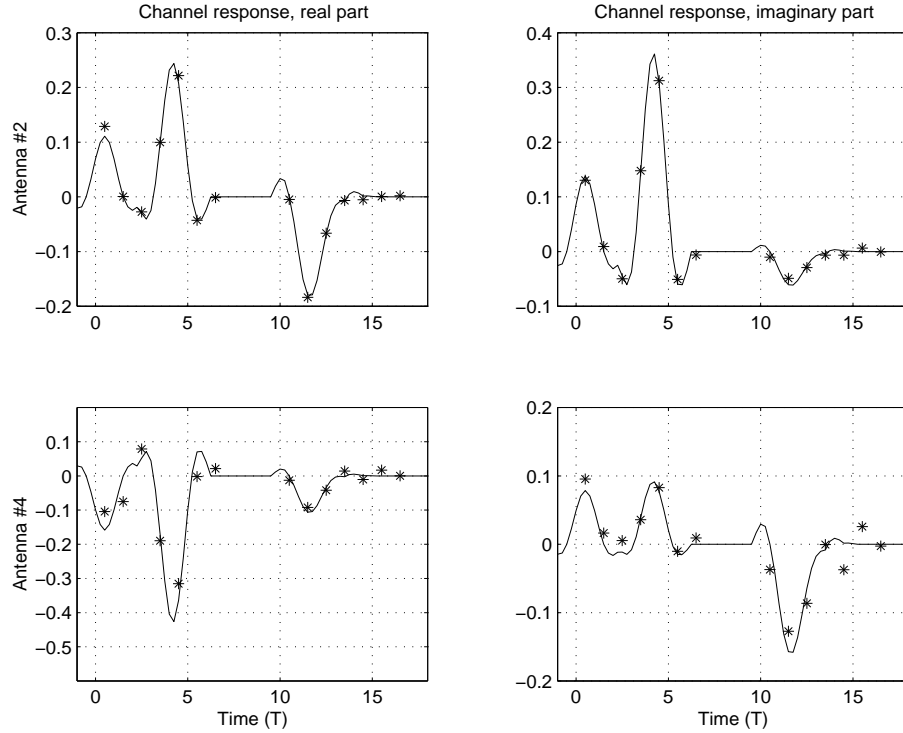
Figure 5.2: Channel estimation for user 1. (— : actual channel, * : estimated channel samples.)

where, † denotes the left pseudo inverse. The estimate of the noise variance $\hat{\sigma}_n^2$ is obtained as the mean of the $ML_cK - K - L + 1$ smallest eigenvalues of $\hat{\mathbf{R}}_x$. The absolute value of the channel gain can be obtained by a $(K + L - 1)$-smoothing on $|\gamma_i|^2$. In order to estimate the unknown phase, we observe that in the noise free case

$$\mathbf{X} = \mathbf{W}\mathbf{\Gamma}\mathbf{S} = \mathbf{W}|\mathbf{\Gamma}|\mathbf{\Phi}\mathbf{S} \tag{5.29}$$

where,

$$|\mathbf{\Gamma}| = \text{diag}\{|\gamma_1|, \ldots, |\gamma_1|, \ldots, |\gamma_R|, \ldots, |\gamma_R|\}$$

$$\mathbf{\Phi} = \text{diag}\{e^{j\phi_1}, \ldots, e^{j\phi_1}, \ldots, e^{j\phi_R}, \ldots, e^{j\phi_R}\}$$

Therefore,

$$\mathbf{\Phi}\mathbf{S} = (\mathbf{W}|\mathbf{\Gamma}|)^{\dagger}\mathbf{X} \tag{5.30}$$

93
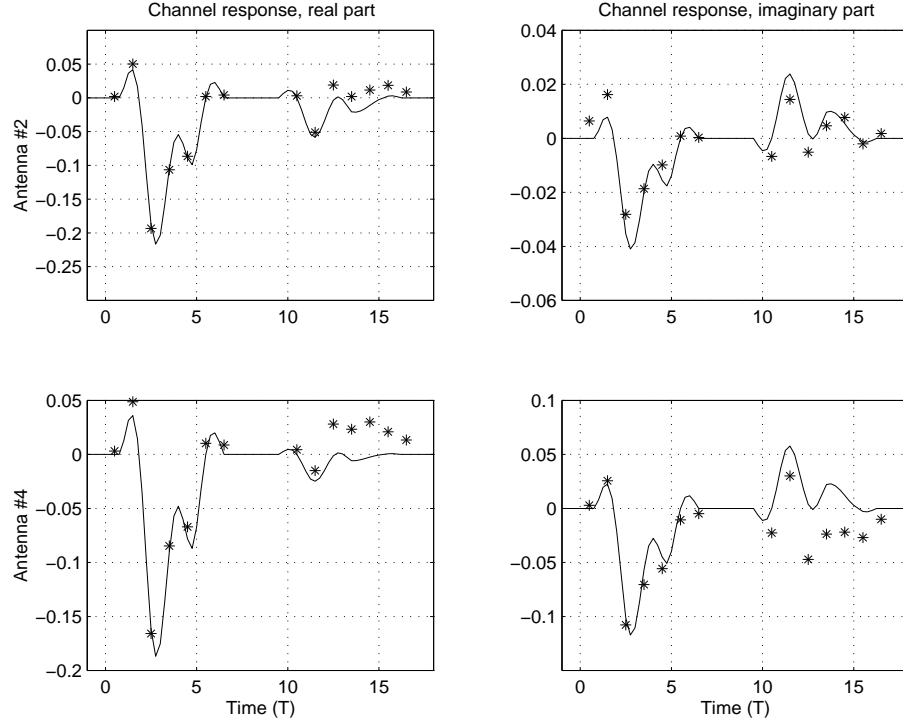
Figure 5.3: Channel estimation for user 2. (— : actual channel, * : estimated channel samples.)

If the entries in $\mathbf{S}$ are either 1 or -1, the phase can be estimated by squaring the entries of both sides of (5.30)

$$(\boldsymbol{\Phi} \odot \boldsymbol{\Phi})(\mathbf{S} \odot \mathbf{S}) = [(\mathbf{W}|\boldsymbol{\Gamma}|)^{\dagger}\mathbf{X}] \odot [(\mathbf{W}|\boldsymbol{\Gamma}|)^{\dagger}\mathbf{X}] \qquad (5.31)$$

where, $\odot$ denotes the Hadamard product. $(\mathbf{S} \odot \mathbf{S})$ is a matrix whose entries are all equal to one, and therefore it is easy to solve $e^{j\phi_i}$ in

$$(\boldsymbol{\Phi} \odot \boldsymbol{\Phi}) = \text{diag}\{\underbrace{e^{j2\phi_1}, \ldots, e^{j2\phi_1}}_{K+L-1}, \ldots, \underbrace{e^{j2\phi_R}, \ldots, e^{j2\phi_R}}_{K+L-1}\} \qquad (5.32)$$

5.5 Simulations

A W-CDMA system is simulated, in which a base station receives signals from $R = 2$ mobile users. The BS has $M = 4$ antennas spaced $\lambda/2$ in a linear array. The carrier
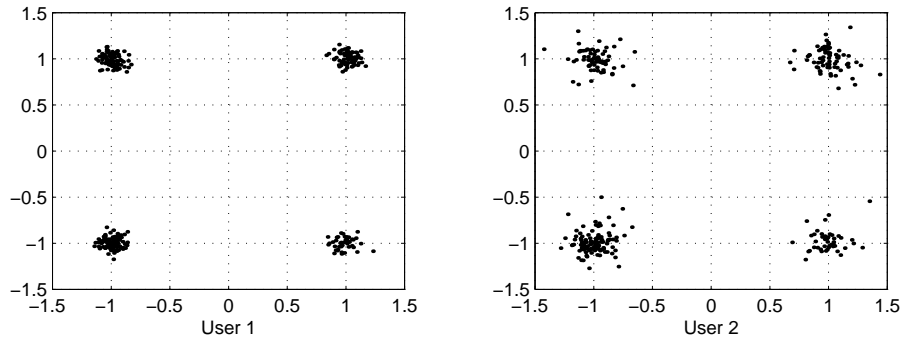
Figure 5.4: Signal constellations of user 1 and user 2.

frequency is 2 GHz. There are two dominant scattering ray bundles from each user arriving at the BS, with nominal DOAs and nominal delays uniformly distributed on $[0, 2\pi)$ and $[0, LcT]$, respectively. T is the chip period. We assume that the nominal DOAs and delays are pre-estimated. Within each ray bundle, there are 3 individual multipaths, with pass losses and delays uniformly distributed on [0 dB, 20 dB] and $[0, 4T]$, respectively. The maximum angle spread is 5 degrees from the nominal DOA.

We generate random QPSK signals for both mobile users, which are then spread by the CDMA spreading code of length $L_c = 16$, and modulated by a raised-cosine pulse function with a roll-off factor of 0.25, truncated to a length of $4T$. The average received power of the signal from user 2 is 6 dB lower than that from user 1.

The proposed method of channel estimation is applied with $N = 100$, $K = 2$. L_g is selected to be 7. Once the channel $\bar{\mathbf{h}}_i$ $(i = 1, 2)$ is estimated, we can construct the signature waveform matrix $\mathbf{W}$ and detect the symbols transmitted by each user.

An example of channel estimation is demonstrated in Figure 5.2 and Figure 5.3, where SNR = 10 dB. They show the agreement of the actual channel and the estimated channel samples at the second and fourth antenna elements of both users. Although the signals are QPSK encoded, the channel gain and the phase can be estimated by a similar approach as in section 5.4. The compensated signal
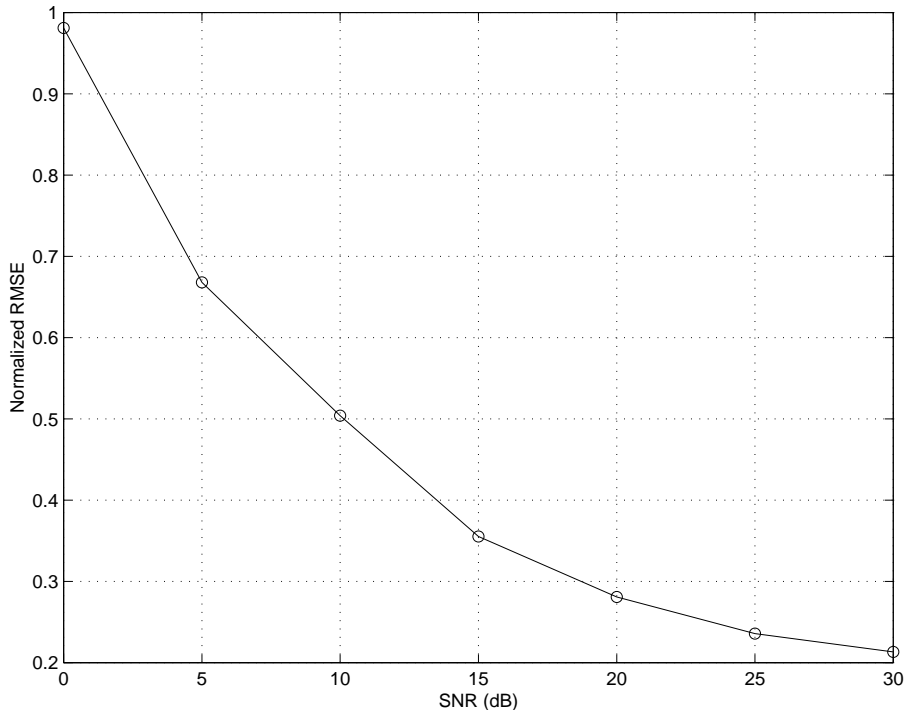
Figure 5.5: Normalized RMSE versus channel output SNR.

constellations are shown in Figure 5.4.

We define the normalized root mean square error as

$$\text{RMSE} = \frac{1}{||\bar{\mathbf{h}}||} \sqrt{\frac{1}{N_t} \sum_{i=1}^{N_t} ||\hat{\bar{\mathbf{h}}} - \bar{\mathbf{h}}||^2} \tag{5.33}$$

where the number of Monte Carlo trials is chosen as $N_t = 1000$. Figure 5.5 shows the normalized RMSE of channel estimation with channel output SNR varying from 0 to 30 dB.

In Figure 5.6, we compare the average bit-error-rate (BER) for the W-CDMA receiver applying the subspace method with that for the RAKE receiver with pseudo inverse beamforming. The 2-finger RAKE receiver has a finger for each dominant ray bundle, and the 6-finger RAKE receiver has a finger for each individual multipath component. The proposed method outperforms the RAKE receiver at high SNR,
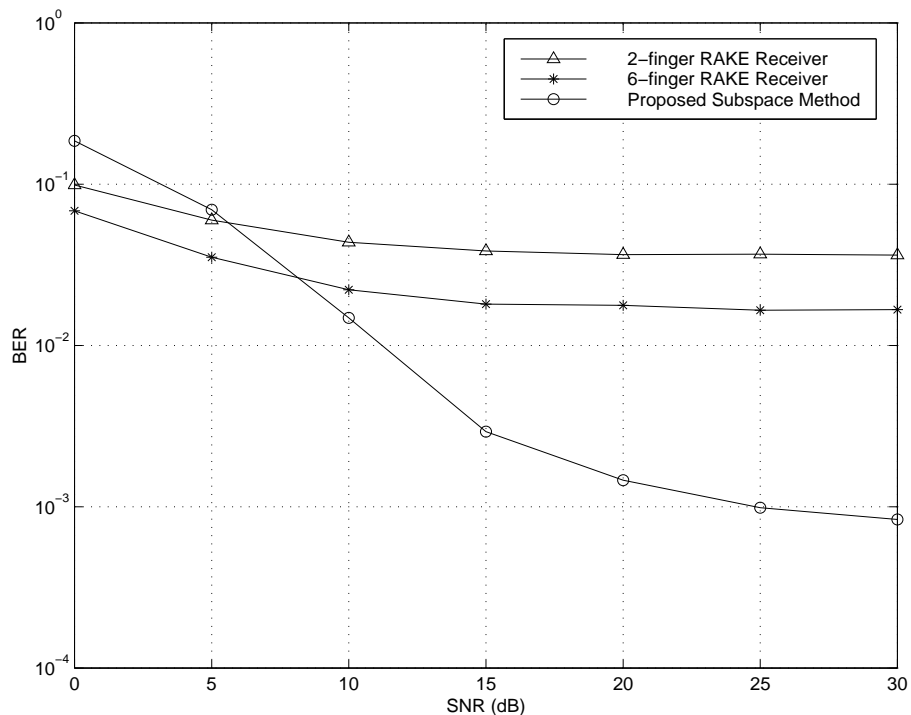
Figure 5.6: Average BER versus channel output SNR.

because it cancels the interference from the other user by estimating both channels.

5.6   Conclusions

We have presented an algorithm for the subspace-based multiuser channel estimation in W-CDMA systems. The algorithm uses information of the slow-varying large-scale structure of the propagation channel and exploits the subspace properties of the received data matrix in a deterministic framework. This approach is computationally efficient, while preserving the performance of the traditional blind channel estimation techniques.

Chapter 6

MIMO Wireless Systems Using Antenna Pattern Diversity

6.1 Introduction

Multiple-input multiple-output (MIMO) wireless communication is one of the most promising technologies for improving the spectrum efficiency of wireless communication systems. It is well known that the use of MIMO antenna systems allows the channel capacity to scale in proportion to the minimum of the number of transmit and receive antennas in uncorrelated Rayleigh fading channels [10, 11]. Of course, real channels do not satisfy these ideal assumptions, thus recent work has focused on measuring and characterizing real MIMO propagation channels [67]. In parallel, work is continuing on efficient space-time coding strategies that achieve the benefits of MIMO communication [7, 8]. However, thus far there has been little work on one of the most important aspects of MIMO communication systems – the antennas that are used at both the transmitter and receiver.

   The correlation between sub-channels of the matrix channel limits the MIMO channel capacity considerably [68, 69]. One way to reduce correlation is to use an-

tennas with different polarizations and radiation patterns [70, 71]. Recent results on polarization diversity show that up to six degrees of freedom are available in the polarization channel, thus the channel capacity can be increased dramatically [72]. However, the sub-channels created by antenna polarization diversity are not completely decorrelated in a real environment, such that the effective degrees of freedom are much less than six, therefore the capacity increase is limited.

In this chapter, we investigated the impact of antenna pattern and polarization on MIMO communication channels. We specialize our results to the case where the antennas are collocated and thus only pattern and polarization, but not antenna spacing, are the parameters of the spatial signatures. This is important for mobile applications where space is extremely limited [71]. First we introduce a general channel model that shows how pattern diversity is the natural generalization of polarization diversity. The MIMO channel is decoupled into sub-channels to quantify the effect of channel correlation. Then we show how orthogonality between patterns decorrelates the signal in highly scattering environments, hence reducing the loss due to channel correlation. Using an electromagnetic ray-tracing simulator, we show that the capacity increase is determined by the selection of antennas of different patterns, and by various propagation environments. Finally, we propose a prototype of MIMO handheld terminal that employs multiple collocated antennas. The capacity gain is provided by the antenna pattern diversity of the system, and it is compared with the capacity gain of a spatial multiplexing system.

This chapter is organized as follows. In Section 6.2, we introduce the channel capacity and the mutual information of the MIMO wireless system, and discuss the correlation between sub-channels. In Section 6.3, the MIMO system that exploits antenna pattern diversity is described, and pattern diversity is included in the channel transfer matrix. Section 6.4 demonstrates the capacity increase obtained through antenna pattern diversity via a ray-tracing simulator. Section 6.5 restates

the necessity of antenna array design for the MIMO handheld terminal. In Section 6.6, we derive the correlation coefficients of collocated antennas with pattern diversity. In Section 6.7, we propose a prototype of the compact handheld terminal, whose antenna array consists of collocated antennas with dissimilar radiation patterns. Finally, conclusions are drawn in Section 6.8.

6.2   MIMO Channel Capacity Under Correlated Fading

Consider a narrowband MIMO wireless system with n_T transmit antennas and n_R receive antennas. The induced voltages at the receive antennas are related to the impressed voltages at the transmit antennas as

$$\mathbf{v}^{(R)} = A\mathbf{H}\mathbf{v}^{(T)} + \mathbf{n} \tag{6.1}$$

where $\mathbf{v}^{(R)} = [v_1^{(R)} v_2^{(R)} \cdots v_{n_R}^{(R)}]^T$ are the voltages at the receive antennas, $\mathbf{v}^{(T)} = [v_1^{(T)} v_2^{(T)} \cdots v_{n_T}^{(T)}]^T$ are the voltages at the transmit antennas. $\mathbf{H}$ is the normalized channel transfer matrix modeling the small-scale fading process, A^2 encompasses the (spatially local-averaged) large-scale path loss and shadowing, and $\mathbf{n}$ is the additive white Gaussian noise (AWGN) vector. If we assume that the channel state information (CSI) is completely known by the receiver but not by the transmitter, the transmitted signal vector is composed of n_T statistically independent Gaussian components with equal power. For a narrowband MIMO channel with uniform power allocation constraint, the mutual information between the transmitter and the receiver is given by [11]

$$M(\mathbf{H}) = \log_2 \left[\det \left(\mathbf{I}_{n_R} + \frac{\rho}{n_T} \mathbf{H}\mathbf{H}^\dagger \right) \right] \tag{6.2}$$

where ρ is the average signal-to-noise-ratio (SNR) at each receive antenna, $\dagger$ denotes conjugate transpose. The ergodic channel capacity C is the expectation of $M(\mathbf{H})$ taken over the probability distribution of $\mathbf{H}$. We will assume $n_T = n_R = n$ throughout the rest of the paper.

Suppose the communication is carried out using bursts (packets). The burst duration is assumed to be short enough such that the channel can be regarded as essentially fixed during a burst, but long enough that the standard information-theoretic assumption of infinitely long code block lengths can be used. In this quasi-static scenario, it is meaningful to associate the "instantaneous" channel capacity with the mutual information given a realization of the channel matrix $\mathbf{H}$. From (6.2), the mutual information can be further expressed as

$$M(\mathbf{H}) = \sum_{i=1}^{n} \log_2 \left(1 + \frac{\rho}{n}\lambda_i\right) \qquad (6.3)$$

where $\{\lambda_i\}$ are the eigenvalues of $\mathbf{H}\mathbf{H}^\dagger$. At high SNR, the mutual information can be approximated by

$$M(\mathbf{H}) \approx \sum_{i=1}^{\text{rank}(\mathbf{H})} \log_2(\frac{\rho}{n}\lambda_i) \qquad (6.4)$$

Since $\lambda_i \leq n$ for a normalized $\mathbf{H}$, an upper bound of the mutual information (at high SNR) can be derived as [72]

$$M(\mathbf{H}) \leq \text{rank}(\mathbf{H}) \log_2 \rho \qquad (6.5)$$

The equality is achieved when a total of $\text{rank}(\mathbf{H})$ sub-channels are uncorrelated. However, complete decorrelation is hard to achieve in a practical scattering environment.

In order to quantify the effect of channel correlation, the MIMO channel is decoupled into n single-input single-output (SISO) sub-channels. Performing the singular value decomposition of the channel matrix $\mathbf{H}$ as $\mathbf{H} = \mathbf{U}\boldsymbol{\Sigma}\mathbf{V}$, we can rewrite the input-output relationship as

$$\mathbf{y} = \boldsymbol{\Sigma}\mathbf{x} + \mathbf{u} \qquad (6.6)$$

where, $\mathbf{y} = \mathbf{U}^\dagger\mathbf{v}^{(R)}$, $\mathbf{x} = A\mathbf{V}\mathbf{v}^{(T)}$, and $\mathbf{u} = \mathbf{U}^\dagger\mathbf{n}$. Because $\boldsymbol{\Sigma}$ is a diagonal matrix, the MIMO channel is transformed into n SISO sub-channels with gains $\sigma_1^2, \sigma_2^2, \ldots, \sigma_n^2$,

where $\{\sigma_i\}$ are the diagonal entries of $\mathbf{\Sigma}$. The mutual information of the MIMO channel is the sum of the mutual information of the n sub-channels [68, 69],

$$M(\mathbf{H}) = \sum_{i=1}^{n} \log_2 \left(1 + \frac{\rho}{n}\sigma_i^2\right) \tag{6.7}$$

where we assume uniform transmitted power allocation on the transmit antennas. This is exactly the mutual information of MIMO channel expressed in (6.3), with $\sigma_i^2 = \lambda_i$ being the eigenvalues of $\mathbf{HH}^\dagger$. The channel capacity is determined by the values of the eigenvalues. When a sub-channel is correlated with another one, the corresponding eigenvalue becomes small, which results in a sub-channel with small gain. From (6.7) we see that the correlated sub-channel contributes little to the total mutual information. The decorrelation of the sub-channel is conventionally provided by spatial diversity, that is, using spatially separated multiple antennas at the transceivers such that each transmitter-receiver pair experiences a different fading channel. With insufficient spacing of local antennas, however, strong correlation can be exhibited between the sub-channels, and consequently the MIMO channel capacity is reduced considerably.

For a narrowband time-invariant MIMO channel with a uform power allocation constraint, the mutual information between an n_T-antenna transmitter and an n_R-antenna receiver is given by (6.2). If the fading of transmitter-receiver pairs is uncorrelated, the entries of $\mathbf{H}$ are i.i.d. complex Gaussian. A general type of correlation of the fading can be represented using a four-dimensional tensor operation on $\tilde{\mathbf{H}}$, where $\tilde{\mathbf{H}}$ is a matrix with uncorrelated complex Gaussian entries [73]. In our case, the antennas at the base station are assumed uncorrelated, whereas the antennas at the handheld terminal are correlated due to insufficient spacing. Therefore, the channel transfer matrix of uplink can be represented by a transformation matrix $\mathbf{K}$ operating on $\tilde{\mathbf{H}}$ as

$$\mathbf{H} = \mathbf{K}\tilde{\mathbf{H}} \tag{6.8}$$

Substituting (6.8) into (6.2) we have

$$M = \log_2 \left[\det \left(\mathbf{I}_{n_R} + \frac{\rho}{n_T} \Psi \tilde{\mathbf{H}} \tilde{\mathbf{H}}^\dagger \right) \right] \tag{6.9}$$

where $\Psi = \mathbf{K}^\dagger \mathbf{K}$ is the spatial covariance matrix of the signals received by the handheld terminal. The entry ψ_{ij} of Ψ is given by the correlation coefficient of the signals received by antennas i and j. The correlation coefficients depend on both the antenna array configuration and the angular spectrum of the incident radio waves.

For spatial diversity in a horizontal plane, the correlation coefficient of the signals received by antenna i and j, separated by distance d_{ij}, and illuminated by an angular spectrum $p(\phi)$ is [30]

$$\rho_{ij} = \int_0^{2\pi} e^{jkd_{ij}\cos(\phi-\alpha)} p(\phi)d\phi, \quad \int_0^{2\pi} p(\phi)d\phi = 1 \tag{6.10}$$

where ϕ is the azimuthal angle of the incident wave, $k = 2\pi f_c/c$ is the wavenumber, and α is the angle of the array orientation. In the case of uniform illumination $p(\phi) = 1/2\pi$, $\rho_{ij} = J_0(kd_{ij})$, where J_0 is the zeroth order Bessel function. To achieve near complete decorrelation, the antennas should be spaced at least $\lambda/2$ apart.

6.3 MIMO Systems Using Antenna Pattern Diversity

To introduce sub-channel decorrelation to the MIMO system which has insufficient antenna spacing, we propose a transceiver array which is composed of antennas with appropriate dissimilarity in radiation patterns, and allow the antenna pattern diversity to be expressed in the channel transfer matrix. The antenna pattern diversity can be exploited in conjunction with spatial diversity to achieve better channel performance in implementation. However, only pattern diversity is addressed in this context for a clear demonstration.

Suppose the transmit antennas are collocated but have different radiation patterns. The receive antennas are also collocated, each of which has a radiation

pattern the same as one of the transmit antennas. For a narrowband channel at fixed carrier frequency $f_c = c/\lambda$, the channel transfer matrix $\mathbf{G} = A\mathbf{H}$, where A is defined as before, $\mathbf{H}$ is the normalized channel transfer matrix modeling both the multipath fading effect and the antenna pattern diversity. By ray-tracing [74] from the transmit antenna to the receive antenna, the voltage on the ith receive antenna excited by the transmission of the kth transmit antenna is (See Appendix C)

$$v_{i,k}^{(R)} = \beta \sum_{m=1}^{M} \mathbf{E}_k^m \cdot \mathbf{F}_i(\theta_m^{(R)}, \phi_m^{(R)}) \tag{6.11}$$

where β is a proportionality constant (assume $\beta = 1$), M is the number of multi-paths in the link, $\mathbf{F}_i(\theta^{(R)}, \phi^{(R)})$ is the ith receive antenna pattern, $(\theta^{(R)}, \phi^{(R)})$ is the receiving angle of each ray, and $\mathbf{E}_k^m$ is the incident field of the mth multipath at the receiver,

$$\mathbf{E}_k^m = \frac{e^{-jk_0 l_m}}{l_m} \mathbf{f}_{m,k}\left(\mathbf{F}_k(\theta_m^{(T)}, \phi_m^{(T)})\right) v_k^{(T)} \tag{6.12}$$

where $k_0 = 2\pi/\lambda$, l_m is the path length of the mth multipath, $\mathbf{f}_{m,k}(\cdot)$ is the functional of reflection and diffraction, and $\mathbf{F}_k(\theta^{(T)}, \phi^{(T)})$ is the kth transmit antenna pattern, $(\theta^{(T)}, \phi^{(T)})$ the transmitting angle. Therefore $\mathbf{G}$ has complex scalar entries

$$G_{i,k} = \sum_{m=1}^{M} \frac{e^{-jk_0 l_m}}{l_m} \mathbf{f}_{m,k}\left(\mathbf{F}_k(\theta_m^{(T)}, \phi_m^{(T)})\right) \cdot \mathbf{F}_i(\theta_m^{(R)}, \phi_m^{(R)}) \tag{6.13}$$

And $\mathbf{G}$ can be expressed as

$$\mathbf{G} = \sum_{m=1}^{M} \frac{e^{-jk_0 l_m}}{l_m} \tilde{\mathbf{G}}_m \tag{6.14}$$

where

$$\tilde{G}_{m,i,k} = \mathbf{f}_{m,k}\left(\mathbf{F}_k(\theta_m^{(T)}, \phi_m^{(T)})\right) \cdot \mathbf{F}_i(\theta_m^{(R)}, \phi_m^{(R)}) \tag{6.15}$$

Because the transmit antennas and the receiver antennas are collocated, the difference in path lengths and phases of the rays travelling between any transmitter-receiver pairs can be neglected. The difference of the entries of $\mathbf{G}$ is solely caused by the antenna pattern diversity implied in $\tilde{\mathbf{G}}_m$.

104

One observation is that using the dual-polarized transmitter-receiver pair where two linear dipoles with equal gain are orthogonally collocated at each end, the two sub-channels are almost uncorrelated with the presence of a strong line-of-sight (LOS) multipath component. The relatively large gains σ_1^2 and σ_2^2 of the sub-channels are provided by the quasi-orthogonal structure of $\mathbf{H}$, and the mutual information reaches its maximum among normalized 2×2 channel realizations. However, the upper bound of mutual information (6.5) introduced in [72] is loose in a MIMO system using pattern diversity of a large number of transmitter-receiver pairs. As we will see in the simulation, the mutual information provided by some sub-channels are nearly zero. Although the rank of $\mathbf{H}$ is guaranteed, the corresponding eigenvalues of $\mathbf{HH}^\dagger$ are small compared to the dominant ones, which is a direct result of severe correlation of the sub-channels.

In order to achieve uncorrelated sub-channels, the goal of antenna design is to make the incident fields of the transmission from one antenna align with the radiation pattern of the desired receive antenna, while being orthogonal to the patterns of other antennas. However, in the real electromagnetic world, the sub-channels, which are characterized by the summation of the dot products in (6.13), may not be completely orthogonal.

6.4   Ray Tracing Simulations

The distribution of MIMO channel capacity can be calculated given the distribution of the eigenvalues of $\mathbf{HH}^\dagger$. However, for a general covariance of fading and pattern diversity and a finite dimensionality, the distribution of eigenvalues can be very difficult to compute. The exact distribution of channel capacity is studied via numerical computation using an electromagnetic ray tracer FASANT [59] in this section. It is a deterministic ray tracing technique based on geometric optics and the uniform theory of diffraction. (See Appendix B).
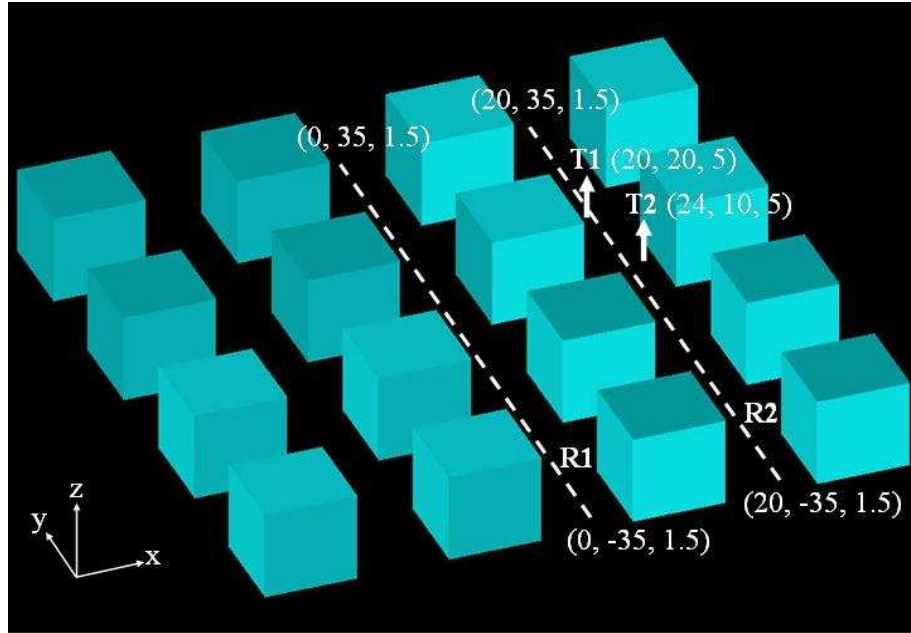
Figure 6.1: Street lattice with transmitter positions T_1 and T_2, and receiver moving tracks R_1 and R_2.

A street lattice in Figure 6.1 is simulated as the geometry input of FASANT. The size of each building block is $(10 \times 10 \times 10)$ m^3, and the street width is 10 m. The material properties for the building walls and the ground are: relative permittivity $\epsilon = 2.0$, relative permeability $\mu = 1.0$, and conductivity $\sigma = 0.08$. There are two transmission points $T_1 : (20, 20, 5)m$ and $T_2 : (24, 10, 5)m$, where T_1 is in the middle of a street crossing. The receiver can move along two streets shown as the tracks R_1 and R_2.

The infinitesimal electric-dipole of electric source $\mathbf{J}$ or current-loop of magnetic source $\mathbf{M}$ is used as the transmit and receive antenna element. At each end of the communication link, two orthogonally placed electric-dipoles with their feed points collocated form a 2×2 MIMO system. Three such orthogonally placed electric-dipoles form a 3×3 MIMO system, and another three orthogonally placed

106
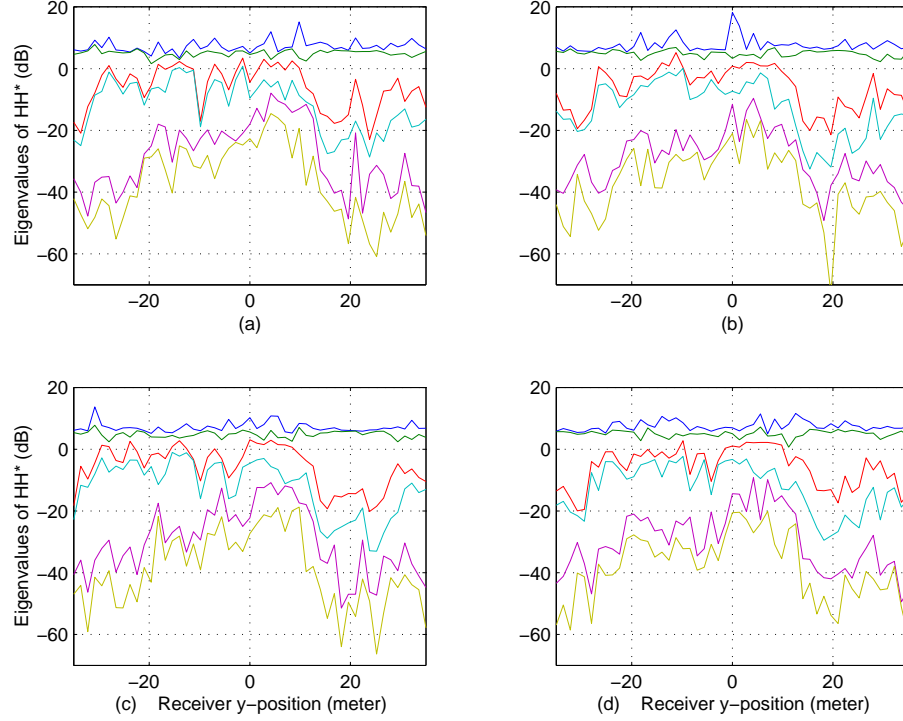
Figure 6.2: Eigenvalues of normalized $\mathbf{H}\mathbf{H}^\dagger$ of the 6×6 MIMO channel in Case 1 . The transmitter is located at T_1, and the receiver moves along 4 tracks as: (a) (-1, -35, 3)$\rightarrow$(-1, 35, 3), (b) (1, -35, 3)$\rightarrow$(1, 35, 3), (c) (-1, -35, 1)$\rightarrow$(-1, 35, 1), (d) (1, -35, 1)$\rightarrow$(1, 35, 1).

current-loops, which are referred to as magnetic-dipoles, collocated with the 3×3 electric-dipoles form a 6×6 MIMO systems. The radiation pattern of the electric-dipole with vertical $\mathbf{J}$ in the spherical coordinate system is $\mathbf{E} = \sin(\theta)\hat{\mathbf{a}}_\theta$, and the radiation pattern of the magnetic-dipole with vertical $\mathbf{M}$ is $\mathbf{E} = -\sin(\theta)\hat{\mathbf{a}}_\phi$. The carrier frequency is 1.8 GHz, that is, a carrier wavelength of 0.167 m.

Case 1   In case 1, the transmit antenna array is located at T_1, and the receive antenna array moves along 4 tracks (-1, -35, 3)$\rightarrow$(-1, 35, 3), (1, -35, 3)$\rightarrow$(1, 35, 3), (-1, -35, 1)$\rightarrow$(-1, 35, 1), and (1, -35, 1)$\rightarrow$(1, 35, 1) on the same street close to track R_1. Therefore, as the receiver changes its position, it experiences both
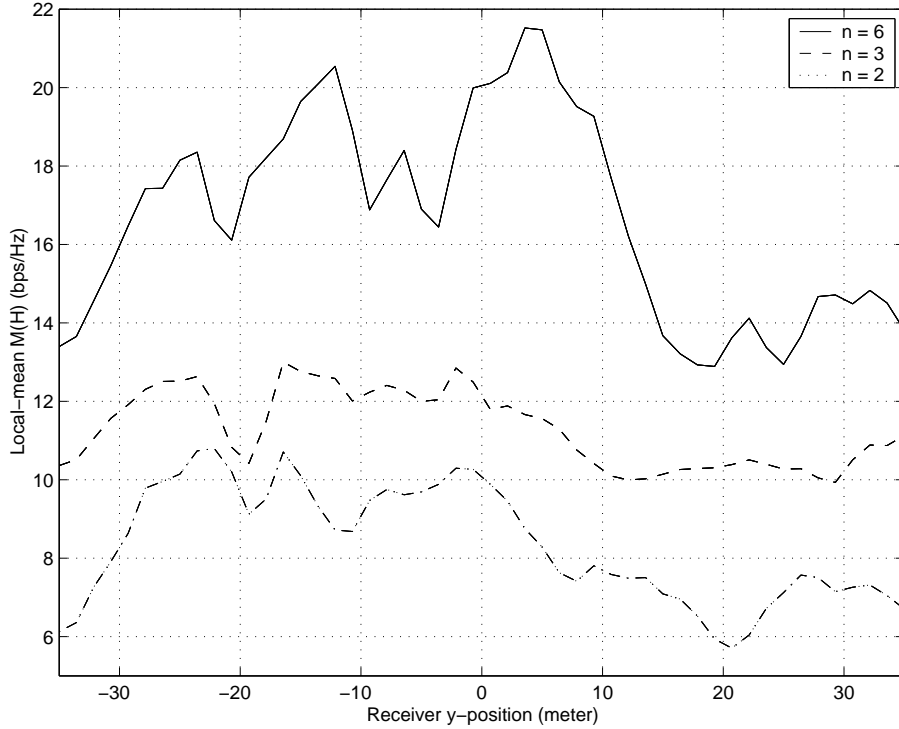
Figure 6.3: Mutual information of the 2×2, 3×3 and 6×6 MIMO channels in Case 1, averaged over neighboring 8 receiving positions. The LOS region is $y \in [13.33, 26.67]$ m.

line-of-sight (LOS) and non-line-of-sight (NLOS) channels.

Figure 6.2 shows the eigenvalues of the normalized $\mathbf{HH}^\dagger$ along each track. Each of the transmit and receive antenna arrays is composed of three electric-dipoles orthogonally placed along x, y, z axes of the Cartesian coordinate system and three such orthogonally placed magnetic-dipoles, therefore every $\mathbf{H}$ along the tracks is a realization of the 6×6 MIMO channel. There are two dominant eigenvalues of $\mathbf{HH}^\dagger$ of each realization of the channel, the next two are about 20 dB down, and the weakest two are about 40 dB down the dominant ones. The drop of weaker eigenvalues, especially in the LOS region from $y = 13.33$ m to $y = 26.67$ m, reveals the strong correlation between the sub-channels.
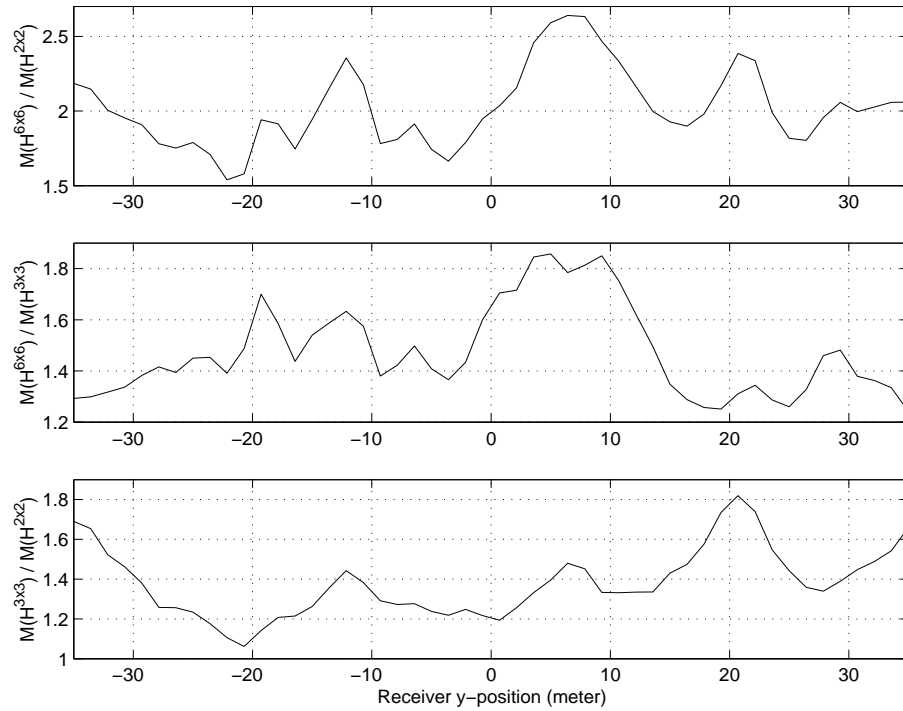
Figure 6.4: Ratios of mutual information of 6×6 to 2×2, 6×6 to 3×3, and 3×3 to 2×2 MIMO systems in Case 1.

Figure 6.3 compares the local-averaged mutual information of the 6×6 MIMO systems with that of the 2×2 and 3×3 MIMO systems. In the 2×2 MIMO system, each of the transmit and receive antenna arrays is composed of two electric-dipoles orthogonally placed along the y and z axes of the Cartesian coordinate system. In the 3×3 MIMO system, the array is composed of three electric-dipoles orthogonally placed along x, y and z axes. The average receive SNR = 20 dB. The figure shows the channel capacity increase of the 6×6 and 3×3 MIMO systems that using collocated antennas exploiting the pattern diversity over the conventional dual-polarized antenna systems as the 2×2 MIMO systems. The antenna pattern diversity is provided by the scattering environment, as a result, the MIMO channel that exploits antenna pattern diversity in the LOS region has less capacity increase

109
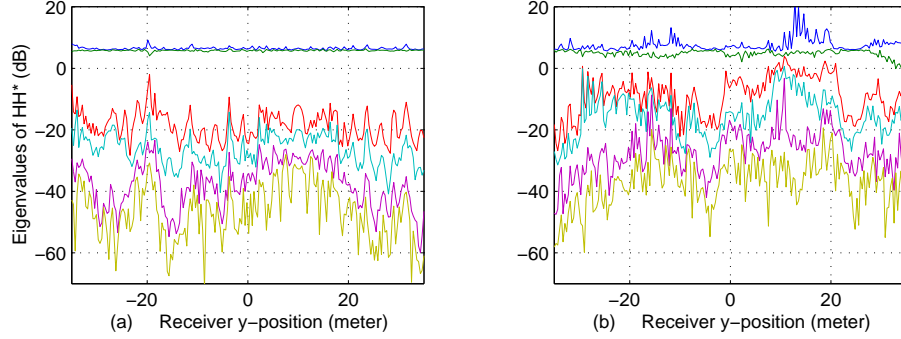
Figure 6.5: Eigenvalues of normalized $\mathbf{HH}^{\dagger}$ of the 6×6 MIMO channel in Case 2. The transmitter is located at T_2, and the receiver moves along 2 tracks as: (a) R_2 LOS case. (b) R_1 NLOS case.

as shown in the figure.

Figure 6.4 shows the ratios of mutual information of systems of different numbers of dimension as above. Comparing mutual information of the 6×6 system with that of the 2×2 system, we find the "instantaneous capacity" in any position of the scattering environment is not ideally tripled, contrast to what is claimed in [72], due to the correlation between sub-channels. This result is expected from the eigenvalue plot of Figure 6.2, because, besides the two dominant sub-channels as in the dual-polarized antenna systems, sub-channels of a system with collocated antennas at transmitter and receiver are correlated in a practical scattering environment. The electrical components and the magnetic components of the field are also highly correlated.

Case 2   In case 2, the transmit antenna array is located at T_2, and the receive antenna array moves along the LOS street $R_2 : (20, -35, 1.5) \rightarrow (20, 35, 1.5)$, and the (almost) NLOS street $R_1 : (0, -35, 1.5) \rightarrow (0, 35, 1.5)$.

Figure 6.5 shows the eigenvalues of the normalized $\mathbf{HH}^{\dagger}$ of the 6×6 MIMO system, where each of the transmitter and receiver antenna arrays has three electric-
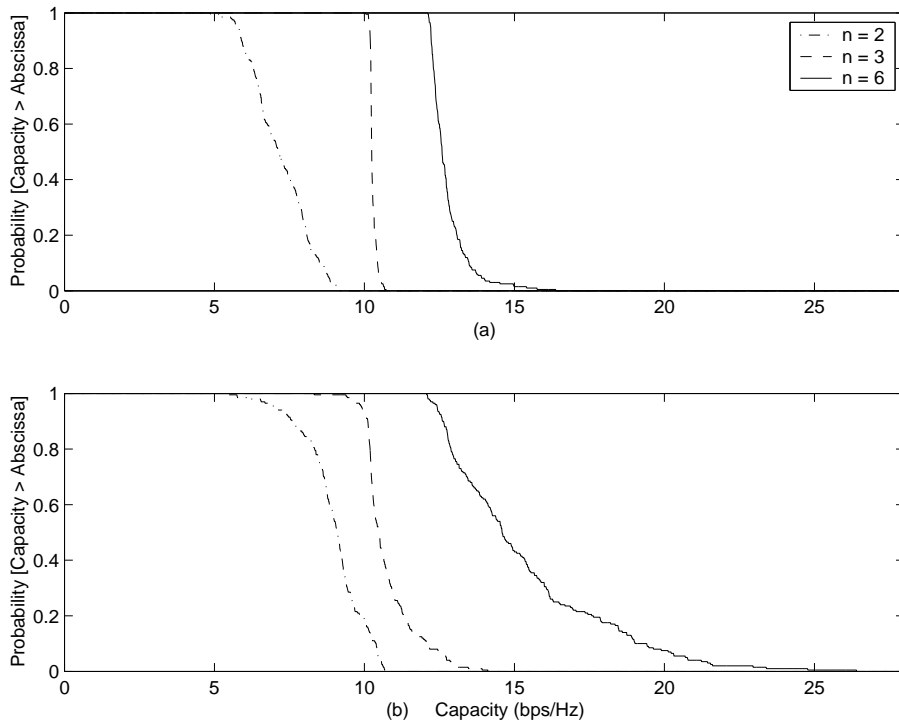
Figure 6.6: CCDFs of instantaneous capacities of the 2×2, 3×3 and 6×6 MIMO channels in Case 2. Average receive SNR = 20 dB. (a) The receiver moves along the LOS street R_2. (b) The receiver moves along the NLOS street R_1.

dipoles, orthogonally placed along x, y, z axes collocated with three such orthogonally placed magnetic-dipoles. Figure 6.5(a) shows the eigenvalues of the channel realizations when the receiver changes its position along $R2$, the LOS region. Figure 6.5(b) shows the eigenvalues of the channel realizations when the receiver changes its position along $R1$, the NLOS region. The better decorrelation effect of the sub-channels in a rich scattering environment (NLOS region) is revealed as the increase in the smaller eigenvalues.

Figure 6.6 compares the complementary cumulative distribution functions (CCDF) of instantaneous channel capacities of the 2×2, 3×3 and 6×6 MIMO systems, when the receiver changes its position along the LOS and NLOS streets.

For the 2×2 MIMO system, the transceiver antenna array is composed of two electric-dipoles along the x and z axes, and this is simply the dual-polarized system in the LOS region. The average receive SNR = 20 dB. As shown in the figure, the large increase in channel capacity of a MIMO system that exploits antenna pattern diversity, referring to a dual-polarized MIMO channel, is more likely to occur in the NLOS region, that is, in the rich-scattering environment.

6.5   Design MIMO Handheld Terminal

Multiple-input multiple-output (MIMO) wireless systems use multiple antennas at both the transmitter and the receiver to offer a large increase in channel capacity [10, 11]. Parallel data pipes can be opened between the transmit and the receive antennas if the fading of the transmitter-receiver pairs is uncorrelated. The base station in a typical mobile radio system is usually located well above surrounding objects, and the angle spread of the multipaths arriving at the base station is typically $1 - 10°$. The necessary antenna spacing for decorrelation is on the order of $5 - 10$ wavelengths [13]. The handheld terminal is usually used in a cluttered environment, and therefore has a large angle spread of the multipath arrivals. For a uniform angular illumination, a minimum antenna spacing of half wavelength is required for decorrelation [30].

Sufficient antenna spacing at the base station is relatively easy to implement. Due to the small size of the handheld terminal, however, sufficient antenna spacing to achieve decorrelation at the mobile unit can be a difficult task. For example at PCS spectrum around 2 GHz, a half wavelength spacing means 7.5 cm apart between antenna elements. This is not suitable for a handheld terminal, especially when more than two antennas are to be equipped for MIMO communication. Further, the assumption of a rich scattering environment with uniform angular illumination is not always valid. This may lead to significant correlation with small antenna

spacing.

In the rest of this chapter, we propose an array structure for the MIMO handheld terminal that exploits antenna pattern diversity instead of spatial diversity [72, 71]. Neglecting the size of the antenna, we regard the antennas in this structure as being collocated. The fading correlation of the terminal antennas is derived, and the mutual information between the transmitter and the receiver is obtained by considering the channel as a combination of the propagation environment and the antenna array configuration [75]. Simulation results show that, in a rich scattering environment, collocated antennas with appropriate dissimilarity in pattern can achieve channel capacity equivalent to a system with half-wavelength antenna spacing. In a scattering environment with small angle spread, collocated antennas with pattern diversity can maintain large channel capacity, however, antenna array that exploits spatial diversity requires at least a few wavelength antenna spacing for near complete decorrelation.

6.6 Collocated Antennas with Pattern Diversity

The complex envelope of the voltage on the receive antenna is given by [30]

$$V(t) = \beta \oint \mathbf{A}(\Omega) \cdot \mathbf{E}(\Omega) e^{-jk\mathbf{u} \cdot \hat{\mathbf{a}}_r(\Omega)t} d\Omega \tag{6.16}$$

where β is a proportionality constant (assume $\beta = 1$), $\mathbf{A}$ is the receiving field pattern of the antenna, $\mathbf{E}$ is the electric field of the incident wave, $e^{-jk\mathbf{u} \cdot \hat{\mathbf{a}}_r(\Omega)t}$ is the Doppler shift caused by the terminal velocity $\mathbf{u}$, $\hat{\mathbf{a}}_r$ is a unit vector in the radial direction, and Ω is the coordinate point on a spherical surface given by (θ, ϕ). Due to the randomness of the incident waves, $V(t)$ is a zero mean random variable, and the correlation coefficient of the received signals, represented by the voltages on antennas i and j, is given by

$$\psi_{ij} = \frac{E\{V_i V_j^*\}}{\sigma_i \sigma_j} \tag{6.17}$$

113

where $\sigma_i^2 = E\{V_i V_i^*\}$, $\sigma_j^2 = E\{V_j V_j^*\}$. It is credible to assume negligible phase change of each incident wave arriving at collocated antennas. We also assume that the phase angles of E_θ and E_ϕ are independently distributed on $[0, 2\pi)$, and they are independent for waves arriving from different directions [30]. Therefore, the correlation coefficient of collocated antennas i and j becomes

$$\psi_{ij} = \frac{1}{\sigma_i \sigma_j} \oint E\{(\mathbf{A}_i(\Omega) \cdot \mathbf{E}(\Omega))(\mathbf{A}_j^*(\Omega) \cdot \mathbf{E}^*(\Omega))\} d\Omega \tag{6.18}$$

With $\mathbf{A}(\Omega) = A_\theta(\Omega)\hat{\mathbf{a}}_\theta + A_\phi(\Omega)\hat{\mathbf{a}}_\phi$, and $\mathbf{E}(\Omega) = E_\theta(\Omega)\hat{\mathbf{a}}_\theta + E_\phi(\Omega)\hat{\mathbf{a}}_\phi$, we have further

$$\psi_{ij} = \frac{1}{\sigma_i \sigma_j} \oint (A_{i\theta}(\Omega) A_{j\theta}^*(\Omega) P_\theta(\Omega) + A_{i\phi}(\Omega) A_{j\phi}^*(\Omega) P_\phi(\Omega)) d\Omega \tag{6.19}$$

where

$$\begin{aligned} P_\theta(\Omega) &= E\{E_\theta(\Omega) E_\theta^*(\Omega)\} \\ P_\phi(\Omega) &= E\{E_\phi(\Omega) E_\phi^*(\Omega)\} \end{aligned} \tag{6.20}$$

We define the angular spectrum of illumination as $P(\Omega) = P_\theta(\Omega) + P_\phi(\Omega)$. Suppose that the base station antennas can transmit various polarized signal waves, and the incident waves arriving at the handheld terminal have uniformly distributed polarization angles, therefore the angular spectrum has equal θ and ϕ components as

$$P_\theta(\Omega) = P_\phi(\Omega) = \frac{P(\Omega)}{2} \tag{6.21}$$

And the correlation coefficient can be written as

$$\psi_{ij} = \frac{1}{2\sigma_i \sigma_j} \oint (\mathbf{A}_i(\Omega) \cdot \mathbf{A}_j^*(\Omega)) P(\Omega) d\Omega \tag{6.22}$$

With incident waves of uniformly distributed angular spectrum, even though the average received power at each antenna is independent of the actual antenna radiation pattern, the correlation coefficient can be adjusted less than one by reducing overlap of antenna patterns. Unlike antenna systems that use spatial diversity, where

114
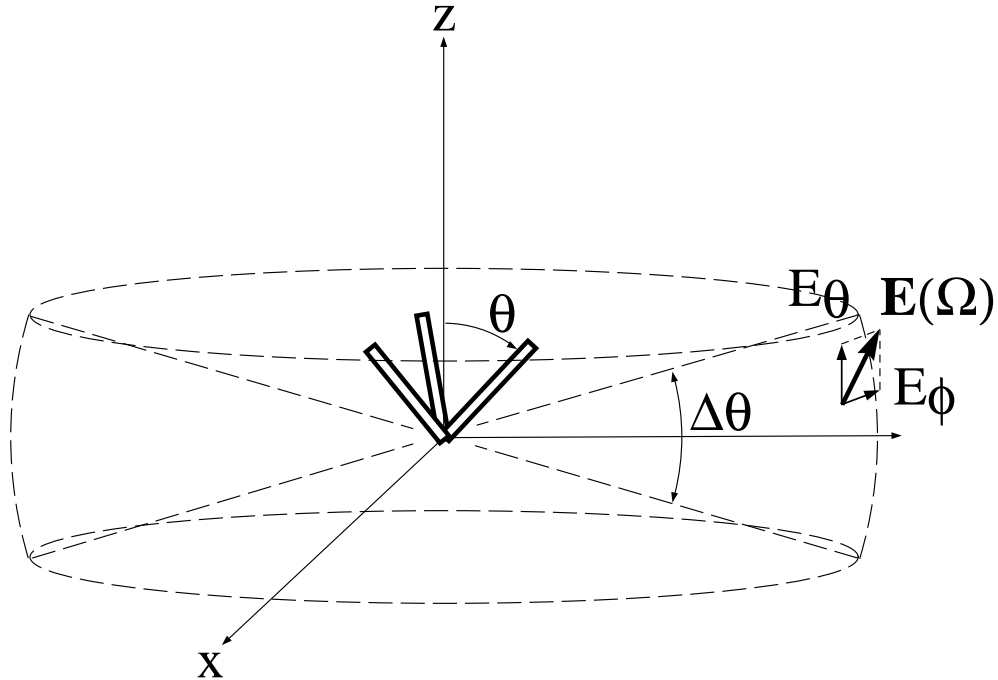
Figure 6.7: Three-element antenna array of handheld terminal.

decorrelation is provided by antenna separation, in antenna systems that exploit pattern diversity, the decorrelation is provided by antenna pattern dissimilarity. As indicated in (6.22), the covariance matrix Ψ is the weighted correlation between local antennas, where the weights are the angular spectrum of illumination at the handheld terminal.

6.7 A Simulated Prototype

We use two collocated antennas or three collocated antennas at the handheld terminal. Figure 6.7 describes the case of the three-antenna array. Each antenna has an "unfolding" polar angle θ opposite to the other antenna(s) in order to create pattern dissimilarity. (For rotation of antenna patterns, see Appendix D). Elec-
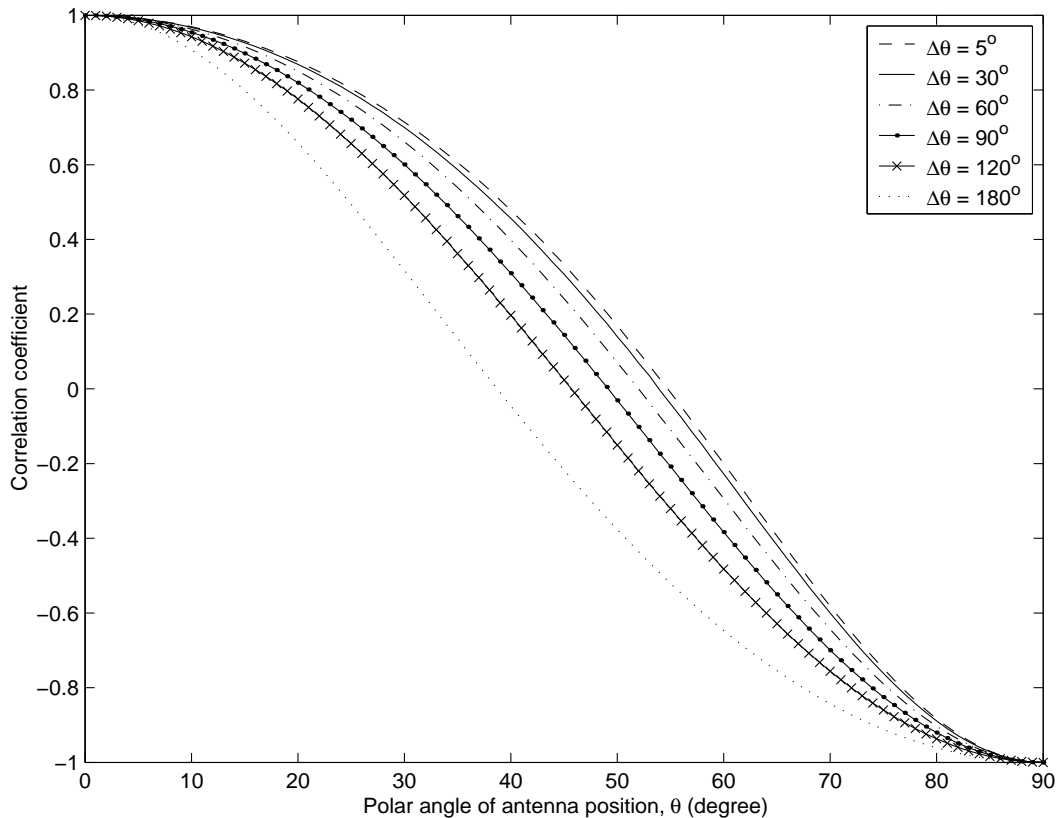
Figure 6.8: Correlation coefficient between antenna elements of the two-element array. Uniform illumination.

trically short dipoles are assumed in the simulation, where the antenna radiation pattern of a vertical dipole $(\theta = 0)$ is $\mathbf{A}(\Omega) = \sin(\theta)\hat{\mathbf{a}}_\theta$. In a cluttered environment, the incident waves at the handheld terminal may come from all azimuthal angles ϕ. Two distributions of the angular spectrum of illumination in ϕ are used: a uniform distribution on $[0, 2\pi)$, and a Gaussian distribution with a standard deviation of $\sigma = 5°$, where the median incident direction is along the broadside of two antennas. We assume uniform distribution of illumination in elevation angle θ. The distribution is restricted to a small angle spread $\Delta\theta$ around the horizontal plane $(\theta = \pi/2)$, depending on the building heights and distances from the base station. Experiments

116
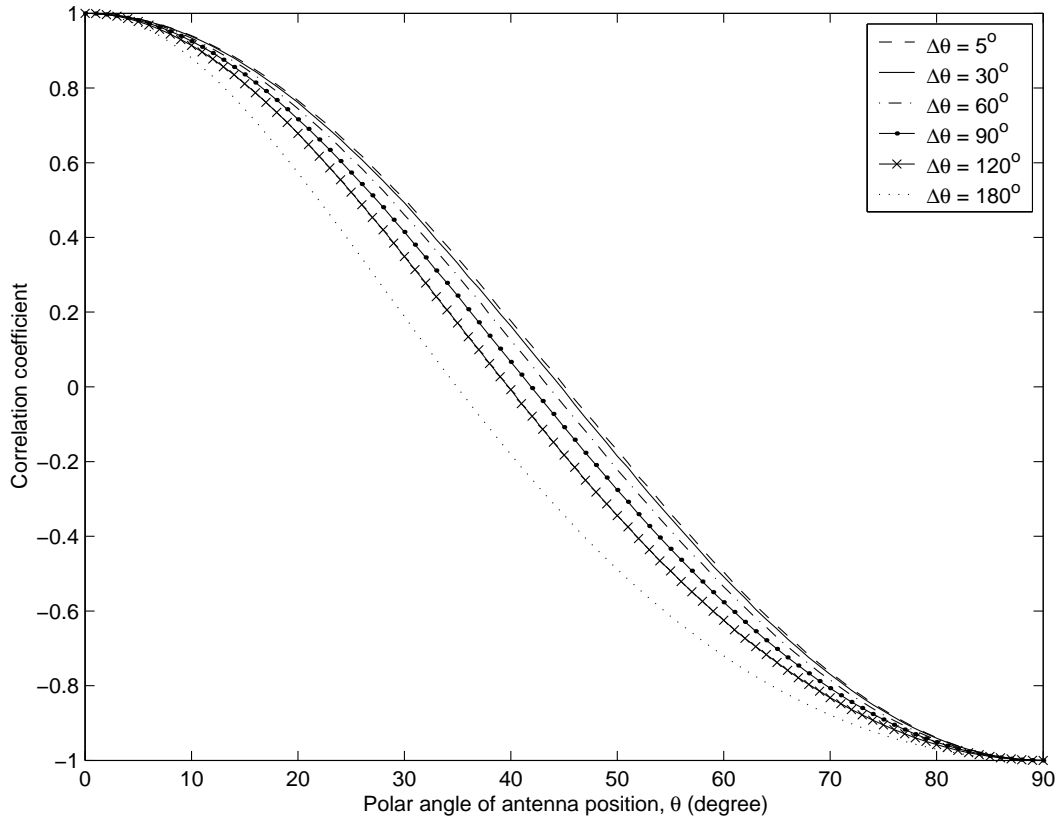
Figure 6.9: Correlation coefficient between antenna elements of the two-element array. Gaussian angular spread at broadside, $\sigma = 5°$.

in suburban and urban environment indicate that distributions extending to $30°$ in elevation are quite common [30].

Figure 6.8 and Figure 6.9 illustrate the dependence of the correlation coefficient ψ on the "unfolding" polar angle of the antennas in the two-dipole array case. The effect of mutual coupling between local antennas is not considered in the simulation. The uniform angular spectrum in θ are restricted to the elevation angle spread of $\Delta\theta = 5°, 30°, 60°, 90°, 120°, 180°$. Both figures show close trend of the change in correlation of various elevation angle spread of illumination. In Figure 6.8, a rich scattering environment is simulated, where the angular spectrum in

ϕ is uniformly distributed on $[0, 2\pi)$. In Figure 6.9, the incident waves have a small angle spread in ϕ, and the angular spectrum is Gaussian distributed with $\sigma = 5°$. The figures demonstrate similar dependence of the correlation on the polar angle of antennas. In both cases, near zero correlation appears when the two dipoles are placed orthogonal to each other, that is, with "unfolding" angle $\theta = 45°$.

We simulate a MIMO system that employs uncorrelated various polarized antennas at the base station, and collocated antennas as constructed above at the handheld terminal. With 3 or 2 antennas at both transceivers, the system has either a 3×3 or a 2×2 MIMO channel. The receive SNR is 10 dB. Figure 6.10 illustrates the dependence of the channel capacities on the "unfolding" polar angle of terminal antennas. The elevation angle spread of illumination is $\Delta\theta = 30°$. The azimuthal angular spectrum is either uniform on $[0, 2\pi)$, or Gaussian with $\sigma = 5°$. The figure shows that in both scattering environments, the terminal antenna array with collocated but orthogonally positioned dipoles can provide capacities that approach the capacities of 3×3 or 2×2 MIMO Rayleigh channels. Note that in order for the dipoles of the three-antenna array to be orthogonal to each other, the "unfolding" polar angle $\theta = \sin^{-1}(\sqrt{2/3}) \approx 54.7°$.

From (6.9) we know that in order to have large channel capacity, the covariance matrix Ψ should be close to an identity matrix. For a uniform elevation illumination with angle spread of $\Delta\theta = 30°$, and a uniform azimuthal illumination on $[0, 2\pi)$, the correlation coefficient of the signals received by the two-dipole array can be calculated as

$$
\begin{aligned}
\psi_{12} &= \frac{1}{2\sigma_1\sigma_2} \int_0^{2\pi} \int_{5\pi/12}^{7\pi/12} \mathbf{A}_1(\theta, \phi) \cdot \mathbf{A}_2^*(\theta, \phi) d\theta d\phi \\
&= \frac{\pi}{48\sigma_1\sigma_2} (9 - \pi + (5\pi + 3)\cos(2\theta_0)) \quad\quad (6.23)
\end{aligned}
$$

where $\mathbf{A}_1$ and $\mathbf{A}_2$ are the receiving field patterns of the antennas "unfolded" by θ_0 to the opposite directions, θ_0 is the "unfolding" angle. For maximum channel capacity, we make Ψ an identity matrix by setting $\psi_{12} = 0$, which corresponds to
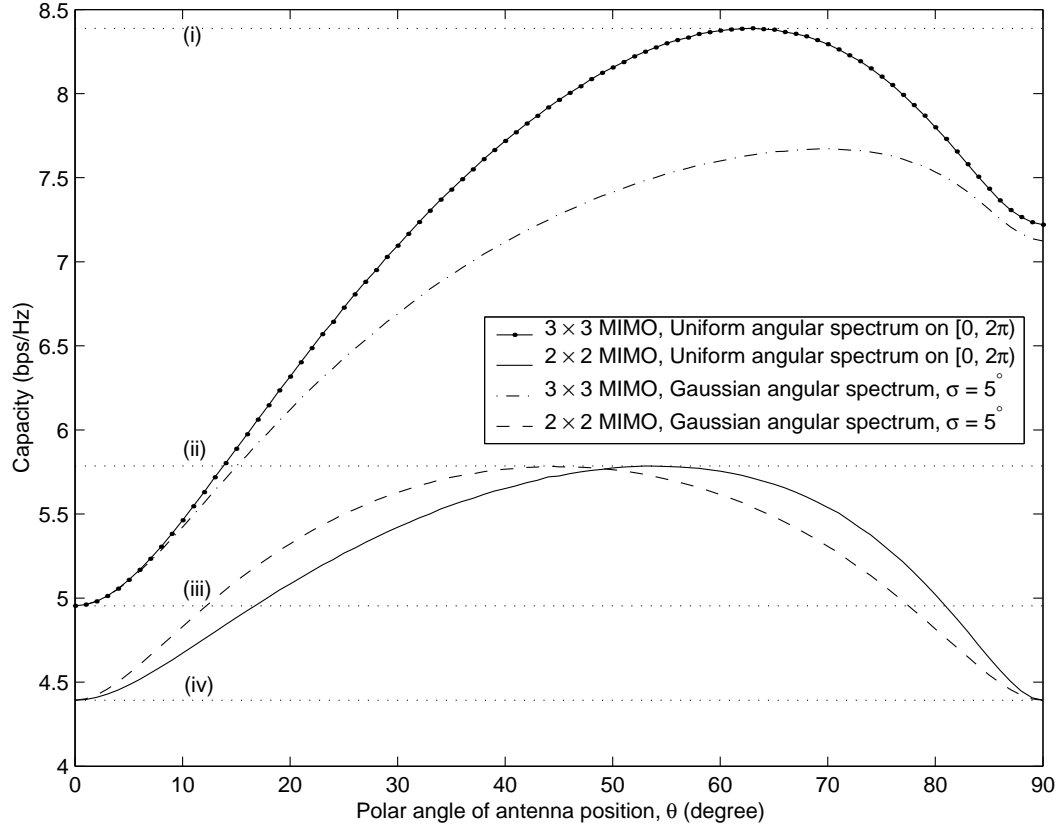
Figure 6.10: Capacity of MIMO channel versus polar angle of antenna position. Receiver SNR = 10 dB. (i) 3×3 Rayleigh channel, (ii) 2×2 Rayleigh channel, (iii) 3×1 Rayleigh channel, (iv) 2×1 Rayleigh channel.

an "unfolding" angle of

$$\theta_0 = \frac{1}{2}\cos^{-1}\left(\frac{\pi - 9}{5\pi + 3}\right) \approx 54.1° \tag{6.24}$$

The correlation coefficient of the signals received by the three-dipole array can be calculated as

$$
\begin{aligned}
\psi_{12} = \psi_{23} = \psi_{31} &= \frac{1}{2\sigma_1\sigma_2}\int_0^{2\pi}\int_{5\pi/12}^{7\pi/12} \mathbf{A}_1(\theta,\phi) \cdot \mathbf{A}_2^*(\theta,\phi)d\theta d\phi \\
&= \frac{\pi}{96\sigma_1\sigma_2}(\pi + 15 + (7\pi + 9)\cos(2\theta_0)) \tag{6.25}
\end{aligned}
$$

By setting $\psi_{12} = 0$, we obtain the "unfolding" angle for maximum channel capacity

119
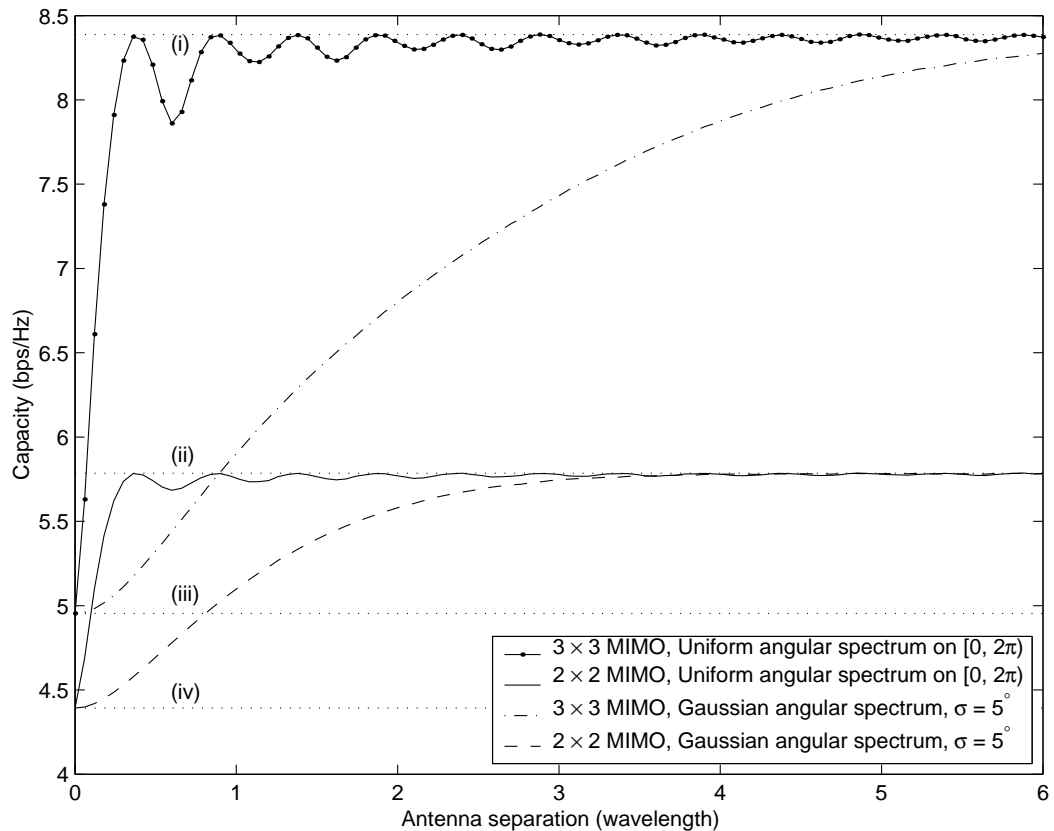
Figure 6.11: Capacity of MIMO channel versus antenna separation. Receiver SNR = 10 dB. (i) 3×3 Rayleigh channel, (ii) 2×2 Rayleigh channel, (iii) 3×1 Rayleigh channel, (iv) 2×1 Rayleigh channel.

as

$$\theta_0 = \frac{1}{2} \cos^{-1} \left(-\frac{\pi + 15}{7\pi + 9} \right) \approx 62.9^\circ \qquad (6.26)$$

These optimum "unfolding" polar angles are revealed in Figure 6.10. For the case of three-antenna array in Gaussian illumination, Ψ can not be exactly an identity matrix due to the asymmetry of correlation coefficients. Therefore, the channel capacity can not be achieved as large as in the 3×3 Rayleigh case, where the fading of transmitter-receiver pairs are uncorrelated.

As a comparison, in the same scattering environments, Figure 6.11 shows
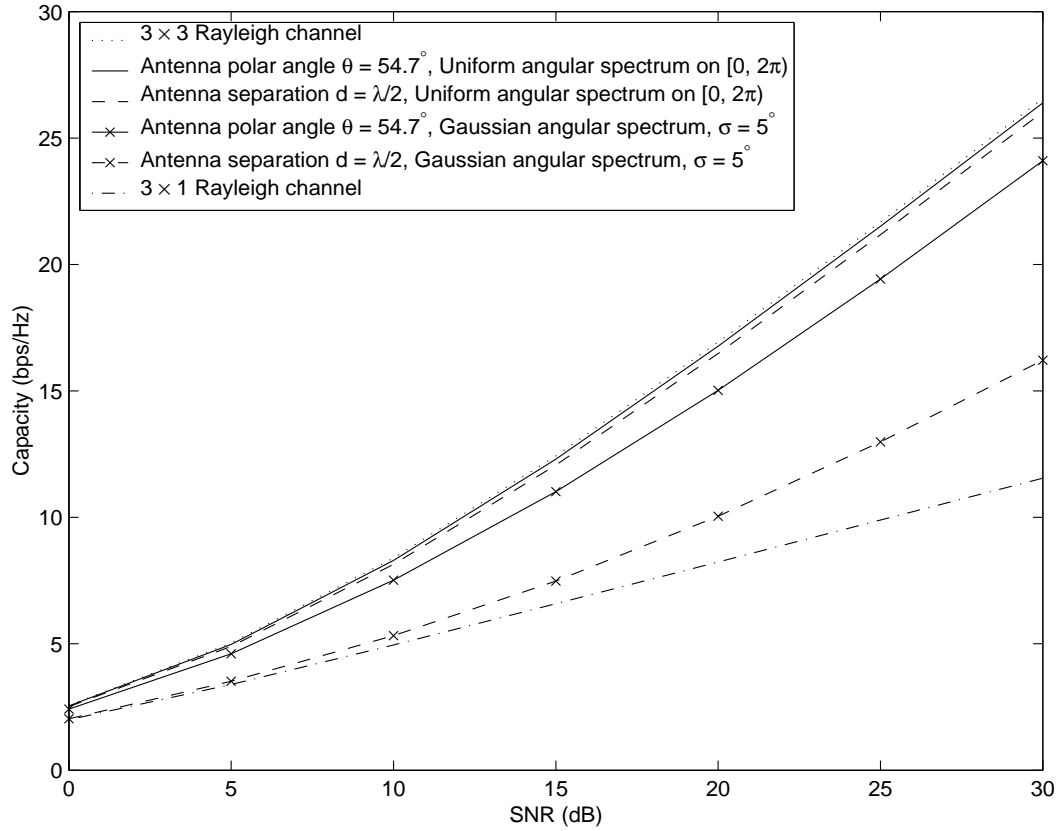
Figure 6.12: Capacities of 3×3 MIMO channels which exploit antenna pattern diversity (antenna polar angle $\theta = 54.7°$) or antenna spatial diversity (antenna separation $d = \lambda/2$).

the capacities of the 3×3 MIMO channel and the 2×2 MIMO channel, where the terminal array is composed of antennas with same radiation patterns. The diversity is provided through antenna spacing, that is, two separated vertical dipoles or three evenly separated vertical dipoles on a circle. When the handheld terminal is in a rich scattering environment with a uniform illumination in ϕ, an antenna separation of a half wavelength is required to achieve channel capacity as large as of the MIMO system with uncorrelated fading. If the incident waves have a small azimuthal angle spread with Gaussian distribution, arriving along the broadside of the array, an

antenna separation of at least a few wavelengths is required to achieve large MIMO channel capacity.

One goal is to build a terminal array with a fixed "unfolding" polar angle that can provide large channel capacity robust to the change of the scattering characteristics. In Figure 6.12, the capacities of a 3×3 MIMO system, where the terminal array is composed of three orthogonally collocated dipoles, are compared with the capacities of a 3×3 MIMO system, where the terminal array is composed of three vertical dipoles with $\lambda/2$ spacing. When the handheld terminal is in a rich scattering environment, both array structures can provide large MIMO channel capacities that approach the capacity of the 3×3 Rayleigh channel. As the scattering environment changes and results in a small angle spread of incident waves, the MIMO system that exploits antenna pattern diversity outperforms the one that exploits antenna spatial diversity, in that the former preserves near complete decorrelation of the transmitter-receiver pairs and its channel capacity does not decrease as much.

6.8   Conclusions

A MIMO wireless system that exploits antenna pattern diversity has been presented. Although the antennas are collocated at the transmitter and receiver, the system offers large capacity increase promised by the MIMO architecture. However, the capacity increase is limited due to the correlation between sub-channels in a practical scattering environment. The MIMO channel capacity is affected not only by the antenna pattern selection, but by the characteristics of the scattering environment as well. Using a computational electromagnetic simulator, we show that: (1) MIMO systems that exploit antenna pattern diversity allow for improvement over dual-polarized antenna systems; (2) The capacity increase of such MIMO systems depends on the characteristics of the scattering environment.

For a MIMO wireless system that has restrictions on the size of the handheld

terminal, we have proposed a scheme to provide fading decorrelation through the antenna pattern diversity. We showed that with appropriate selection of antenna patterns, the array with collocated antennas can provide channel capacity equivalent to the MIMO terminal that employs antenna array with sufficient antenna spacing. The fading correlation, therefore channel capacity, of a MIMO system that exploits antenna pattern diversity is less affected by the scattering characteristics than that of a MIMO system that exploits antenna spatial diversity. The ongoing research efforts include the analysis of the proposed array structure with antenna mutual coupling in a real propagation environment, and the capacity study of MIMO systems that employ more transmit and receive antennas, where pattern diversity is exploited in conjunction with spatial diversity.

Chapter 7

Conclusions

7.1 Dissertation Summary

The main focus of this dissertation has been the development and application of advanced array signal processing techniques to mobile broadband systems that have practical implementation complexity and high performance. In particular, we have focused on the characterization, modeling and prediction of fast fading vector channels, and have developed a series of new techniques for mobile broadband systems, such as blind channel estimation, power control and adaptive beamforming. We have also explored MIMO channels in non-ideal scattering environment, especially MIMO systems that exploit antenna pattern diversity.

We have briefly described the wireless channels of adaptive antenna systems, and discussed how the fast fading effect and the large delay spread of multipath channels challenge the implementation of mobile broadband communications. In fact, most of the current techniques of adaptive antenna systems have it as a premise that the channel is time-invariant over an uplink/downlink frame, and the algorithm complexity becomes unbearable when attempting to recover signals with receiving delays spread over symbol periods.

We have modeled the channel fading as an AR process, and verified the validity of using models with low order in a scattering environment. In practice, not all the AR model coefficients can be precisely estimated from a noisy signal. We have exploited the redundancy of the fading characteristics, either in the channel transfer functions at different frequencies, in the access channel and the traffic channel, or in the signals received at multiple antennas, to obtain a better estimation of the model coefficients. These solutions to channel estimation have paved the road for the development of our joint wideband channel prediction, dynamic uplink power control, and predictive downlink beamforming.

The uplink power control and the adaptive downlink beamforming, implemented at the mobile site and the base station respectively, were both developed in an effort to combat fast Rayleigh fading. The dynamic power control and the predictive beamforming can track the channel variation within an uplink/downlink frame, such that they are able to compensate the deep fades within a frame, provided the necessary hardware modifications. We have also exploited the subspace of the spatial covariance matrix of received signals at the base station antennas. The stability of the channel subspaces provides a platform to develop our subspace-based beamforming algorithm against fast fading. This technique has overcome the impairment of independent fading in uplink and downlink because of the negligible distance between uplink and downlink subspaces in a practical FDD system, and it can be implemented effectively without any feedback requirement.

Confronting the large delay spread of the wideband channel, we have proposed a blind channel estimation algorithm, which can be combined with a RAKE receiver. The algorithm is of low complexity, because the space-time structure of the wideband channel helps to reduce the number of the unknown model parameters.

This dissertation has also been extended from vector channel study to matrix channel study. The matrix channel is used to describe the wireless link of MIMO sys-

tems. We have discussed the channel capacity of MIMO systems, and analyzed the correlation between sub-channels, which imposes limitations on the linear capacity increase promised by MIMO configuration. In the search for improved decorrelation, we have included the antenna pattern diversity into the channel matrix. Through a ray tracing simulator, we have compared the capacity increases in various scattering environments. Finally, an antenna array that exploits pattern diversity has been proposed for compact MIMO handheld terminals.

7.2   Primary Contributions

This dissertation has analyzed the mobile vector channels for broadband antenna systems, and has consequently laid the foundation for the array signal processing of broadband wireless communications. A series of new techniques for mobile broadband systems have been developed. The primary contributions of this dissertation include:

1. **Characterization of mobile broadband channels**   We study the multipath fading effect of mobile broadband channels. The delay spread and the Doppler spread are investigated, which leads to the bridging of correlation functions of a WSSUS channel model. We also explore the structure of broadband vector channels to simplify channel estimation algorithms.

2. **Modeling and prediction of broadband vector channels**   We model time-varying vector channels as low-order autoregressive (AR) processes. The suitability of the AR model for the scattering radio channel is verified. We predict the channel transfer function of the wideband system, as the prediction coefficients are jointly found over the frequency band to reduce prediction error.

3. **An estimation algorithm of low complexity for broadband channels**

With careful study of the model constraints of the broadband channel, we propose a blind estimation algorithm for the CDMA vector channel. This algorithm alleviates the computational burden of the subspace-based estimation, which is conventionally extensive. Therefore, it is favorable to be implemented in any real-time systems.

4. **A power control scheme for fast mobiles**   We propose an open-loop dynamic power control scheme for the mobile unit. This uplink power control enables the base station to receive constant signal power over a fast fading channel. The power control relies on the channel prediction, which takes advantage of the usage of access channel and traffic channel in the CDMA protocol.

5. **Adaptive beamforming to combat fast Rayleigh fading**   We propose two adaptive beamforming approaches for mobile broadband communications. Both of them can transmit desired downlink signals effectively despite the fast Rayleigh fading effect. The first beamforming is based on the efficient vector channel prediction. It can be directly implemented in time division duplex (TDD) systems, and only needs moderate channel feedback if implemented in frequency division duplex (FDD) systems. The second one is based on the analysis of channel subspaces, and it can be directly implemented in both TDD and FDD systems.

6. **Verification of algorithms by ray tracing simulations**   We perform simulations on the computer-aided design (CAD) models of propagation environments through a ray tracer, FASANT. The field parameters it provides, which are much closer to reality than mathematical models, are mingled with our communication channel representations to evaluate system performance such as bit error rate (BER) and channel capacity.

7. **Channel modeling and capacity study of MIMO systems that exploit antenna patter diversity** We explore the MIMO wireless system that exploits antenna pattern diversity, while studying the channel capacity and its dependence on the scattering characteristics of a practical electromagnetic surrounding. The pattern diversity is expressed in the channel transfer matrix for a better capture of the system capacity.

8. **Design of a MIMO handheld terminal with compact antenna array** Having characterized the fading correlation between sub-channels of a MIMO system, we propose an array design for the handheld terminal that exploits antenna pattern diversity. The antenna array consists of multiple collocated antennas with dissimilar radiation patterns, such that the terminal remains its compact size, whereas the generated pattern diversity guarantees large channel capacity.

7.3 Future Research

Work continues on smart antenna systems and MIMO systems for mobile broadband communications. Although MIMO wireless systems have been extensively studied due to its unique advantage for high-data-rate wireless communication, previous researches have been focused on the fixed MIMO wireless access, most of which have been limited to narrowband channels. (The narrowband MIMO can still achieve high data rate, thanks to the multi-carrier techniques such as orthogonal frequency-division multiplexing (OFDM).) How to bridge the current techniques of fixed MIMO and the rapidly growing demand for mobile broadband communications will be an exciting research topic.

Future research may include issues pertinent to MIMO mobile cellular systems, with emphases on mobile broadband MIMO channel modeling, OFDM-based

mobile broadband MIMO communications, and smart antenna mobile-assisted hand-off of multi-cell MIMO systems. The multiplexing of MIMO systems that exploit antenna pattern diversity and/or spatial diversity will be further explored. This will involve space-time coding for MIMO fading channels, transceiver deployment and compact antenna design. By analyzing characteristics of the propagation environment, implementation algorithms will be developed for mode switching between MIMO for diversity gain and MIMO for multiplexing gain, as well as algorithms for tuning of adaptive modulation at different cell locations.

The study of wireless communication systems with high mobility can be extended to the research on mobile Ad-hoc networks. Such network is composed of mobile-to-mobile links only, but no fixed base stations. Therefore, the relative speed of mobile units results in a wireless channel of even higher mobility.

Indoor measurement will be taken to support research on the MIMO wireless data link and wireless networking. Outdoor vehicular measurement will be taken, or computational electromagnetics used, to study the MIMO system with high mobility.

Appendix A

Distance Between Uplink and Downlink Subspaces

As a mobile communicates with a base station which has an M-element circular array, the effective uplink channel subspace $\mathcal{A}^{(u)} \subseteq \mathbb{C}^M$ and the effective downlink channel subspace $\mathcal{A}^{(d)} \subseteq \mathbb{C}^M$ are given by

$$\begin{aligned}
\mathcal{A}^{(u)} &= \text{span}\{\mathbf{v}_1^{(u)}, \mathbf{v}_2^{(u)}, \ldots, \mathbf{v}_L^{(u)}\} \\
\mathcal{A}^{(d)} &= \text{span}\{\mathbf{v}_1^{(d)}, \mathbf{v}_2^{(d)}, \ldots, \mathbf{v}_L^{(d)}\}
\end{aligned} \tag{A.1}$$

where

$$\begin{aligned}
\mathbf{v}_i^{(\cdot)} &= [e^{j2\pi R f_c^{(\cdot)} \cos(\theta_i)/C}, e^{j2\pi R f_c^{(\cdot)} \cos(\theta_i + 2\pi/M)/C}, \cdots, e^{j2\pi R f_c^{(\cdot)} \cos(\theta_i + 2\pi(M-1)/M)/C}]^T \\
& \quad i = 1, \ldots, L
\end{aligned}$$

Suppose that $\text{rank}(\mathcal{A}^{(u)}) = \text{rank}(\mathcal{A}^{(d)}) = L \leq M$. Let $P^{(u)} \in \mathbb{C}^{M \times M}$ and $P^{(d)} \in \mathbb{C}^{M \times M}$ be the orthogonal projections onto $\mathcal{A}^{(u)}$ and $\mathcal{A}^{(d)}$, respectively. For an arbitrary unit-norm vector $\mathbf{a}^{(d)} \in \mathcal{A}^{(d)}$, let $\mathbf{a}^{(u)} = P^{(u)}\mathbf{a}^{(d)} \in \mathcal{A}^{(u)}$. For the algorithm developed in this paper, we want to show that the norm of $\mathbf{a}^{(u)}$ is close to the norm of $\mathbf{a}^{(d)}$ in a practical FDD system. First we examine the case when $L = 1$. Let

$\mathbf{a}^{(d)} = \alpha\mathbf{v}_1^{(d)}$, where α is a scaler. Since $\mathbf{a}^{(d)}$ has unit norm, $|\alpha| = 1/\sqrt{M}$. The orthogonal projection onto $\mathcal{A}^{(u)}$ is

$$P^{(u)} = \frac{\mathbf{v}_1^{(u)}\mathbf{v}_1^{(u)H}}{\mathbf{v}_1^{(u)H}\mathbf{v}_1^{(u)}} = \frac{1}{M}\mathbf{v}_1^{(u)}\mathbf{v}_1^{(u)H} \tag{A.2}$$

Therefore,

$$\begin{aligned}
||\mathbf{a}^{(u)}|| &= ||P^{(u)}\mathbf{a}^{(d)}|| = \frac{|\mathbf{v}_1^{(u)H}\mathbf{v}_1^{(d)}|}{M}||\alpha\mathbf{v}_1^{(u)}|| \\
&= \frac{1}{M}\left|\sum_{k=0}^{M-1}e^{j2\pi R\Delta f_c\cos(\theta_1+2\pi k/M)/C}\right| \tag{A.3}
\end{aligned}$$

where $\Delta f_c = f_c^{(d)} - f_c^{(u)}$. At the PCS spectrum about 1.9 GHz, though the difference of the two carriers can be as large as 10%, if the array radius R is only about half wavelength of the carrier, $R\Delta f_c/C \approx 0.05$. Therefore the exponential terms in the above sum are close to 1.

When $L = 2$, the unique orthogonal projection for each link is

$$P^{(\cdot)} = \frac{\mathbf{v}_1^{(\cdot)}\mathbf{v}_1^{(\cdot)H} + \mathbf{v}_2^{(\cdot)}\mathbf{v}_2^{(\cdot)H} - \beta\mathbf{v}_1^{(\cdot)}\mathbf{v}_2^{(\cdot)H} - \beta^*\mathbf{v}_2^{(\cdot)}\mathbf{v}_1^{(\cdot)H}}{M(1-|\beta|^2)} \tag{A.4}$$

where $\beta = \frac{\mathbf{v}_1^{(\cdot)H}\mathbf{v}_2^{(\cdot)}}{M}$. The distance between subspaces $\mathcal{A}^{(u)}$ and $\mathcal{A}^{(d)}$ is defined by [76]

$$\mathcal{D}(\mathcal{A}^{(u)}, \mathcal{A}^{(d)}) = ||P^{(d)} - P^{(u)}||_2 \tag{A.5}$$

Therefore,

$$\begin{aligned}
||\mathbf{a}^{(u)}|| &= ||P^{(u)}\mathbf{a}^{(d)}|| \\
&= (||\mathbf{a}^{(d)}||^2 - ||(I - P^{(u)})\mathbf{a}^{(d)}||_2^2)^{\frac{1}{2}} \\
&= (1 - ||(P^{(d)} - P^{(u)})\mathbf{a}^{(d)}||_2^2)^{\frac{1}{2}} \\
&\geq (1 - ||P^{(d)} - P^{(u)}||_2^2 \cdot ||\mathbf{a}^{(d)}||^2)^{\frac{1}{2}} \\
&= (1 - ||P^{(d)} - P^{(u)}||_2^2)^{\frac{1}{2}} \\
&= (1 - \mathcal{D}^2(\mathcal{A}^{(u)}, \mathcal{A}^{(d)}))^{\frac{1}{2}} \tag{A.6}
\end{aligned}$$
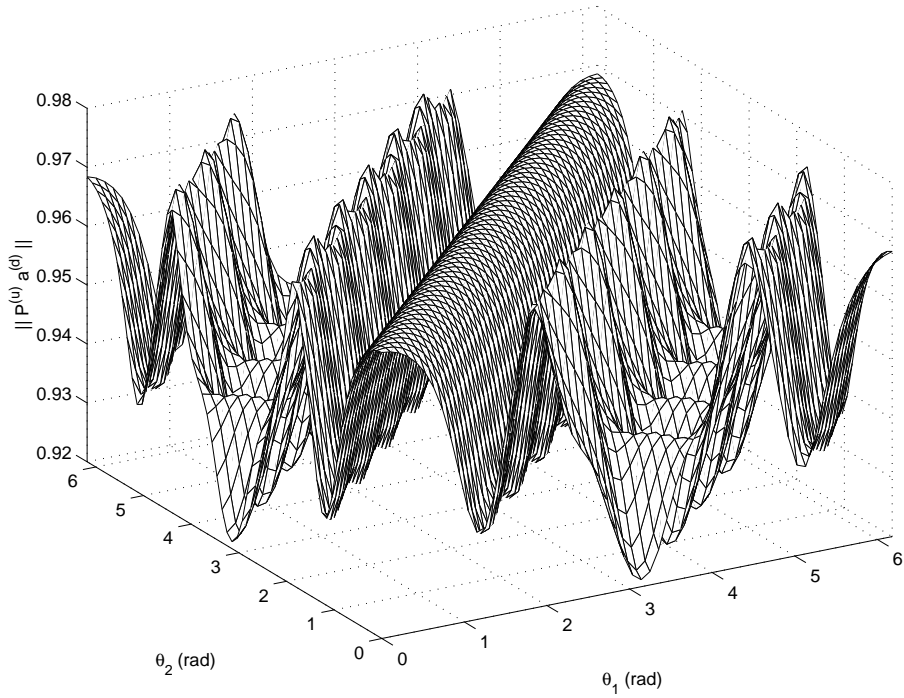
Figure A.1: Lower bound of $||P^{(u)}\mathbf{a}^{(d)}||$, $L = 2$.

Figure A.1 shows the lower bound of $||P^{(u)}\mathbf{a}^{(d)}||$ as θ_1 and θ_2 vary independently in $[0, 2\pi)$, where $R = 0.085$ m, $f_c^{(u)} = 1.8$ GHz and $f_c^{(d)} = 2.0$ GHz. The lower bound is close to 1, which means the norm of the downlink channel vector projected onto the effective uplink channel subspace is comparatively large. Notice that when $\theta_1 = \theta_2$, it devolves to be the case of $L = 1$, where the lower bound of $||P^{(u)}\mathbf{a}^{(d)}||$ is approximately 0.9686.

132

Appendix B

Channel Representations of FASANT Simulation

FASANT output file OUTPUT.OUT contains information of each individual incident ray at the observation points: the e-field contribution E_x, E_y, E_z, the path length d, and the angles θ, ϕ of the direction of arrival (DOA). In our experiment using dipole antennas with linear polarization, we only need E_z and azimuth angle ϕ.

TOTAL.OUT shows the total field at each point. IPOINT.OUT contains the information of the intermediate points of each ray, which is not of interest here.

Complex value E_z represents the phasor at each observation points, i.e.

$$E_z = -A \; e^{-j \; (2\pi f_c \frac{d}{C} \; + \; \psi)} \tag{B.1}$$

where, f_c is the RF carrier frequency, d is the ray length from transmitter to receiver, ψ is the random phase change when the ray is reflected or diffracted by some objects. (For line-of-sight rays, obviously $\psi = 0$). Real number A is the peak field value, which decays when d increases. The negative sign on the right hand side explains the fact that the E_z component at the transmission point heading down

along the z axis due to the definition of θ.

Multipath Channel Model   Assuming there are p rays impinging on the receiver at a particular observation point. With transmitted signal $s(t)$ being modulated to the carrier frequency f_c as $s(t)e^{j2\pi f_c t}$, the received signal is

$$
\begin{aligned}
x(t) &= \sum_{k=1}^{p} E_z^{(k)}\ e^{j\ 2\pi f_c t}\ s(t - \tau_k) \\
&= \sum_{k=1}^{p} -A_k\ e^{-j\ (2\pi f_c \frac{d_k}{C}\ +\ \psi_k)}\ e^{j\ 2\pi f_c t}\ s(t - \tau_k)
\end{aligned}
\tag{B.2}
$$

The baseband signal is therefore,

$$
x(t) = \sum_{k=1}^{p} E_z^{(k)}\ s(t - \tau_k)
\tag{B.3}
$$

Hence the channel

$$
h(\tau) = \sum_{k=1}^{p} \alpha_k\ \delta(\tau - \tau_k)
\tag{B.4}
$$

where, the complex amplitude $\alpha_k = E_z^{(k)}$ is a function of f_c. Note that with different carrier frequencies, the phase difference between two arriving rays at a fixed observation point is different, i.e.

$$
\Delta \Psi_{ij} = 2\pi f_c \frac{d_j - di}{C} + \psi_j - \psi_i
$$

Doppler Spread and Time-varying Channel   For a receiver moving with velocity $\vec{v}$, the Doppler frequency shift correspondent to one individual ray is

$$
f_d = \frac{v \cos(\varphi)}{\lambda} = \frac{v \cos(\varphi)}{C} f_c
\tag{B.5}
$$

where λ is the carrier wavelength. φ is the angle between $\vec{v}$ and the DOA of this ray, which can be calculated from output azimuth angle ϕ. The baseband received

signal at one particular observation point with instantaneous velocity $\vec{v}$ is therefore

$$x(t) = \sum_{k=1}^{p} E_z^{(k)} \ e^{j \ 2\pi f_d^{(k)} t} \ s(t - \tau_k) \tag{B.6}$$

Hence the time-varying channel

$$h(\tau; t) = \sum_{k=1}^{p} E_z^{(k)} \ e^{j \ 2\pi f_d^{(k)} t} \ \delta(\tau - \tau_k) \tag{B.7}$$

Finite Bandwidth Receiver Resolution   For a finite bandwidth receiver, the resolution of the arriving rays is limited. Multipath rays with close delays cluster at the receive end and become indistinguishable in time, though they may have different DOAs. Assuming there are L such clusters of all arriving rays, the channel model can be well approximated as

$$h(\tau; t) = \sum_{l=1}^{L} \beta_l(t) \ \delta(\tau - \tau_l) \tag{B.8}$$

where,

$$\beta_l(t) = \sum_{i=1}^{p_l} E_z^{(i)} \ e^{j \ 2\pi f_d^{(i)} t} \tag{B.9}$$

We made the assumption that $\tau_i \approx \tau_l \ (i = 1, \ldots, p_l)$, which is validated by the bandwidth limitation. With relatively large number p_l, $\beta_l(t)$ expresses Rayleigh distribution, or Ricean distribution if there is a strong line-of-sight.

Channel Representation Steps

1. Extract the z component of the e-field E_z, path length d, azimuth angle ϕ of DOA of each ray at the observation point. RF carrier frequency is f_c.

2. Derive path delay τ_k from path length d_k. From (B.5), derive Doppler shift f_d of each ray from assumed velocity v, ϕ and f_c.

3. Obtain time-varying channel expression by (B.7). Note that the channel is f_c-dependent.

4. For narrowband signal, the delay difference is neglected. For wideband signal, cluster close rays accordingly to exercise channel model (B.8).

Appendix C

Received Signal at Patterned Antenna

In order to derive the voltage on a receive antenna caused by the incident electromagnetic field, let us ignore the antenna scattering and consider two equivalent problems of one receive antenna. One is to calculate the received voltage v_i caused by the incident field $\mathbf{E}_i, \mathbf{H}_i$, and the other is to generate the radiated field $\mathbf{E}_r, \mathbf{H}_r$ excited by the current source $\mathbf{J}_r$. By the Lorentz Reciprocity Theorem, we have

$$- \oint_S (\mathbf{E}_i \times \mathbf{H}_r - \mathbf{E}_r \times \mathbf{H}_i) \cdot d\mathbf{s} = \int_V (\mathbf{E}_i \cdot \mathbf{J}_r - \mathbf{E}_r \cdot \mathbf{J}_i) dv \qquad (C.1)$$

Note that $\mathbf{J}_i = 0$, the right side of (C.1) becomes

$$\int_V \mathbf{E}_i \cdot \mathbf{J}_r dv = I_r \int_L \mathbf{E}_i \cdot d\mathbf{l} = I_r v_i \qquad (C.2)$$

where, I_r is the current on the antenna. Therefore, the received voltage at the antenna can be derived as

$$
\begin{aligned}
v_i &= \frac{1}{I_r} \oint_S (\mathbf{E}_r \times \mathbf{H}_i - \mathbf{E}_i \times \mathbf{H}_r) \cdot \hat{\mathbf{r}} ds \\
&= \frac{1}{I_r} \oint_S \left(\mathbf{E}_r \times \frac{1}{\eta}(-\hat{\mathbf{r}} \times \mathbf{E}_i) - \mathbf{E}_i \times \frac{1}{\eta}(\hat{\mathbf{r}} \times \mathbf{E}_r) \right) \cdot \hat{\mathbf{r}} ds \\
&= \frac{1}{\eta I_r} \oint_S [-(\mathbf{E}_r \cdot \mathbf{E}_i)\hat{\mathbf{r}} + (\hat{\mathbf{r}} \cdot \mathbf{E}_i)\mathbf{E}_r - (\mathbf{E}_i \cdot \mathbf{E}_r)\hat{\mathbf{r}} + (\hat{\mathbf{r}} \cdot \mathbf{E}_r)\mathbf{E}_i] \cdot \hat{\mathbf{r}} ds \\
&= -\frac{2}{\eta I_r} \oint_S (\mathbf{E}_i \cdot \mathbf{E}_r) ds \quad\quad\quad\quad\quad\quad\quad (\text{C.3})
\end{aligned}
$$

Perform the integration on the spherical surface with radius R, where the receive antenna is at the center of the sphere. R is large enough such that the antenna far-field assumption is valid. Suppose the antenna has an effective receiving area ds_0 seen from all arriving angles. Therefore, for the mth ray arriving at the receive antenna with path length is l_m, the receiving area on the integral surface is $ds_m = \frac{l_m - R}{l_m} ds_0$. Therefore, we can express the integration by a summation as

$$
\begin{aligned}
v^i &\propto \sum_{m=1}^{M} \tilde{\mathbf{E}}_i^m \cdot \tilde{\mathbf{E}}_r^m ds_m \\
&= \sum_{m=1}^{M} \frac{l_m}{l_m - R} \mathbf{E}_i^m e^{jk_0 R} \cdot \frac{1}{R} \mathbf{F}_r(\theta_m, \phi_m) e^{-jk_0 R} ds_m \\
&= \sum_{m=1}^{M} \mathbf{E}_i^m \cdot \mathbf{F}_r(\theta_m, \phi_m) \frac{ds_0}{R} \quad\quad\quad\quad\quad\quad (\text{C.4})
\end{aligned}
$$

where $\tilde{\mathbf{E}}_i^m$ and $\tilde{\mathbf{E}}_r^m$ denote the fields on the integral sphere with radius R. With normalization, this leads to the relationship between the voltage on the receive antenna and the incident field as expressed in (6.11).

138

Appendix D

Rotation of Antenna Radiation Pattern in 3D Cartesian Coordinate System

Two 3D-vectors $\mathbf{p}$ and $\mathbf{p}'$, $\mathbf{p}'$ is obtained from $\mathbf{p}$ by the *Euler* rotation angles $[\alpha, \beta, \gamma]$ about "X then Y then Z", then a (unitary) rotation matrix $\mathbf{R}$ may represent the rotation:

$$\mathbf{p}' = \mathbf{R}\mathbf{p} \tag{D.1}$$

where,

$$\mathbf{R} = \begin{pmatrix} \cos(\gamma)\cos(\beta) & -\cos(\beta)\sin(\gamma) & \sin(\beta) \\ \cos(\alpha)\sin(\gamma) + \cos(\gamma)\sin(\beta)\sin(\alpha) & \cos(\gamma)\cos(\alpha) - \sin(\gamma)\sin(\beta)\sin(\alpha) & -\cos(\beta)\sin(\alpha) \\ -\cos(\gamma)\cos(\alpha)\sin(\beta) + \sin(\gamma)\sin(\alpha) & \cos(\gamma)\sin(\alpha) + \sin(\gamma)\sin(\beta)\cos(\alpha) & \cos(\beta)\cos(\alpha) \end{pmatrix}$$

The rotation of the vector is equivalent to the rotation of the Cartesian coordinates (with opposite direction) as shown in Figure D.1. Suppose the radiation pattern at point p due to the antenna in original position 1 is $\mathbf{E}_1$. $\mathbf{E}_1$ is given by

$$\mathbf{E}_1 = A_x(x, y, z)\hat{\mathbf{x}} + A_y(x, y, z)\hat{\mathbf{y}} + A_z(x, y, z)\hat{\mathbf{z}} \tag{D.2}$$
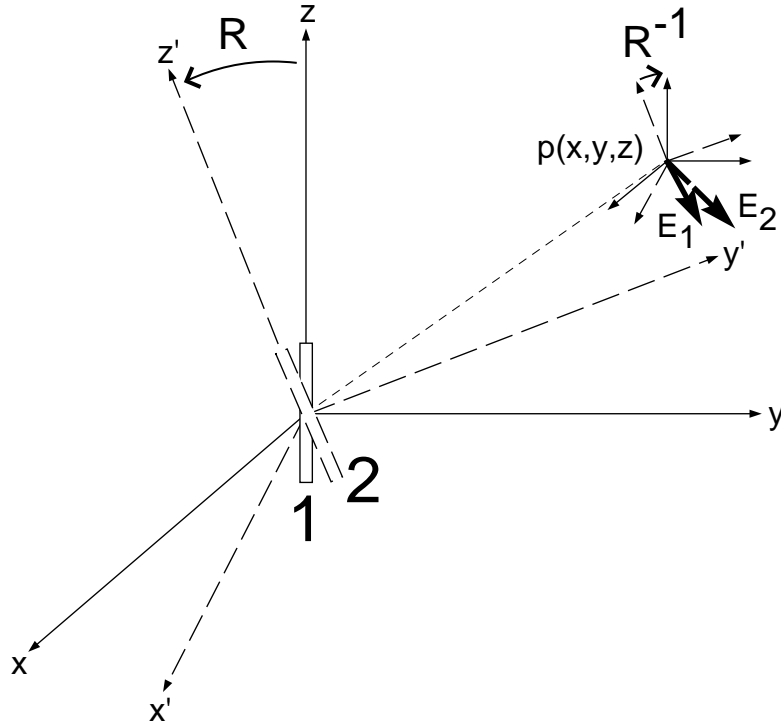
Figure D.1: Rotation of the antenna radiation pattern

When the antenna is rotated to position 2, or equivalently the Cartesian axes are rotated to (x', y', z'), the radiation pattern at point p is $\mathbf{E}_2$. $\mathbf{E}_2$ in the (x', y', z') coordinate system is given by

$$\mathbf{E}_2 = A_x(x', y', z')\hat{\mathbf{x}'} + A_y(x', y', z')\hat{\mathbf{y}'} + A_z(x', y', z')\hat{\mathbf{z}'} \tag{D.3}$$

where

$$\begin{pmatrix} x' \\ y' \\ z' \end{pmatrix} = \mathbf{R} \begin{pmatrix} x \\ y \\ z \end{pmatrix} \tag{D.4}$$

140

To be expressed in the (x, y, z) coordinate system, this pattern vector is again rotated back by

$$\begin{pmatrix} E_x \\ E_y \\ E_z \end{pmatrix} = \mathbf{R}^{-1} \begin{pmatrix} A_x(x', y', z') \\ A_y(x', y', z') \\ A_z(x', y', z') \end{pmatrix} \tag{D.5}$$

Finally, we have the radiation pattern of the rotated antenna (in position 2). The field component at point p is given by

$$\mathbf{E}_2 = E_x(x, y, z)\hat{\mathbf{x}} + E_y(x, y, z)\hat{\mathbf{y}} + E_z(x, y, z)\hat{\mathbf{z}} \tag{D.6}$$

Bibliography

[1] T. S. Rappaport, *Wireless Communications*, Prentice Hall, NJ, 1996.

[2] W. C. Y. Lee, "The most spectrum-efficient duplexing systems: CDD," *IEEE Commum. Mag.*, vol. 40, no. 3, pp. 163–166, Mar. 2002.

[3] F. J. Velez and L. M. Correia, "Mobile broadband services: classification, characterization, and deployment scenarios," *IEEE Commun. Mag.*, vol. 40, no. 4, pp. 142–150, Apr. 2002.

[4] R. D. Murch and K. B. Letaief, "Antenna systems for broadband wireless access," *IEEE Commun. Mag.*, vol. 40, no. 4, pp. 76–83, Apr. 2002.

[5] J. H. Winters, "Smart antennas for wireless systems," *IEEE Pers. Commun. Mag.*, vol. 5, no. 1, pp. 23–27, Feb. 1998.

[6] A. Paulraj and C. Papadias, "Space-time processing for wireless communications," *IEEE Signal Processing Mag.*, pp. 49–83, Nov. 1997.

[7] V. Tarokh, N. Seshadri, and A. R. Calderbank, "Space-time codes for high data rate wireless communication: performance criterion and code construction," *IEEE Trans. Inform. Theory*, vol. 44, no. 2, pp. 744–765, Mar. 1998.

[8] V. Tarokh, H. Jafarkhani, and A. R. Calderbank, "Space-time block codes

from orthogonal designs," *IEEE Trans. Inform. Theory*, vol. 45, no. 5, pp. 1456–1467, July 1999.

[9] V. Tarokh, H. Jafarkhani, and A. R. Calderbank, "Space-time block coding for wireless communications: performance results," *IEEE J. Select. Areas Commun.*, vol. 17, no. 3, pp. 451–460, Mar. 1999.

[10] A. Paulraj and T. Kailath, "U.S. pattern No. 5345599: Increasing capacity in wireless broadcast systems using distributed transmission/directional reception (DTDR)," Sept. 1994.

[11] G. J. Foschini and M. J. Gans, "On limits of wireless communications in a fading environment when using multiple antennas," *Wireless Personal Commun.*, vol. 6, no. 3, pp. 311–335, Mar. 1998.

[12] G. J. Foschini, "Layered space-time architecture for wireless communication in a fading environment when using multi-element antennas," *Bell Labs Tech. J.*, vol. 1, no. 2, pp. 41–59, 1996.

[13] A. Lozano, F. Rashid-Farrokhi, and R. A. Valenzuela, "Lifting the limits on high-speed wireless data access using antenna arrays," *IEEE Commun. Mag.*, vol. 39, no. 9, pp. 156–162, Sept. 2001.

[14] L. Dong, G. Xu, and H. Ling, "Prediction of fast fading mobile radio channels in wideband communication systems," in *Proc. IEEE GLOBECOM'01*, Nov. 2001, pp. 3287–3291.

[15] L. Dong and G. Xu, "Dynamic uplink power control for cellular radio systems over fast fading channel," in *Proc. IEEE VTC'01*, May 2001, pp. 2849–2853.

[16] L. Dong, G. Xu, and H. Ling, "Predictive downlink beamforming for wireless cdma over rayleigh fading channels," *submitted to IEEE Trans. Wireless Commun.*, Apr. 2002.

[17] L. Dong and G. Xu, "Subspace-base beamforming for fast rayleigh fading signals," *submitted to IEEE Trans. Commun.*, June 2002.

[18] L. Dong, G. Xu, and H. Ling, "Subspace-based channel estimation for wideband cdma communication systems," in *Proc. IEEE MILCOM'01*, Oct. 2001, pp. 1205–1209.

[19] L. Dong, H. Ling, and R. W. Heath, "Multiple-input multiple-output wireless communication systems using antenna pattern diversity," *to be presented at IEEE GLOBECOM'02*, 2002.

[20] L. Dong, R. W. Heath, and H. Ling, "MIMO wireless handheld terminals using antenna pattern diversity," *submitted to IEEE Trans. Wireless Commun.*, July 2002.

[21] A. Duel-Hallen, S. Hu and H. Hallen, "Long-range prediction of fading signals," *IEEE Signal Processing Mag.*, vol. 17, no. 3, pp. 62–75, May 2000.

[22] R. Vaughan, P. Teal and R. Raich, "Short-term mobile channel prediction using discrete scatterer propagation model and subspace signal processing algorithms," in *Proc. IEEE VTC'00*, Sept. 2000, pp. 751–758.

[23] T. Eyceoz, A. Duel-Hallen, and H. Hallen, "Deterministic channel modeling and long range prediction of fast fading mobile radio channels," *IEEE Commun. Lett.*, vol. 2, pp. 254–256, Sept. 1998.

[24] J. Hwang and J. Winters, "Sinusoidal modeling and prediction of fast fading processes," in *Proc. IEEE GLOBECOM'98*, Nov. 1998, pp. 892–897.

[25] J. Andersen, J. Jensen, S. Jensen and F. Frederiksen, "Prediction of future fading based on past measurements," in *Proc. IEEE VTC'99*, Sept. 1999, pp. 151–155.

[26] T. Ekman and G. Kubin, "Nonlinear prediction of mobile radio channels: measurements and MARS model designs," in *Proc. IEEE ICASSP'99*, May 1999, vol. 5, pp. 2667–2670.

[27] R. Roy and T. Kailath, "ESPRIT – estimation of signal parameters via rotational invariance techniques," *IEEE Trans. Acoust., Speech, Signal Processing*, vol. 37, no. 7, pp. 984–995, July 1989.

[28] R. H. Clarke, "A statistical theory of mobile-radio reception," *Bell Syst. Tech. Jour.*, vol. 47, pp. 957–1000, 1968.

[29] P. A. Bello, "Characterization of randomly time-variant linear channel," *IEEE Trans. Commun. Syst.*, vol. CS-11, pp. 360–393, 1963.

[30] W. C. Jakes, *Microwave Mobile Communications*, John Wiley and Sons, New York, 1974.

[31] R. D. Yates, "A framework for uplink power control in cellular radio systems," *IEEE J. Select. Areas Commun.*, vol. 13, no. 7, pp. 1341–1347, Sept. 1995.

[32] F. Rashid-Farrokhi, L. Tassiulas, and K. J. R. Liu, "Joint optimal power control and beamforming in wireless networks using antenna arrays," *IEEE Trans. Commun.*, vol. 46, no. 10, pp. 1313–1324, Oct. 1998.

[33] B. Sklar, "Rayleigh fading channels in mobile digital communication system part II: Mitigation," *IEEE Commun. Mag.*, pp. 103–109, July 1997.

[34] D. Astély and B. Ottersten, "The effects of local scattering on direction of arrival estimation with MUSIC," *IEEE Trans. Signal Processing*, vol. 47, no. 12, pp. 3220–3234, Dec. 1999.

[35] M. H. Hayes, *Statistical Digital Signal Processing and Modeling*, John Wiley and Sons, 1996.

[36] C. W. Therrien, *Discrete Random Signals and Statistical Signal Processing*, Prentice Hall, NJ, 1992.

[37] M. Torlak, G. Xu, B. L. Evans, and H. Liu, "Fast estimation of weight vectors to optimize multi-transmitter broadcast channel capacity," *IEEE Trans. Signal Processing*, vol. 46, no. 1, pp. 243–246, Jan. 1998.

[38] J. H. Winters, J. Salz, and R. D. Gitlin, "The impact of antenna diversity on the capacity of wireless communications systems," *IEEE Trans. Commun.*, vol. 42, no. 2/3/4, pp. 1740–1751, Feb./Mar./Apr. 1994.

[39] A. F. Naguib, A. Paulraj, and T. Kailath, "Capacity improvement with base-station antenna arrays in cellular CDMA," *IEEE Trans. Veh. Technol.*, vol. 43, no. 3, pp. 691–698, Aug. 1994.

[40] J. H. Winters, "Optimum combining in digital mobile radio with cochannel interference," *IEEE J. Select. Areas Commun.*, vol. SAC-2, no. 4, pp. 528–539, July 1984.

[41] A. Arredondo, K. R. Dandekar, and G. Xu, "Vector channel modeling and prediction for improvement of downlink received power," *to appear in IEEE. Trans. Commun.*

[42] A. Akaike, "A new look at the statistical model identification," *IEEE Trans. Automat. Contr.*, vol. AC-19, pp. 716–723, Dec. 1974.

[43] G. Schwartz, "Estimating the dimension of a model," *Ann. Stat.*, vol. 6, pp. 461–464, Oct. 1978.

[44] J. Rissanen, "Modeling by shortest data description," *Automatica*, vol. 14, pp. 465–471, 1978.

[45] J. G. Proakis, *Digital Communications*, New York: McGraw Hill, 3rd edition, 1995.

[46] D. Gerlach and A. Paulraj, "Adaptive transmitting antenna arrays with feedback," *IEEE Signal Processing Lett.*, vol. 1, no. 10, pp. 150–152, Oct. 1994.

[47] G. Xu and H. Liu, "An effective transmission beamforming scheme for frequency-division-duplex digital wireless communication systems," in *Proc. IEEE ICASSP'95*, 1995, vol. 3, pp. 1729–1732.

[48] G. G. Raleigh, S. N. Diggavi, V. K. Jones, and A. Paulraj, "A blind adaptive transmit antenna algorithm for wireless communication," in *Proc. IEEE ICC'95*, 1995, vol. 3, pp. 1494–1499.

[49] Y.-C. Liang and F. Chin, "Two suboptimal algorithms for downlink beamforming in FDD DS-CDMA mobile radio," *IEEE J. Select. Areas Commun.*, vol. 19, no. 7, pp. 1264–1275, July 2001.

[50] Y.-C. Liang, F. Chin, and K. J. R. Liu, "Downlink beamforming for DS-CDMA mobile radio with multimedia services," *IEEE Trans. Commun.*, vol. 49, no. 7, pp. 1288–1298, July 2001.

[51] K. Hugl, J. Laurila, and E. Bonek, "Downlink beamforming for frequency division duplex systems," in *Proc. IEEE GLOBECOM'99*, 1999, pp. 2097–2101.

[52] S. Haykin, *Adaptive Filter Theory*, Prentice-Hall, NJ, 1996.

[53] M. Dell'Anna and A. H. Aghvami, "Performance of optimum and suboptimum combining at the antenna array of a W-CDMA system," *IEEE J. Select. Areas Commun.*, vol. 17, no. 12, pp. 2123–2137, Dec. 1999.

[54] S. Choi and D. Shim, "A novel adaptive beamforming algorithm for a smart antenna system in a CDMA mobile communication enviroment," *IEEE Trans. Veh. Technol.*, vol. 49, no. 5, pp. 1793–1806, Sept. 2000.

[55] A. Barron, J. Rissanen, and B. Yu, "The minimum description length principle in coding and modeling," *IEEE Trans. Inform. Theory*, vol. 44, no. 6, pp. 2743–2760, Oct. 1998.

[56] M. Wax and T. Kailath, "Detection of signals by information theoretic criteria," *IEEE Trans. Acoust., Speech, Signal Processing*, vol. ASSP-33, no. 2, pp. 387–392, Apr. 1985.

[57] G. Liang, D. M. Wilkes, and J. A. Cadzow, "ARMA model order estimation based on the eigenvalues of the covariance matrix," *IEEE Trans. Signal Processing*, vol. 41, no. 10, pp. 3003–3009, Oct. 1993.

[58] M. F. Catedra, J. Perez, F. Saez de Adana, and O. Gutierrez, "Efficient ray-tracing techniques for three-dimensional analysis of propagation in mobile communications: application to picocell and micorcell scenarios," *IEEE Antenna Propagat. Mag.*, vol. 40, pp. 15–28, Apr. 1998.

[59] J. Perez, F. Saez de Adana, O. Gutierrez, I. Gonzalez, F. Catedra, I. Montiel, and J. Guzman, "FASANT: fast computer tool for the analysis of on-board antennas," *IEEE Antenna Propagat. Mag.*, vol. 41, pp. 84–98, Apr. 1999.

[60] L. Tong, G. Xu, and T. Kailath, "Blind identification and equalization based on second-order statistics: A time domain approach," *IEEE Trans. Inform. Theory*, vol. 40, no. 2, pp. 340–349, Mar. 1994.

[61] M. Torlak and G. Xu, "Blind multiuser channel estimation in asynchronous CDMA systems," *IEEE Trans. Signal Processing*, vol. 45, no. 1, pp. 137–147, Jan. 1997.

[62] A. J. van der Veen, S. Talwar, and A. Paulraj, "A subspace approach to blind space-time signal processing for wireless communication systems," *IEEE Trans. Signal Processing*, vol. 45, no. 1, pp. 173–190, Jan. 1997.

[63] X. Wang and H. V. Poor, "Blind equalization and multiuser detection in dispersive CDMA channels," *IEEE Trans. Commun.*, vol. 46, no. 1, pp. 91–103, Jan. 1998.

[64] A. J. Weiss and B. Friedlander, "Synchronous DS-CDMA downlink with frequency selective fading," *IEEE Trans. Signal Processing*, vol. 47, no. 1, pp. 158–167, Jan. 1999.

[65] L. Perros-Meilhac, E. Moulines, K. Abed-Meraim, P. Chevalier, and P. Duhamel, "Blind identification of multipath channels: A parametric subspace approach," *IEEE Trans. Signal Processing*, vol. 49, no. 7, pp. 1468–1480, July 2001.

[66] S. Dennett, *The cdma2000 ITU-R RTT Candidate Submission*, July 1998.

[67] A. F. Molisch, M. Steinbauer, M. Toeltsch, E. Bonek, and R. S. Thomä, "Capacity of MIMO systems based on measured wireless channels," *IEEE J. Select. Areas Commun.*, vol. 20, no. 3, pp. 561–569, Apr. 2002.

[68] D.-S. Shiu, G. J. Foschini, M. J. Gans, and J. M. Kahn, "Fading correlation and its effect on the capacity of multielement antenna systems," *IEEE Trans. Commun.*, vol. 48, no. 3, pp. 502–513, Mar. 2000.

[69] I. E. Telatar and D. N. C. Tse, "Capacity and mutual information of wideband multipath fading channels," *IEEE Trans. Inform. Theory*, vol. 46, no. 4, pp. 1384–1400, July 2000.

[70] B. Lindmark, S. Lundgren, J. R. Sanford, and C. Bechman, "Dual-polarized

array for signal-processing applications in wireless communications," *IEEE Trans. Antennas Propagat.*, vol. 46, no. 6, pp. 758–763, June 1998.

[71] C. B. Dietrich, K. Dietze, J. R. Nealy, and W. L. Stutzman, "Spatial, polarization, and pattern diversity for wireless handheld terminals," *IEEE Trans. Antennas Propagat.*, vol. 49, no. 9, pp. 1271–1281, Sept. 2001.

[72] M. R. Andrews, P. P. Mitra, and R. deCarvalho, "Tripling the capacity of wireless communications using electromagnetic polarization," *Nature*, vol. 409, pp. 316–318, Jan. 2001.

[73] D. Chizhik, F. Rashid-Farrokhi, J. Ling, and A. Lozano, "Effect of antenna separation on the capacity of BLAST in correlated channels," *IEEE Commun. Lett.*, vol. 4, no. 11, pp. 337–339, Nov. 2000.

[74] P. F. Driessen and G. J. Foschini, "On the capacity formula for multiple input multiple output wireless channels: A geometric interpretation," *IEEE Trans. Commun.*, vol. 47, no. 2, pp. 173–176, Feb. 1999.

[75] D.-S. Shiu, G. J. Foschini, M. J. Gans, and Kahn J. M., "Fading correlation and its effect on the capacity of multielement antenna systems," *IEEE Trans. Commun.*, vol. 48, no. 3, pp. 502–513, Mar. 2000.

[76] G. H. Golub and C. F. Van Loan, *Matrix Computations*, Johns Hopkins Press, Baltimore and London, 3rd edition, 1996.

Vita

Liang Dong was born in Shanghai, China, on February 15, 1974 . He received the B.S. degrees in applied physics and computer engineering from Shanghai Jiaotong University, China, in July 1996, and the M.S. degree in electrical engineering from the University of Texas at Austin, in December 1998. Since then, he started his doctoral studies in telecommunications and signal processing in the Department of Electrical and Computer Engineering at the University of Texas at Austin. His research has been in the area of wireless communications.

Mr. Dong worked for IBM China in 1995. From May 1998 to May 1999, he was employed as a software engineer for Cwill Telecommunications, Inc. in Austin, Texas. He is a member of Tau Beta Pi, Phi Kappa Phi and Sigma Xi.

Permanent Address: 9B, No.3, Lane 826, Jiang Ning Road

Shanghai, China, 200041

This dissertation was typeset with $\text{\LaTeX}\,2_\varepsilon$[1] by the author.

---

[1] $\text{\LaTeX}\,2_\varepsilon$ is an extension of $\text{\LaTeX}$. $\text{\LaTeX}$ is a collection of macros for $\text{\TeX}$. $\text{\TeX}$ is a trademark of the American Mathematical Society.